Department of Spatial Sciences

Application of Advanced Techniques for the Remote Detection, Modelling and Spatial Analysis of Mesquite (*Prosopis* spp.) Invasion in Western Australia

Todd Peter Robinson

This thesis is presented for the Degree of
Doctor of Philosophy
of
Curtin University of Technology

June 2008

ABSTRACT

Invasive plants pose serious threats to economic, social and environmental interests throughout the world. Developing strategies for their management requires a range of information that is often impractical to collect from ground based surveys. In other cases, such as retrospective analyses of historical invasion rates and patterns, data is rarely, if ever, available from such surveys. Instead, historical archives of remotely sensed imagery provides one of the only existing records, and are used in this research to determine invasion rates and reconstruct invasion patterns of a ca 70 year old exotic mesquite population (Leguminoseae: *Prosopis* spp.) in the Pilbara Region of Western Australia, thereby helping to identify ways to reduce spread and infill. A model was then developed using this, and other, information to predict which parts of the Pilbara are most a risk. This information can assist in identifying areas requiring the most vigilant intervention and pre-emptive measures. Precise information of the location and areal extent of an invasive species is also crucial for land managers and policy makers for crafting management strategies aimed at control, confinement or eradication of some or all of the population. Therefore, the third component of this research was to develop and test high spectral and spatial resolution airborne imagery as a potential monitoring tool for tracking changes at various intervals and quantifying the effectiveness of management strategies adopted. To this end, high spatial resolution digital multispectral imagery (4 channels, 1 m spatial resolution) and hyperspectral imagery (126 channels, 3 m spatial resolution) was acquired and compared for its potential for distinguishing mesquite from coexisting species and land covers. These three modules of research are summarised hereafter.

To examine the rates and patterns of mesquite invasion through space and time, canopies were extracted from a temporal series of panchromatic aerial photography over an area of 450 ha using unsupervised classification. Non-mesquite trees and shrubs were not discernible from mesquite using this imagery (or technique) and so were masked out using an image acquired prior to invasion. The accuracy of the mesquite extractions were corroborated in the field and found to be high ($R^2 = 0.98$, $P<0.001$); however, accuracy varied between classes ($R^2 = 0.55$ to 0.95). Additional sampling may be required in some of the wider class intervals, particularly the

moderate density class (30 to 90%) as sampling frequency was poor within the range of 60 to 90%. This is a direct result of there being relatively few quadrats available to be randomly selected in this class. That is, quadrats with between 60-90% cover were only evident in 4% of the test area. A more robust approach would, therefore, be to split this class into two (e.g. 30-60% and 60-90%) and select an additional 15 quadrats in the 60-90% range. The resolution of the imagery (1.4 m) precluded mapping shrubs smaller than 3 m^2. Rates and patterns were compared to mesquite invasions in its native range. It was determined that: (i) the shift from grass to mesquite domination had been rapid, with rates of increase in canopy cover comparable to invasive populations where it is native; (ii) rate of patch recruitment was high in all land types (stony flats, red-loamy soils and the riparian zone), but patch expansion and coalescence primarily occurred over the riparian zone and red-loamy soils; (iii) mesquite had been spread by sheep and macropods and the recent switch to cattle is likely to exacerbate spread as it is a far more effective dispersal vector; and (iv) early successional patterns, such as high patch initiation followed by coalescence of existing stands are similar to where mesquite is native, but patch mortality did not occur.

A knowledge based model was used to predict which parts of the Pilbara region are most at risk. Several limitations of models often employed in predicting suitability ranges of invasive plants were identified and include: (i) an inability to incorporate the notion that within a suitability range there is likely to be a scale of favourability; (ii) an inability to assign greater importance to evidence that is likely to have more importance in defining the areas suitable for invasion; and (iii) an inability to control the level of conservatism in the final results. These three shortcomings were mitigated through the use of: (i) fuzzy membership functions to derive a range of favourability from poor to best; (ii) pairwise comparison to derive higher weights for layers perceived to be more important and vice versa; and (iii) the use of ordered weighted averaging to directly control the level of conservatism (or risk) inherent in the models produced. Based on the outcomes of the historical reconstruction of spatial rates and patterns, data sources included land types, land use, and the derivation of a steady state wetness index from spot height data. Model outputs were evaluated using two methods: the area under the curves (AUC) produced from relative operating characteristic (ROC) plots and by the maximum Kappa procedure.

Both techniques agreed that the model most representative of the validation data was the one assuming the most risk. To create a Boolean output representing areas suitable/not suitable for invasion, optimal cut-points were derived using the point closest to the top left hand corner of the ROC plot and by the maximum Kappa method. Both methods obtained identical cut-points, but it is argued that the coefficient produced by the maximum Kappa method is more easily interpreted. The highest AUC was found to be 0.87 and, based on the maximum Kappa method, can be described as good to very good agreement with the validation records used.

Digital multispectral imagery (DMSI), acquired in the visible and near infrared portions of the spectrum (3 visible bands, 1 near infrared) with a spatial resolution of 1 m and hyperspectral imagery (126 bands, 3 m spatial resolution) was acquired to assess the potential of developing a reliable and repeatable mapping tool to facilitate the monitoring of spread and the effects of control efforts. Woody vegetation was extracted from the images using unsupervised classification and grouped into patches based on contiguity. Various statistics (e.g. maximum, minimum, median, mean, standard deviation, majority and variety) were assigned to these patches to garner more information for species separation. These statistics were explored for their ability to separate mesquite from coexisting species using Tukey's Honestly Significantly Different (HSD) test and, to reduce redundancy, followed by linear discriminant analysis.

Two approaches were taken to select the patch statistics offering the best discrimination. The first approach selected patch statistics that best discriminated all species (named "overall separation"). This was compared to a second approach, which selected the best patch statistics that separated each species from mesquite on a pairwise basis (named "pairwise separation"). The statistics offering the best discrimination were used as input in an Artificial Neural Network (ANN) to assign class labels. An incremental cover evaluation, whereby producer's accuracy was computed from mesquite patches grouped into various size-classes, showed that identification of mesquite patches smaller than 36 m^2 was relatively low (43-51%) regardless of the method used for choosing between the patch statistics or image type. Accuracy improved for patches >36 m^2 (66-94%) with both approaches and image types. However, both approaches used on the hyperspectral imagery were

more reliable at capturing patches >36 m2 than the DMSI using either approach. The lowest omission and commission rates were obtained using pairwise separation on the hyperspectral imagery, which was significantly more accurate than DMSI using an overall separation approach ($Z=2.78$, $P<0.05$), but no significant differences were found between pairwise separation used on either media. Consequently, all methods and imagery types, except for DMSI processed using overall separation, are capable of accurately mapping mesquite patches >36m^2. However, hyperspectral imagery processed using pairwise separation appears to be superior, even though not statistically different to hyperspectral imagery processed using overall separation or DMSI processed using pairwise separation at the 95% confidence level. Mapping smaller patches may require the use of very high spatial resolution imagery, such as that achievable from unmanned airborne vehicles, coupled with a hyperspectral instrument. Alternatively, management may continue to rely on visual airborne surveys flown at low altitude and speed, which have proven to be capable at mapping small and isolated mesquite shrubs in the study area used in this research.

ACKNOWLEDGEMENTS

Something worth doing is worth doing well. In this case, that "something" was this thesis, and I can only hope it is considered to have been done well. Regardless, I have no doubt that it would not have been done nearly as well without the enormous support of others, whom I acknowledge hereafter. For those that I might overlook, please accept my gratitude for the role that you have played.

I give my upmost gratitude to Dr. Graciela Metternicht, formerly of Curtin University of Technology, and Dr. Rieks van Klinken from CSIRO (Entomology) for their tireless assistance as supervisors/advisers. I would never have contemplated doing a PhD without Graciela's encouragement and belief in my ability, and for that I am hugely grateful. Graciela's knowledge and experience in remote sensing and spatial modelling were most valuable in setting up this thesis correctly from the beginning to the end. Our frequent face to face meetings and phone conversations always realigned this research to its core objectives. Rieks has a meticulous eye for critical details. He has made me analyse what the results of my research are really saying and how best to present this to my potential readership. He has shown me how to write concisely and clearly and look outside the square. Without his guidance in many of the ecological principles presented in this research, this thesis may have missed its true audience. I thank him for taking my calls at 4.55 pm and giving me hours of his time at the drop of a hat. I thank both for their patience and transference of skills that I can take with me in my professional career. I would also like to thank Dr. Bert Veenendaal of Curtin University of Technology for taking over as chief supervisor after Graciela's movement to the University of South Australia and for making that transition as smooth as possible.

I would also like to acknowledge the support and depth of knowledge and experience of all the staff at the Department of Spatial Sciences of Curtin University of Technology. It has been great to get feedback on snippets of this thesis via presentations and other discussions. Most notably, I would like to thank Drs. Bert Veenendaal, Rob Corner and Will Featherstone for their inputs into various modules of this thesis. They often asked questions or gave advice that offered me food for

thought. Thank you to Mrs Lori Patterson for her assistance with formatting, editing and associated issues.

Without funding this study would not have been possible. For that I would like to acknowledge the ARC-Linkage (LP0454890) grant, awarded to Dr. Graciela Metternicht, which assisted in acquiring most of the imagery used in this project. I would also like to thank the Department of Agriculture and Food Western Australia (DAFWA) for acting as a partner in this study and most notably Damian Shepherd from DAFWA for his assistance with datasets and various other contributions of this and related research. Linda Anderson from the Pilbara Mesquite Management Committee Inc. provided field assistance and logistical support. Logistical support was also provided by the Mardie Station Managers (Richard and Lindy Climas) and the leaseholders of Mardie Station (Thompson Family, Four Seasons Inc.). I would also like to thank SpecTerra Services for their support with the collection of the high resolution digital multispectral imagery (DMSI) used in this research and, in particular, Andrew Malcolm for preliminary discussions on which filters and spatial resolution to use. Thank you also to Peter Cocks from HyMap (hyperspectral imagery), who was only too kind in assisting me with processing and correcting the hyperspectral imagery acquired for this project. A Curtin University Postgraduate Scholarship (CUPS) provided the majority of personal funding throughout this research.

Thank you to my fellow lab rats at the Department of Spatial Sciences for their time, support and friendship, most notably, Dr. Georgina Warren, Deavi Purnomo and Dan McIntyre. I would also like to thank Dan for the exchange of ideas relating to invasive plants and updates of his work on Patterson's Curse.

Thank you to my parents for spending uncountable dollars on my education and providing invaluable support throughout my studies. Apologies for not getting down to see you as regularly as I would have liked, but you were never far from my thoughts. Without your unwavering support none of us would have become what we did, especially me. I'd like to also thank my close friends for their patience and understanding after knocking back invite after invite.

Finally, I would like to thank my own family. Firstly, thank you to my loyal Labrador, Karri, who kept me company during endless nights of reading. Yes, we can play ball now! But, more importantly, thank you to Mandy for her support and endurance through this time and making it feel worth it. Mandy thought it was all over after Honours, but I had some bad news for her. Without a hiccup she supported my decision. Thanks for doing all the family stuff alone, editing my chapters for spelling and grammar and apologies for being, at times, as thorny as a mesquite shrub. Mandy, three lines from a song by Lonestar (*Always in the band*) sums it up best:

Sometimes this dream demands more than I can give it
But even still I don't regret a single minute
Thank god she understands.

TABLE OF CONTENTS

ABSTRACT i
ACKNOWLEDGEMENTS v
TABLE OF CONTENTS viii
LIST OF FIGURES xiv
LIST OF TABLES xvii

1 INTRODUCTION 1
1. 1 Woody Plant Invasion: A Global Phenomenon 1
1. 2 Mesquite: The Space Invader 2
1. 3 Problem Statement 3
1. 4 Thesis Objectives 4
1. 5 Thesis Structure 5

2 LITERATURE AND METHODOLOGICAL REVIEW 8
2. 1 Introduction 8
2. 2 Spectral Properties of Vegetation 9
2. 3 Remote Sensing for Invasive Plant Detection 10
2.3.1 Step 1: Assess likelihood of successful discrimination 11
2.3.1.1 Flower, fruit or bract colour 11
2.3.1.2 Early “green-up” and/or early senescence 12
2.3.1.3 Canopy architecture 13
2.3.1.4 Seasonal colouration (leaves) 13
2.3.1.5 Growth habit 13
2.3.1.6 Stress/disease resulting in defoliation and colour change 14
2.3.2 Step 2: Choose appropriate imagery for the task 14
2.3.2.1 Spatial resolution 14
2.3.2.2 Spectral resolution 15
2.3.2.3 Radiometric resolution 16
2.3.2.4 Temporal resolution 16
2.3.3 Step 3: Choose a classification method 17

2.3.3.1 Parametric, hard unsupervised classification: ISODATA 19
2.3.3.2 Parametric, hard supervised classification: maximum likelihood (ML)……..... 19
2.3.3.3 Non-parametric, hard supervised classification 20
2.3.3.3.1 Artificial neural networks (ANNs)..... 21
2.3.3.3.2 Minimum-distance-to-means (MDM)..... 21
2.3.3.3.3 Parallelepiped..... 22
2.3.3.4 Non-parametric, soft supervised classification 23
2.3.3.4.1 Linear spectral unmixing (LSU) 23
2.3.3.4.2 Matched-filtering and Mixture Tuned Matched Filtering..... 25
2.3.3.4.3 Spectral angle mapper (SAM)..... 25
2.3.3.5 Manual image interpretation 26
2.3.3.6 Object-oriented (OO) classification 27
2.3.4 Step 4: Assessment of classification accuracy 27
2.3.4.1 Overall accuracy..... 27
2.3.4.2 Producer's accuracy and errors of omission 28
2.3.4.3 User's accuracy and errors of commission 29
2.3.4.4 Overall Kappa 29
2.3.4.5 Per-class Kappa..... 31
2.3.5 Review of the past success for mapping invasive plants 32
2.3.5.1 Panchromatic aerial photography..... 32
2.3.5.2 Colour and colour-infrared aerial photography..... 32
2.3.5.3 Airborne multispectral imagery 34
2.3.5.4 Satellite multispectral imagery..... 35
2.3.5.5 Hyperspectral imagery 36
2.3.5.5.1 Studies using SAM..... 38
2.3.5.5.2 Studies using LSU..... 38
2.3.5.5.3 Studies using MF or MTMF 39
2.3.5.5.4 Studies using ANNs..... 39
2.3.5.5.5 Dealing with spectral redundancy..... 40
2. 4 Spatial and Temporal Assessment of Invasion 41
2. 5 Predicting the Suitability of a Region to Plant Invasion..... 43
2.5.1 Data-driven models..... 44
2.5.1.1 Profile techniques..... 44

2.5.1.2 Group discrimination techniques 45
2.5.2 Knowledge-driven models 45
2.5.2.1 The weed invasion susceptibility prediction (WISP) model 46
2.5.2.2 Models incorporating fuzzy standardisation 46
2.5.3 Hutchinson's niche model – impact on model choice 49
2.5.4 Model validation techniques 49
2.5.4.1 The threshold dependent measure 50
2.5.4.2 The threshold independent measure 51
2. 6 Summary 52

3 STUDY AREA AND DATASETS 54
3. 1 Introduction 54
3. 2 Study Area 54
3.2.1 Control methods 55
3.2.2 Vegetation 56
3.2.3 Climate 57
3.2.3.1 Rainfall 57
3.2.3.2 Temperature and humidity 58
3.2.4 Topography 59
3. 3 Remotely Sensed Datasets 59
3.3.1 Airborne survey 60
3.3.2 Aerial photographs 62
3.3.3 Digital multispectral imagery (DMSI) 64
3.3.4 Hyperspectral imagery 66
3. 4 Datasets to Predict Suitability for Mesquite Invasion 69
3.4.1 Land types of the Pilbara 69
3.4.2 Pastoral potential 70
3.4.3 Land uses of the Pilbara 71
3.4.4 Digital elevation model 72
3. 5 Software 73
3. 6 Summary 73

4 EXAMINATION OF THE SPATIAL AND TEMPORAL RATES AND PATTERNS OF MESQUITE INVASION 75

4. 1 Introduction 75
4. 2 Methodology 77
4.2.1 Image classification and construction of vegetation layers 77
4.2.2 Mapping land types 79
4.2.3 Analysis of mesquite cover and temporal change 79
4.2.3.1 Patch dynamics 79
4.2.3.2 Change detection 80
4.2.3.3 Analysis of cover 81
4.2.4 Field verification of image processing 81
4. 3 Results 82
4.3.1 Analysis of mesquite cover and temporal change 82
4.3.2 Patch dynamics 83
4.3.3 Change detection 85
4.3.4 Analysis of cover 85
4.3.5 Ground verification of canopy cover densities within quadrats 87
4. 4 Discussion 88
4. 5 Summary 91

5 MODELLING THE SUITABILITY OF THE PILBARA REGION TO MESQUITE INVASION 93
5. 1 Introduction 93
5. 2 Description of Techniques 95
5.2.1 Weighted linear combination (WLC) 95
5.2.2 Standardisation of categorical maps 96
5.2.3 Pairwise comparison for weight estimation 97
5.2.4 Trade-off and risk 98
5.2.5 Manipulating trade-off and risk using ordered weighted averaging (OWA) 100
5. 3 Model Design 101
5.3.1 Step 1: Define layers 101
5.3.2 Step 2: Standardise layers 103
5.3.3 Step 3: Derive and apply weights 106
5.3.4 Step 4: Apply ordered weights 106
5.3.5 Step 5: Validate model 107

5.3.6 Step 6: Examine optimal cut-points 108
5. 4 Results 108
5. 5 Discussion 113
5. 6 Summary 117

6 ASSESSMENT OF HIGH SPATIAL RESOLUTION MULTISPECTRAL AND HYPERSPECTRAL IMAGERY FOR DISCRIMINATING BETWEEN MESQUITE AND OTHER WOODY SPECIES 118
6. 1 Introduction 118
6. 2 Artificial Neural Networks (ANNs) 121
6.2.1 Network architecture and forward propagation 121
6.2.2 Adjusting interconnecting weight values: Backpropagation 123
6. 3 Methodology 125
6.3.1 Collection of training and testing data 125
6.3.2 Step 1: Patch extraction 126
6.3.3 Step 2: Assignment of patch statistics 126
6.3.4 Step 3: Normalisation 127
6.3.5 Step 4: Exploratory analysis 127
6.3.6 Step 5: Discriminant analysis 127
6.3.6.1 Identifying patch statistics for overall and pairwise separation 128
6.3.7 Step 6: Classification using an ANN 128
6.3.8 Step 7: Class accuracy assessment 129
6.3.9 Step 8: Size-class accuracy assessment 129
6.3.10 Step 9: Accuracy comparisons 130
6. 4 Results 130
6.4.1 Exploratory analysis of DMSI 130
6.4.2 Exploratory analysis of hyperspectral imagery 132
6.4.3 Discriminant analysis 134
6.4.4 Class accuracy assessment 135
6.4.4.1 Overall separation approach: DMSI 135
6.4.4.2 Pairwise separation approach: DMSI 135
6.4.4.3 Overall separation approach: Hyperspectral imagery 136
6.4.4.4 Pairwise separation approach: Hyperspectral imagery 136
6.4.5 Size-class accuracy assessment 137

6.4.6 Accuracy comparisons 137
6. 5 Discussion 141
6. 6 Summary 144

7 SUMMARY AND RECOMMENDATIONS 146
7. 1 Introduction 146
7. 2 Spatial and Temporal Invasion Rates and Patterns 146
7.2.1 Recommendations 147
7. 3 Modelling the Suitability of the Pilbara to Mesquite Invasion 147
7.3.1 Recommendations 149
7. 4 Development of a Mapping and Monitoring Tool 149
7.4.1 Recommendations 150

REFERENCES 152

APPENDIX A 170

LIST OF FIGURES

Figure 2.1 Typical reflectance characteristics for healthy green grass, dead or senescing grass and bare dry soil for the wavelength interval from 400 to 1100 nm…….…..9

Figure 2.2 Summary of the different kinds of image processing techniques suitable for classifying remotely sensed imagery into meaningful classes…….....18

Figure 2.3 Conceptual rendition of the maximum likelihood algorithm……..20

Figure 2.4 Conceptual rendition of the minimum-distance-to-means algorithm 22

Figure 2.5 Conceptual rendition of the parallelepiped classification method….23

Figure 2.6 Hypothetical illustration of LSU……24

Figure 2.7 Conceptual rendition of the SAM algorithm……. 26

Figure 2.8 Examples of fuzzy membership functions (FMFs)……47

Figure 2.9 Illustration of a ROC plot……...52

Figure 3.1 The distribution of mesquite by density class, as recorded visually from an airborne (helicopter) survey……..55

Figure 3.2 (a) Biological control, leaf tier (*Evippe* sp. #1); (b) Close up photograph showing the yellowing of the leaves and partial defolation of a mesquite shrub caused by the leaf tier…….56

Figure 3.3 Annual rainfall for Mardie, WA, Australia, 1930-2004…….58

Figure 3.4 Overhead views of mesquite brush at different aerial cover values. Photographs were taken from the helicopter during the survey…….61

Figure 3.5 Typical shrub/tree densities used to categorise the percentage of mesquite canopy cover found within a surveyed grid cell into different class definitions……...62

Figure 3.6 Location map and display of the chosen aerial photographs……..64

Figure 3.7 False colour composite (R=NIR, G=Red, B=Green) of the digital multispectral imagery (DMSI)……67

Figure 3.8 False colour composite (R=800nm, G=680nm, B=550nm) of the hyperspectral imagery…….68

Figure 3.9 Map of the different land types throughout the Pilbara Region……..69

Figure 3.10 Map of the six classes of pastoral potential……71

Figure 3.11 Map of the various land uses of the Pilbara Region……..….72

Figure 3.12 Digital Elevation Model (DEM) of the Pilbara Region……..73
Figure 4.1 Flowchart of the algorithm used to extract the mesquite canopies from the aerial photography……78
Figure 4.2 Illustration of how the ISODATA technique assigns pixels to different clusters……78
Figure 4.3 Relationship between the variance of estimated mesquite cover (%) and quadrat size……...80
Figure 4.4 Density of mesquite patches by size class for 1970 (black bars) and 2001 (open bars): (a) stony flats, (b) red loamy soils, (c) riparian zone…… 84
Figure 4.5 The distribution of land type and mesquite across the test area showing presence of mesquite (circles and triangles) and increase in mesquite cover within a quadrat above the change threshold (circles) in (a) 1970 and (b) 2001……..86
Figure 4.6 Field measurements of canopy cover plotted against estimates of canopy cover found from image processing within 60 randomly selected 20 x 20 (400 m^2) quadrats…….88
Figure 5.2 Compound Topographic Index (CTI) derived for the Pilbara Region……...103
Figure 5.3 Fuzzy membership values assigned to each of the pastoral potential ratings……104
Figure 5.4 Fuzzy membership values assigned to each of the land uses……104
Figure 5.5 Fuzzy membership values assigned to the CTI layer……105
Figure 5.6 Model outputs illustrating the suitability of the study area to mesquite invasion: (a) Fuzzy Conservative; (b) Fuzzy WLC; and (c) Fuzzy Risky…….109
Figure 5.7 Relative Operating Receiver (ROC) plots for the three models implemented……..110
Figure 5.8 Map showing the suitability of the Pilbara to mesquite invasion split into two classes…….112
Figure 6.1 Neural network architecture of a multilayer perceptron used for the classification of remotely sensed data……...122
Figure 6.3 Spectral reflectance curves of mesquite and associated species derived from the DMSI……..131

Figure 6.4 Spectral reflectance curves of mesquite and associated species derived from the hyperspectral imagery……133

Figure 6.5 Percentage of mesquite patches correctly detected (producer's perspective) for two size-classes for a) the DMSI and b) the hyperspectral imagery……...138

Figure 6.6 Sample map of the hyperspectral imagery classified using patch statistics identified by pairwise separation……...140

LIST OF TABLES

Table 2.1 Common invasive plants, their distinguishable traits and examples of the best time for image acquisition…….12

Table 2.2 Summary of the various kinds of imagery available in terms of spatial, spectral, radiometric and temporal resolution……15

Table 2.3 Illustration of an error matrix and associated statistics used for assessing the accuracy of a classification……...28

Table 2.4 Examples of the accuracy achieved in previous studies using various classification methods and either colour/colour infrared (CIR) aerial photography, airborne multispectral or satellite multispectral imagery……...34

Table 2.5 Examples of the accuracy achieved in previous studies using various classification methods and hyperspectral imagery…….37

Table 2.6 The various error types used to validate a prediction model……..50

Table 3.1 Summary of monthly rainfall data for Mardie…….58

Table 3.2 Summary of monthly temperature data for Mardie……59

Table 3.3 Descriptions and proportions of the study area occupied for the mosaic of 20 land types surveyed……...70

Table 3.4 Area and percentage of the 6 pastoral potential classes……..71

Table 3.5 Descriptions and proportions of the study area occupied for the 8 land uses……..72

Table 4.1 Statistical breakdown of the canopy cover changes for the 1943, 1970 and 2001 images over the three land types…….82

Table 4.2 Summary statistics for patches greater than 100m^2 in 2001, broken down by land type……...83

Table 5.1 The fundamental scale on which pairwise comparisons are based….97

Table 5.2 Random Inconsistency Index (RI)……..98

Table 5.3 Pairwise comparison matrix used to weight each individual layer prior to assigning order weights……106

Table 5.4 Order weights used to control the risk-trade-off continuum for the three knowledge driven models computed……...107

Table 5.5 Average suitability values for presence and absence records for the three models implemented……109

Table 5.6 Error matrix representing the number of pixels observed versus the number predicted from the 'fuzzy risky' model for the top 10% of pixels…….111

Table 6.1 Description of the statistics calculated for each patch……..126

Table 6.2 Patch statistics of mesquite and associated species derived from the DMSI after normalisation…….132

Table 6.3 Summary of the patch statistics found from discriminant analysis that best separate all species (overall separation method)……...134

Table 6.4 Summary of the patch statistics found from discriminant analysis that best separate mesquite from each species in turn (pairwise separation method)…….134

Table 6.5 Confusion matrix and associated statistics based on the patch statistics derived from the DMSI that gave the best overall separation……..135

Table 6.6 Confusion matrix and associated statistics based on the patch statistics derived from the DMSI that gave the best pairwise separation……136

Table 6.7 Confusion matrix and associated statistics based on the patch statistics derived from the hyperspectral imagery that gave the best overall separation……..136

Table 6.8 Confusion matrix and associated statistics based on the patch statistics derived from the hyperspectral imagery that gave the best pairwise separation……..137

Table 6.9 Errors of omission and commission for both image types and both approaches for patches >36 m^2…….139

1 INTRODUCTION

1. 1 Woody Plant Invasion: A Global Phenomenon

Invasive woody plants have been observed on every continent where arid and semi-arid rangelands occur (Archer, 1994; Hudak and Wessman, 1998). These plants have the potential to dramatically alter biodiversity (Gibbens et al., 1992), vary the temporal and spatial distribution of water, nitrogen and other soil resources (Schlesinger et al., 1990) and impact on primary production by reducing the amount of pastoral land available for grazing (Henessy et al., 1983; Goslee et al., 2003).

The proximate causes for the recent global shift from grasslands to woodlands are multi-faceted and controversial. Popular theories include globally rising carbon dioxide levels, which theoretically favour woody plants that have a C_3 photosynthetic pathway over C_4 grasses (Polley et al., 1994; Derner et al., 2005) and may also enhance the water efficiency of woody plants, thereby increasing the likelihood of establishment and survival in arid to semi-arid regions (Polley, 1997). However, this theory is deemphasised by Archer et al. (1995) who argue that the relationship is not entirely cause and effect. Relatively recent climate changes causing, for example, more intense episodic periods of rainfall, extended wet seasons or droughts may also explain some cases of proliferation (e.g. Bowman et al., 2001). However, this is controversial since edaphically similar areas on adjacent paddocks have been observed to show dramatic differences in invasion rates (Van Auken, 2000). At the landscape level, woody plants that produce nutritious pods (e.g. mesquite) may have high invasion rates due to introduced dispersal vectors (e.g. cattle). Mesquite has a thick seed coat that requires scarification, which occurs during mastication; the seed survives passage through the gut of cattle and is deposited in a moist, nutrient rich, dung (Brown and Archer, 1987; Brown and Archer, 1989; Brown and Carter, 1998).

In many parts of the world, fire frequencies have decreased since settlement and subsequent pastoralism practices have been adopted. These reductions in fire frequencies are a result of fine-fuel removal by livestock grazing, cessation of ignition by indigenous populations and active fire suppression. In Australia, active and accidental use of fire by Aboriginals in the 40,000 years prior to European

settlement is well documented (e.g. Bowman, 1998), and it is thought that cessation of traditional Aboriginal land management has resulted in woody thickening in some parts of northern Australia (Bowman et al., 2001). Sufficient fire-free intervals can enable some woody plants to reach an appreciable size and age whereby they become highly tolerant to fire and eventually overtop the herbaceous cover (Van Auken, 2000; Scholes and Archer, 1997). Altered fire regimes throughout the world are, therefore, thought to be a major cause of the invasion of woody species into grasslands in the recent past (Bowman, 1998; Van Auken, 2000; Bowman et al., 2001).

An increased frequency of gaps in the herbaceous layer caused by herbivory enables greater opportunities for woody plant establishment. Contrarily, the long life-span of woody plants means that the frequency of gap formation in wooded areas is relatively low. Differences in rates and frequencies of gap formation associated with grass and woody plant life-history traits may explain why successional transitions between grass and woody plant-dominated states are highly asymmetrical and why conversion back to grasslands is highly unlikely (Scanlan and Archer, 1991; Archer, 1994). Put simply, once the successional process is initiated, the probability of grasslands (g) converting into woodlands (w) is far greater than the reverse occurring (i.e. $P(g \rightarrow w) > P(w \rightarrow g)$) (Archer, 1994).

1. 2 Mesquite: The Space Invader

Mesquite is a leguminous shrub that grows to about 3 m in height and often forms impenetrable thickets, resulting in serious economic (e.g. lost production, increased control and management costs), environmental (e.g. increased land degradation, loss of soil moisture, altered biodiversity and provision of refuges for feral animal populations) and social costs (Hennessy et al., 1983; Gibbens et al., 1992; Goslee et al., 2003). Mesquite was widely planted on properties throughout northern Australia in the early 1900s for a variety of purposes including shade, as a possible food source for stock (pods), and for soil stabilisation around mining sites. By the 1920s and and 1930s, it was widely distributed throughout Queensland, the Northern Territory and Western Australia (van Klinken and Campbell, 2001). Naturalised and hybrid species of mesquite are now found in every state and territory in Australia, with the exception of Tasmania and the Australian Capital Territory (Osmond et al., 2003).

Due primarily to its invasiveness, potential for spread and economic and environmental impacts, mesquite is regarded as one of the worst weeds in Australia, and is currently listed as one of the top 20 weeds of national significance to Australia (Thorp and Lynch, 2000).

In the 1930s, mesquite was introduced to the Mardie Pastoral Station in the northwest Pilbara Region of Western Australia to serve as a shade and emergency fodder plant (Meadly, 1962). Initially, plants showed little tendency to spread, and it was not until after the 1945 floods in Western Australia that the invasive potential of mesquite became evident. Anecdotal evidence suggests that a small number of trees planted in the 1930s around the Mardie Station homestead and shearing shed rapidly multiplied, resulting in the worst infestation in the country (Osmond et al., 2003). Here, it is estimated to have established over 150,000 ha of potential grazing land, of which 30,000 ha has been identified as dense (van Klinken et al., 2003).

Mesquite possesses many characteristics that make it a very aggressive invader of grasslands. Such characteristics include an extensive root system that can access water from both shallow and deep soil horizons (Lopez-Portillo and Montana, 1999), a long life-span with low post-establishment mortality rates (Archer, 1989), an ability to fix nitrogen (Shearer et al., 1983) and a capability to germinate over a wide range of soil types, temperatures, moisture regimes and light conditions (Hennessy et al., 1983; Gibbens et al., 1992; El-Keblawy and Al-Rawai, 2005).

1. 3 Problem Statement

As mentioned above, mesquite is a threatening process to rangelands throughout Australia. Failure to curb invasion will only amplify its impacts as it continues to spread and increase in density. Traditionally, information such as invasion processes and the location and spatial extent of invasive plants is acquired by field surveys; however, this may not always be practical or timely, particularly over large, highly inaccessible regional areas. Spatial science, which in this context covers geographic information science and remote sensing science, offers the potential to supply this information in a more timely and practical manner. Three key problems that may be addressable by combining ecological principles with the manipulation, extraction and formulation of geographic information are identified hereafter.

Firstly, the process of invasion needs to be considered within the context of the landscape in which it is invading. There are a wide range of processes through which weeds can invade a landscape and these processes need to be understood prior to the implementation of coherent management schemes. For example, management strategies may differ for invasive plants that invade along a population front, solely through riparian corridors or that are dispersed long distances and subsequently in-fill. Furthermore, it is likely that in any setting, rates of invasion will vary spatially and temporally and may be regulated by various factors including soil types, soil moisture and the presence of an effective dispersal vector and these factors need to be identified, and where possible, quantified.

Secondly, predicting the potential distribution of invasion at a regional level offers important information for preventing spread into high risk areas, identifying priority areas to control and directing where to acquire remote sensing data to monitor for early outbreaks and thereby craft early intervention strategies (Morisette et al., 2006).

Thirdly, a major challenge confronting ecologists and land managers in their vision to effectively manage invasive plant species is a lack of information concerning their precise location and extent. Remote sensing offers a potential solution for mapping and monitoring invasive plants, but has not yet been adopted as a standard survey tool because of past limitations in spatial and/or spectral resolution. This has hindered the mapping of plants at a sufficient resolution for targeted control/eradication, particularly for invasive plants that do not exhibit highly distinguishable biological traits relative to coexisting species present within the same landscape. However, current technology can provide very high spatial resolution (e.g. <1 m) and very high spectral resolution imagery (e.g. >100 bands, acquired at 10 to 15 nm intervals). Furthermore, classification algorithms have also become more sophisticated since the early attempts at classifying the more challenging species.

1. 4 Thesis Objectives

Based on the above problem statement, the objectives of this study are threefold:

(i) Determine the rates and patterns of mesquite invasion since introduction. In particular, identify:

a. Rates of invasion and compare to rates where mesquite is native;
b. Patterns of invasion;
c. Rates and patterns of invasion over different land types; and
d. Whether invasion patterns are consistent with dispersal by known vectors.

(ii) Predict the potential distribution of the mesquite population throughout the Pilbara Region using advanced knowledge driven modelling. The parameters for the model are heavily reliant on the knowledge gained from objective (i) above. In particular, this model will include suitable land types, soil moisture and the presence of effective dispersal vectors; and

(iii) Determine the effectiveness of high spatial resolution digital multispectral imagery (e.g. 1 m) and high spectral resolution imagery (e.g. hyperspectral imagery) for differentiating between mesquite and coexisting species, with the aim of developing a robust tool for future mapping and monitoring. This objective will also identify any limitations of the method (e.g. smallest patch size reliably detected).

1. 5 Thesis Structure

This thesis consists of seven chapters. Chapter 1 introduces the problem of invasion of grasslands by woody weeds, potential causes and briefly describes the invasive plant under study (mesquite). It then describes information that can augment management practices and how this information can be derived from digital information (e.g. geographic and remotely sensed data). Objectives are directly derived from three data requirements for crafting effective management strategies.

Chapter 2 reviews relevant literature and methodologies to satisfy the three objectives of the study (reconstructing historical invasion rates and patterns; construction of a suitability template for mesquite invasion and mapping mesquite using remotely sensed imagery). The chapter begins with the role of remote sensing

for mapping individual species on the basis of distinguishable biological traits. A four step methodology is presented to identify the likelihood of successful mapping as well as for guiding the choice of imagery and classification method. Accuracy measures are also given to quantify and compare the success of mapping using different datasets and techniques. The success of previous studies is reviewed for a wide range of image types, classification techniques and invasive plants. The success of previous studies aimed at examining historical invasion rates is then reviewed. Finally, methods for modelling habitat suitability are reviewed and advantages and disadvantages of current approaches highlighted in order to derive the most appropriate, novel and robust model for this study. Methods for model validation are also given.

Chapter 3 describes the location and characteristics of the mesquite population under study. All data sources used in subsequent chapters are presented. The main software packages used to analyse, present and derive the various outputs of this study are described.

Chapter 4 focuses on objective (i) above. Historical aerial photographs are used to reconstruct past rates and patterns of mesquite invasion and highlight the similarities and differences of this population to native range populations. This work has been published in the Journal of Arid Environments (Robinson et al. 2008)

Chapter 5 extrapolates information derived from Chapter 4 (e.g. dispersal vectors, suitability to land types and the influence of soil moisture), using a knowledge driven approach, over the Pilbara Region to identify areas of high and low suitability for mesquite invasion (objective ii). Levels of conservatism inherent in the models are altered by using ordered weighted averaging. Models are validated using relative operating characteristic (ROC) plots and Kappa statistics.

Chapter 6 examines the potential of DMSI and hyperspectral imagery for differentiating mesquite from coexisting species, thereby defining the precise location and distribution of mesquite throughout the landscape (objective iii). Confusion matrices and the approximate patch size that can be reliably mapped using these technologies are examined.

Chapter 7 presents a summary of the thesis, including salient conclusions and opportunities for further research.

2 LITERATURE AND METHODOLOGICAL REVIEW

2. 1 Introduction

This chapter reviews the role of remote sensing and spatial modelling for the study and management of invasive plants, with a particular focus on invasive plant mapping, the use of longitudinal assessment of weed invasions to understand invasion processes, and habitat suitability modelling.

The first section covers the spectral properties of vegetation, highlighting: (i) changes that can be expected in the signature characteristics of different species and vegetation types at different phenological stages; and (ii) that species differentiation relies on the existence of detectable differences between the spectra of all coexisting species.

The next section summarises the process of classifying invasive species from remotely sensed imagery into four broad steps:

(i) examine the biological traits of the target weed and other coexisting species to determine if the spectra of all species are likely to be separable;
(ii) choose appropriate imagery to maximise the chances of successful mapping;
(iii) give consideration as to which classification method may be most appropriate; and
(iv) assess classification accuracy.

This discussion is followed by a review of a cross-section of studies aimed at mapping invasive plants.

The third section discusses how reconstructing historical invasion patterns can assist in predicting future patterns, determining causes for accelerated invasion, quantifying the long term success of control strategies, and revealing land type preferences.

The final section discusses methods to extrapolate existing knowledge over large areas to assist in the prioritisation of management activities. In particular, a wide

range of models are reviewed in terms of their strengths and weaknesses in order to derive a more robust model in this research.

2. 2 Spectral Properties of Vegetation

Remote sensing involves the measurement and analysis of reflected radiation. Typical reflectance characteristics for healthy green vegetation, dead or senescent vegetation and dry bare soil are shown in Figure 2.1. Around 70 to 90% of blue (e.g. 400 to 500 nm) and red (e.g. 600 to 700 nm) light are absorbed by healthy green vegetation to provide energy for the process of photosynthesis. The slight reflectance peak around 500 to 600 nm (green light) is known as the "green peak" and is the reason that most actively growing vegetation appears green to the human eye. Non-photosynthetically active vegetation lacks this "green peak" (Mather, 2004).

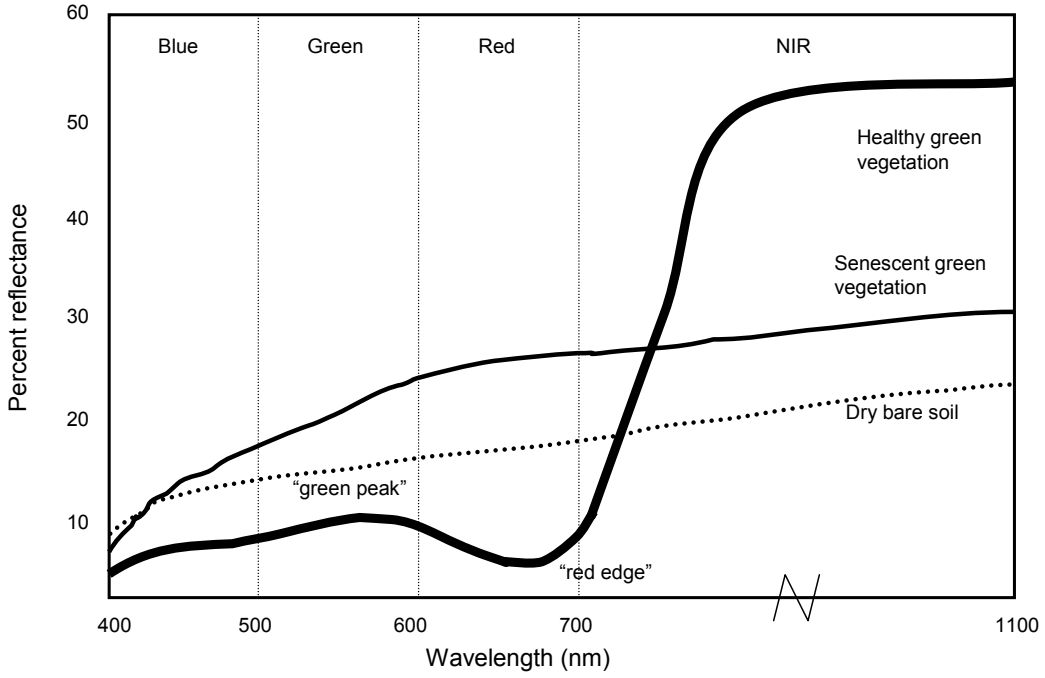

Figure 2.1 Typical reflectance characteristics for healthy green grass, dead or senescing grass and bare dry soil for the wavelength interval from 400 to 1100 nm (adapted from Jensen, 1996).

For photosynthetically active vegetation, the spectral reflectance curve rises sharply between approximately 700 and 800 nm and remains high in the near infrared region between 750 and 1350 nm. The "red edge" refers to the region of rapid change in reflectance of chlorophyll at approximately 680 to 700 nm, with maximum

reflectance at approximately 800-900 nm (Figure 2.1). The "red-edge" point for plants undergoing greater photosynthesis will generally begin to rise at longer wavelengths of the near-infrared portions of the spectrum (Vogelmann, 1993). As the plant senesces, the level of reflectance in the near infrared region declines first, with reflectance in the visible part of the spectrum not being affected significantly. However, the relative maximum in the green portion of the spectrum is likely to decline as pigments other than chlorophyll begin to dominate and the leaf begins to lose its greenness. Stress (e.g. from drought, disease or herbivory) can also produce a spectral response that is similar to senescence (Mather, 2004).

Importantly, it is the difference in the spectral reflectance curves of different land covers that enable their classification from remotely sensed imagery – land covers would not be distinguishable from one another if the spectral reflectance curves are almost identical. Likewise the discrimination of plant species depends on the existence of detectable differences between the spectra of all coexisting species (see Section 2.3.1).

2. 3 Remote Sensing for Invasive Plant Detection

Any study aimed at mapping specific species usually proceeds in four steps. Firstly, remote sensing experts, often in collaboration with ecologists and land managers, ascertain the likelihood that the species can be mapped with success. This is normally achieved by identifying if the target species possess some distinguishable trait relative to other species present at and around the invasion sites (see Section 2.3.1). The second step is the identification of the smallest patch or individual that must be detected for effective management. This step largely influences the spatial resolution (pixel or cell size) of the imagery required (see Section 2.3.2). Additionally, the spectral resolution required (e.g. the number and width of the spectral bands) also needs to be identified. For example, if it is determined from step 1 that the distinguishable characteristics of the target species are subtle, higher spectral resolution imagery may be required. Identification of the spectral/spatial resolution required generally assists in deciding which sensor (or range of sensors) may be most appropriate for the task at hand.

The third step is to choose an appropriate classification routine, which may be dependent on which instrument was used to capture the imagery. For example, a range of techniques that might be applicable to hyperspectral imagery (very high spectral resolution imagery) might not be applicable to aerial photography (see Section 2.3.3). The final step involves an assessment of the accuracy of the classification procedure implemented. In general, it is appropriate to outline a target accuracy *a priori* that must be achieved in order to consider the application of remote sensing for mapping the invasive species a success for management purposes (see Section 2.3.4).

2.3.1 Step 1: Assess likelihood of successful discrimination

Many successful studies aimed at differentiating invasive species from coexisting species have usually relied on timing the acquisition of remotely sensed imagery to coincide with a period where the focal species exhibits a unique trait, relative to coexisting species (Hunt et al., 2003). Such traits can include:

(i) Flower, fruit or bract colour;
(ii) Early "green-up"/senescence or late senescence;
(iii) Canopy architecture;
(iv) Seasonal colouration (leaves);
(v) Growth habit; and
(vi) Stress/disease resulting in defoliation and colour change.

Table 2.1 shows examples of studies where successful species discrimination was achieved on the basis of one or more of the abovementioned traits.

2.3.1.1 Flower, fruit or bract colour

During peak flowering, invasive plants that would otherwise be indistinguishable from other vegetation types may be identified and therefore timing imagery to coincide with this period is crucial for success. For example, leafy spurge (*Euphorbia esula*) produces yellow bracts around June each year causing its visible reflectance to increase from 630 to 690 nm, which is higher than other species common to the area (Everitt et al., 1995). Other species mapped on the premise of unique flower, bract or fruit colour are shown in Table 2.1.

Table 2.1 Common invasive plants, their distinguishable traits and examples of the best time for image acquisition.

Category	Species (Common Name)	Scientific Name	Distinguishing Traits	Image Timing (Examples)	Related Studies
Unique flower, fruit or bract colour	Huisache	*Acacia farnesiana*	Orange-yellow flowers	Winter	Everitt and Villarreal (1987)
	Mexican polo-verde	*Parkinsonia aculeata*	Yellow flowers	Spring	
	Common goldenweed	*Isocoma cornopifolia*	Golden-yellow flowers	Early to mid autumn	Everitt et al. (1992a)
	Drumond goldenweed	*Isocoma dummondii*	Golden-yellow flowers	Late autumn to early winter	Everitt et al. (1992a)
	Leafy spurge	*Euphorbia esula*	Bright yellow bracts	Early summer	Everitt et al. (1995)
Early "green-up" and/or early senescence	Cheatgrass (aka Downy brome)	*Bromus tectorum*	Early greenup and early senescence	Early spring (for early greenup); Mid-summer (for early senescence)	USGS (2003)
Canopy architecture	Broom snakeweed	*Guitierezia sorathrae*	Erectophile (erect leaves) canopy structure.	Any time during growing season	Everitt et al. (1992b)
	Spiny aster	*Aster spinosus*	Erectophile (erect leaves) canopy structure.	Any time during growing season	Everitt et al. (1992b)
Seasonal colouration (leaves)	Chinese tamarisk	*Tamarix chinensis*	Unique orange brown leaf colour in autumn	Autumn	Everitt and Deloach (1990); Everitt et al. (1996)
	Redberry Juniper	*Juniperus pinchottii*	Evergreen foliage	Autumn if other species are deciduous	Everitt et al. (2001)
Growth habit (e.g. thickets)	Blackberry	*Rubus fruiticosis*	Dense thickets reflect higher in NIR region	Summer to early autumn	Frazier (1998); Ullah et al. (1989).
	Giant Reed	*Arundo donax*	Dense thickets reflect higher in NIR region	Summer and autumn.	Everitt et al. (2004).
Stress/disease resulting in defoliation and colour change	Oak (with oak wilt disease)	*Quercus spp.*	Defoliated crowns	When most defoliated.	Everitt et al. (1999).

2.3.1.2 Early "green-up" and/or early senescence

Invasive plants or grasses that "green-up" before the "green-up" of other species or senesce before other species can be good targets for mapping using remote sensing

technologies. For example, cheatgrass (*Bromus tectorum*) "greens-up" early in the spring and then senesces before other grasses; and can therefore be distinguished from other species by acquiring imagery at green-up or senescence, or both (USGS, 2003; Table 2.1).

2.3.1.3 Canopy architecture

Canopy architecture is also potentially useful for detecting invasive plants. For example, due to an erectophile canopy structure (e.g. erect leaves) the near-infrared reflectance of broom snakeweed (*Guitierezia sorathrae*) and spiny aster (*Aster spinosus*) was found to be lower than that of other rangeland species in a study by Everitt et al. (1992b) (Table 2.1).

2.3.1.4 Seasonal colouration (leaves)

The reduction in chlorophyll in deciduous plants during autumn has been used effectively in species discrimination by allowing other more unique pigments, relative to other species, to be detected. For example, Everitt and DeLoach (1990) and Everitt et al. (1996) mapped Chinese tamarisk (*Tamarix chinensis*) by taking advantage of its unique orange-brown colour prior to leaf drop, while coexisting species remained evergreen. Mack (2005) suggests that any invasive species with the potential to undergo distinct seasonal colour change may a candidate for aerial assessment. This principle can also be used in reverse. For example, Everitt et al. (2001) successfully mapped redberry juniper (*Juniperus pinchottii*) by taking advantage of its evergreen foliage by obtaining imagery in winter when other species were dormant (Table 2.1).

2.3.1.5 Growth habit

Invasive plants that grow in monospecific stands (e.g. thickets) may produce unique spectral characteristics to enable detection. The vegetative density and crown vigour of these stands often results in fewer gaps in their canopy, relative to individual plants. As a result, the reflectance in the near infrared band is often higher than that of other species that do not form thickets. Everitt et al. (2004) and Frazier (1998) have utilised this principle for mapping giant reed (*Arundo donax*) and blackberry (*Rubus fruiticosis*), respectively (Table 2.1).

2.3.1.6 Stress/disease resulting in defoliation and colour change

Trees/plants that are stressed or diseased will often show signs of dieback of the upper crown coupled with discolouration and wilting/defoliation of the foliage. Everitt et al. (1999) were able to map oak (*Quercus* spp.) suffering from oak wilt disease as the defoliation effects of the disease resulted in lower reflectance values in the near infrared region, relative to healthy oak trees (Table 2.1)

2.3.2 Step 2: Choose appropriate imagery for the task

The strength of remotely sensed imagery for detecting invasive plants is a function of the chosen sensor's spatial, spectral, radiometric and temporal resolution, as discussed hereafter.

2.3.2.1 Spatial resolution

Spatial resolution can be defined as a measure, in meters, of the ground projected instantaneous field of view (IFOV) of the sensor. For example, the Landsat Thematic Mapper (herein referred to as Landsat) ground-projected IFOV is 30x30 m. Generally, the higher the spatial resolution the greater the resolving power of the sensor (Jensen, 1996).

The ability to resolve light and scattered weed infestations is a commonly highlighted limitation of the application of remote sensing to invasive plant detection that is linked to the achievable spatial resolution of current remote sensing technologies. For example, the required spatial resolution for mapping weed patches has been estimated as less than one-quarter of the smallest patches that need to be mapped (Hunt et al., 2005). This 'detection limit' needs to be identified prior to obtaining imagery. For example, sensors must be able to detect small and isolated populations if classification outputs are to be useful in invasive plant eradication programmes (c.f. Moody and Mack, 1988). Table 2.2 highlights the spatial resolution of many available remotely sensed products from both airborne and satellite platforms. Hence, if the intention of the study is to precisely identify the location of isolated/scattered invasive plants then those sensors with a spatial resolution higher than the weed manager's detection limit can, in general, be ruled out.

Table 2.2 Summary of the various kinds of imagery available in terms of spatial, spectral, radiometric and temporal resolution.

Platform	Type	Sensor(s)/ Products	Spatial Resolution[1]	Spectral Resolution	Rad. Res.[2]	Temporal Resolution
Aircraft	Film Photography	Panchromatic	e.g. <2 m	Low	8	Generally archived
		Colour/ colour infrared	e.g. <2 m	Low	8	On demand
	Digital Photography	Colour	e.g. <2 m	Low	8	On demand
	Digital videography	CCD cameras record to VHS	Poorest of airborne	Low	n/a	On demand
	Multispectral scanners	DMSI[3]	0.25 to 4 m	Low	12	On demand
		ADAR[4]	0.25 to 4 m	Low	8	On demand
		MEIS[5]	e.g. 0.4 m	Low	8	No longer operational
	Hyperspectral	Hymap/Probe	1 to 10 m	V. High	16	On demand
		CASI-2[6]	1 to 10 m	High	12	On demand.
Satellite	Low spatial resolution imagery	AVHRR[7]	1.1 km	Low	10	2 per day
		MODIS[8]	250 m to 1 km	High	12	1-2 days
	Moderate spatial resolution imagery	Landsat	30 m	Low	8	16 days
		SPOT-5[9]	10 m	Low	8	26 days
	High spatial resolution imagery	Quickbird	2.4 m	Low	11	Must be tasked
		IKONOS	4 m	Low	11	Must be tasked
	Hyperspectral	Hyperion	30 m	V. High	12	16 days

[1]The spatial resolution of airborne products is dependent on the height at which the imagery is flown. Please consult your vendor for what is currently achievable; [2]Number of bits; [3]DMSI=Digital Multispectral Imagery; [4]ADAR=Airborne Data Acquisition and Registration; [5]MEIS=Multispectral Earth Imaging System; [6]CASI=Compact Airborne Spectrographic Imager; [7]AVHRR=Advanced Very High Resolution Radiometer; [8]MODIS=Moderate Resolution Imaging Spectroradiometer; [9]SPOT=Satellite Pour l'Observation de la Terre.

2.3.2.2 Spectral resolution

Spectral resolution refers to the number and width of spectral bands of a particular sensor (Mather, 2004). In general, the greater the spectral resolution, the greater the likelihood of distinguishing invasive plants from their surroundings (Hunt et al., 2005). More specifically, to provide reliable identification of a particular plant species on a remotely sensed image, the spectral resolution of the sensor must match as closely as possible to the spectral reflectance curve of the particular plant in question (Mather, 2004).

The spectral resolution achievable with current and past sensors can be broadly categorised into three types: panchromatic, multispectral and hyperspectral sensors. Panchromatic images have commonly been collected using aerial photography, although some satellites also have a panchromatic channel (e.g. IKONOS, SPOT, Landsat ETM+). Multispectral sensors are sensitive to radiation within several wavelengths (e.g. Landsat 7 acquires imagery in 7 bands or "channels") from the visible (red, green and blue light) and often into at least the near infrared portions of the spectrum. By utilising several bands, multispectral imagery has improved power over panchromatic imagery for discriminating land covers. However, as the bandwidths of these sensors are generally quite large, subtle differences (e.g. between like vegetation types) may not be distinguishable (Mather, 2004). Hyperspectral sensors acquire many more bands of imagery than multispectral imagery (e.g. >100 bands) at narrower bandwidths (e.g. 10 nm wide, but can be narrower). This precise information may enable the capturing of more subtle differences in land covers (and, potentially, subtle differences between invasive plant species) than either multispectral or panchromatic imagery.

2.3.2.3 Radiometric resolution

Radiometric resolution refers to the number of digital quantisation levels (expressed in binary digits (bits)) used to store and "communicate" the data collected by the sensor. In general, the greater the number of quantisation levels the greater the detail in the information collected by the sensor. For example, 256 levels of grey is expressed using 8 bits (2^8), whereas 10 bit data can store up to 1024 levels of grey (2^{10}). Theoretically, as the latter has a larger dynamic range of grey levels, it has an enhanced ability for detecting subtle differences in absorption/reflectance of land covers. Table 2.2 details the radiometric resolution of many common sensors.

2.3.2.4 Temporal resolution

Temporal resolution refers to the revisit rate of the sensor (Jensen, 1996). As discussed in Section 2.3.1, mapping invasive plants often relies on acquiring imagery at a specific time of the year when the target species exhibits a unique difference, relative to other species. One disadvantage of some satellite products is that it can sometimes be difficult to acquire the imagery when these unique differences are at

their peak. For example, if the temporal resolution of the satellite is many days apart, a distinct biological trait may be missed. This is further magnified if weather conditions preclude obtaining acceptable quality (e.g. cloud free) images when it revisits. Additionally, satellites that have to be tasked (e.g. QuickBird, IKONOS) may not be available at the most opportune times (Lass et al., 2005). In contrast, airborne imagery can, in theory, be collected at most times as long as there is sufficient light and cloud free conditions at the height of acquisition.

2.3.3 Step 3: Choose a classification method

The following describes many of the classification algorithms used in the literature for mapping invasive plants and follows the categorisation illustrated in Figure 2.2, highlighting advantages and disadvantages of and between methods where applicable. It is provided here for completeness and so that readers not familiar with the concepts have some background understanding when the algorithms are mentioned under the review of the past success for mapping invasive plants (Section 2.3.5). Readers with a sound knowledge of classification algorithms, as applied to different media, may choose to skip to Section 2.3.4.

Figure 2.2 illustrates the different families of classification algorithms used to process remotely sensed imagery into meaningful classes. While it is incorrect to assume that one classification method is, or always will be, superior to other methods, the following aims to give guidelines for choosing between many of them, based on hypothetical examples, the distribution of the remotely sensed data (e.g. parametric versus non-parametric methods) and whether a decision needs to be made between choosing either a soft or a hard classification.

Non-parametric methods are those that do not rely on statistical information from the sample data (e.g. means, variances) but rather are trained on the sample data directly. They make no assumptions concerning the frequency distribution of the data and can thus incorporate non-remotely sensed data such as slope or soil type into the classification. Non-metric methods, such as decision trees, can also incorporate nominal data into the classification. In contrast, parametric methods use parameters derived from the training data, such as the mean and variance/covariance matrices for each of the classes. These methods assume that the frequency distribution of each

class is normally distributed, and hence, if this is not the case there is justification in avoiding them (Mather, 2004).

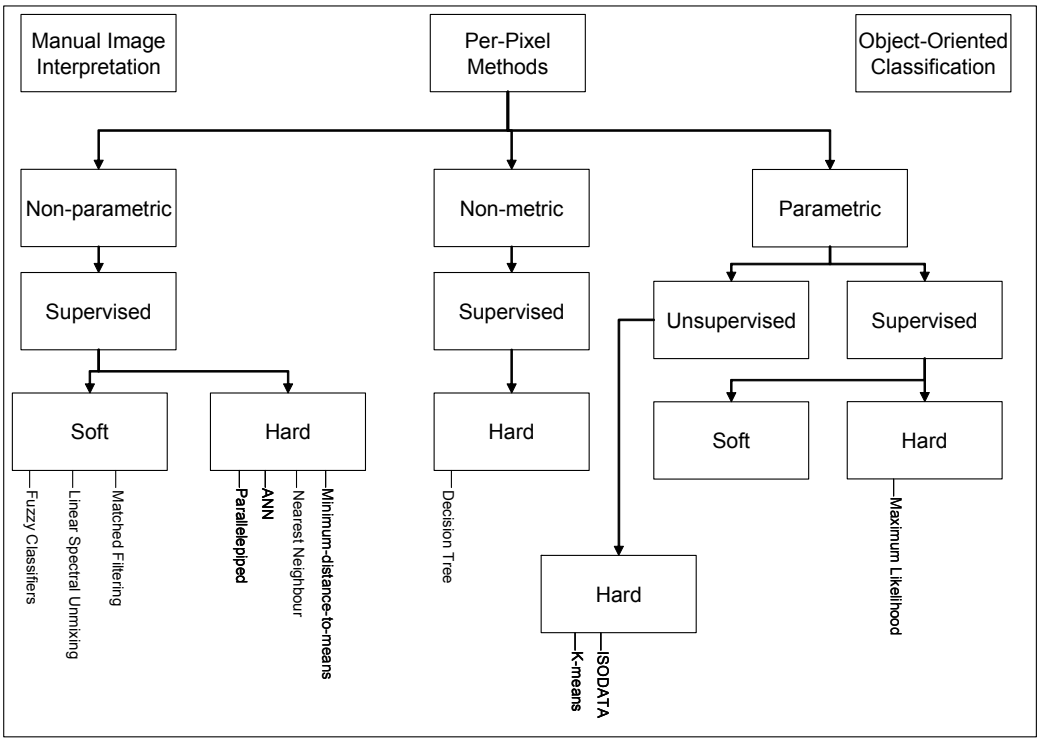

Figure 2.2 Summary of the different kinds of image processing techniques suitable for classifying remotely sensed imagery into meaningful classes.

Unsupervised classification methods can be used without knowledge of the spectral characteristics of the land covers present in the image (i.e., training data). In essence, unsupervised classification routines form clusters by grouping together pixels with similar spectral characteristics (Hunt et al., 2005). In contrast, supervised classification routines require information (i.e., training pixels) on the spectral characteristics of the land covers (e.g. species types) present within the scene in order to group pixels of similar spectral response. Supervised classification algorithms, whether parametric, non-parametric or non-metric can be dichotomised into hard or soft classifiers (see Figure 2.2).

Hard classifiers are so named because they reach a hard decision about the class to which each pixel belongs. For example, if a pixel contains a mix of land covers, the dominant land cover (e.g. the one with the highest percentage of cover in that pixel)

will be assigned (Eastman, 2006). Unlike hard classifiers, soft classifiers defer making a definitive judgement of any pixel in favour of a group of statements about the degree of membership of that pixel in each of the possible classes. The output is not a single classified land cover map, but rather a set of images (one per class) that express, for each pixel, the degree of membership in the class in question.

2.3.3.1 Parametric, hard unsupervised classification: ISODATA

Perhaps the most well known unsupervised classification is ISODATA. This method repeatedly iterates over arbitrary seed values and then reassigns pixel values to particular clusters based on their closeness to these seed values. As the number of iterations increase, the mean class values gravitate towards natural breaks in the distribution of image pixels (Anderson and Cobb, 2004; Mather, 2004). The main benefits of this method are that it is easy to apply and no training data is required. The main disadvantages of this method are that the number of clusters chosen is arbitrary, and often requires a trial and error approach and clusters may not be well separated and therefore mis-classification can be significant. Additionally, class labels need to be assigned by the operator, which involves a degree of subjectivity. Hence, any accuracy statement is assessing a combination of spectral discrimination and the user's assignment to those classers.

2.3.3.2 Parametric, hard supervised classification: maximum likelihood (ML)

The ML algorithm uses the mean and variance/covariance data of the signatures to estimate the posterior probability (from Bayesian probability theory) that a pixel belongs to each class. By incorporating information about the covariance between bands as well as their inherent variance, the ML algorithm produces what can be conceptualised as an elliptical zone of characterisation of the signature (Figure 2.3; Mather, 2004; Eastman, 2006).

An advantage of the ML approach is that prior knowledge can be taken into account. For example, *a priori* knowledge of the proportion of the area to be classified that is covered by each class can be expressed as a vector of prior probabilities. The probabilities are proportional to the area covered by each class, and can be thought of as weights. A high prior probability for class *i* in comparison with class *j* means that any pixel selected at random is more likely to be placed in class *i* than class *j*,

because class *i* is given more weight (Mather, 2004). A second advantage of this method is that, unlike the minimum-distance-to-means (MDM) classifier (see Section 2.3.3.3.2), it can account for spreads of data in particular spectral directions.

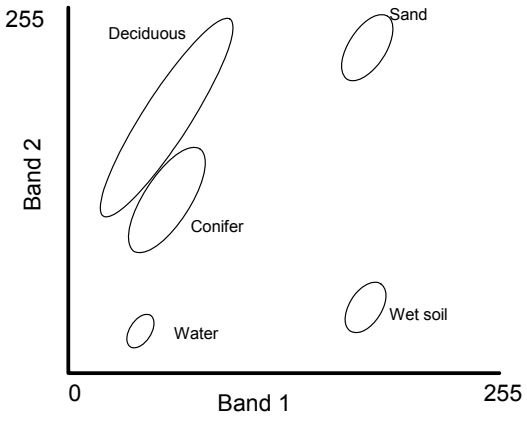

Figure 2.3 Conceptual rendition of the maximum likelihood algorithm (after Eastman, 2006).

A disadvantage of this method is that it requires a relatively large sample size, when compared to many of the non-parametric methods (e.g. artificial neural networks or MDM), for each of the classes in order to compute a robust covariance matrix (Richards and Jia, 1998). In addition, compared to MDM or the parallelepiped method (see Section 2.3.3.3.3) or artificial neural networks (see Section 2.3.3.3.1), the ML method requires considerable computation effort (Jensen, 1996). While this may be considered less of an issue with contemporary computers, the increasing trend towards higher spatial and spectral resolution imagery will require more memory and processing time than for classifying conventional moderate resolution datasets (e.g. Landsat) and, in such cases, may be justification for using a classifier that is more parsimonious in terms of computer resources.

2.3.3.3 Non-parametric, hard supervised classification

As discussed above, non-parametric, hard classifiers are those that do not take into account the distribution of the data and output one class per pixel. These include artificial neural networks (ANNs), the minimum-distance-to-means (MDM) classifier and the parallelepiped method. These methods are discussed hereafter.

2.3.3.3.1 Artificial neural networks (ANNs)

Over the last ten to fifteen years, the ANN has become an increasingly popular tool for the classification of remotely sensed imagery, particularly because (Lee et al., 1990; Benediktsson et al., 1990; Atkinson and Tatnall, 1997; Mather, 2004):

(i) they are free from restrictive assumptions such as requiring multivariate normal distributions;
(ii) are able to generalise;
(iii) are tolerant to noisy training data;
(iv) do not require as extensive training sets as, for example, ML;
(v) have been demonstrated, under some circumstances, to be a more accurate technique than statistical classifiers (e.g. ML);
(vi) are faster at classification when compared to ML; and
(vii) have the ability of simultaneously using data from different sensors or sources.

In simplified terms, an ANN learns how to classify imagery by comparing an input (a pixel) to an expected output (e.g. class of the pixel, known from training data). If there is a difference between the two, a set of weights are adjusted and the process is reiterated. This process continues until the ANN gets the correct answers, in which case it is considered to have learnt all possible patterns. The main disadvantage of ANNs is that they require considerable expertise in setting up the architecture (e.g. the number of hidden layers, the number of nodes) and choosing between some of the important parameters that are associated with their ability to learn (e.g. learning coefficient, momentum parameter, termination time). See Mather (2004) for more details on these parameters.

2.3.3.3.2 Minimum-distance-to-means (MDM)

The MDM classifier characterises each class based on its mean position on each band. To classify an unknown pixel, the distance from that pixel to each class is determined and assigned to that of the nearest class. The main limitation of this method is related to signature variability. If some classes are inherently more variable than others, there can be considerable mis-classification (Eastman, 2006). For example, for a particular species of deciduous shrub there may be a large

variability in the degree of defoliation at any one time throughout the population (e.g. dependent on sun light, canopy position, nutrients and water availability) which would create significant signature variability. On the other hand, the land cover "sand" may be relatively homogenous throughout the image. The variability of the two classes is illustrated by the circles, representing two standard deviations from the mean (Figure 2.4).

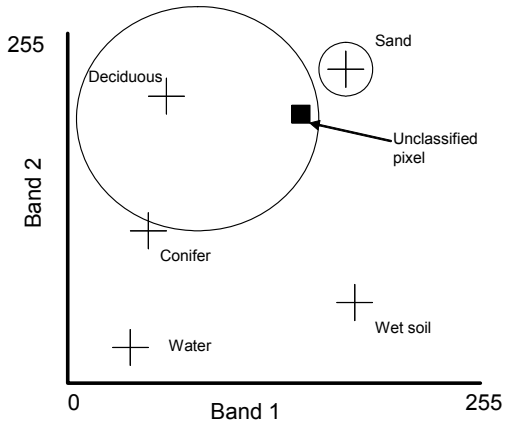

Figure 2.4 Conceptual rendition of the minimum-distance-to-means algorithm assuming 8 bit imagery with only two bands and two classes (after Eastman, 2006). Using this method the unclassified pixel would have been incorrectly classified as "sand" (see text).

From Figure 2.4 it can be seen that the unclassified pixel lies within the variability range of the deciduous class. However, because of this variability, the *mean* reflectance of the unclassified pixel is actually closer to the mean for sand and will therefore be classed as such. The main advantages of this method are that it is fast and requires fewer samples for each class, when compared to ML.

2.3.3.3.3 Parallelepiped

The parallelepiped method characterises each class by the range of expected values on each band. This range is typically an array of standard deviations from the mean (e.g. ± 2 standard deviations from the mean). These ranges form an enclosed box-like polygon, known as the parallelepiped. Unclassified pixels are then given the class of any parallelepiped box they fall into (Figure 2.5). Whilst the parallelepiped is a fast and simple classifier to train and use, it has at least two fundamental drawbacks: (i) if a parallelepiped overlaps, the choice of class is arbitrary, as shown between the conifer and deciduous classes in Figure 2.5 (Mather, 2004; Eastman,

2006); and (ii) if a pixel falls outside the parallelepipeds then it will not be classified (unlike MDM and ML, which classifies all pixels) (Richards and Jia, 1998).

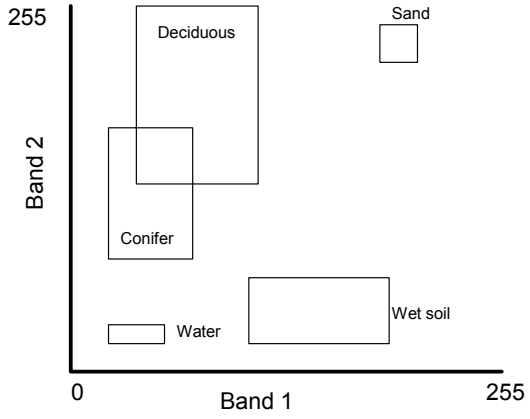

Figure 2.5 Conceptual rendition of the parallelepiped classification method (after Eastman, 2006). The overlapping parallelepipeds for deciduous and coniferous classes cannot be separated and class label will be arbitrary. Pixels falling outside the parallelepipeds will not be classified (see text).

2.3.3.4 Non-parametric, soft supervised classification

Non-parametric, soft classifiers are capable of determining the relative proportion of land covers present within a pixel, and include linear spectral unmixing, matched filtering and an extension of matched filtering known as mixture tuned matched filtering. Spectral angle mapper is considered by some authors to be in this category (e.g. Mather, 2004), however, the output is often 'hardened' to show the dominant landcover of each pixel by methods that are explained below (Section 2.3.3.4.3). All four methods are described in more detail hereafter.

2.3.3.4.1 Linear spectral unmixing (LSU)

LSU assumes that a pixel is a linear combination of all spectral components (land covers) present in the scene. For example, a pixel containing only a single plant should have the same value as reflected in a plant patch with 100% cover. If an invasive plant covers 50% of a pixel and the remainder is made up of bare soil then the pixel value should be the mean of the reflectance values for the invasive plant and bare soil (Figure 2.6).

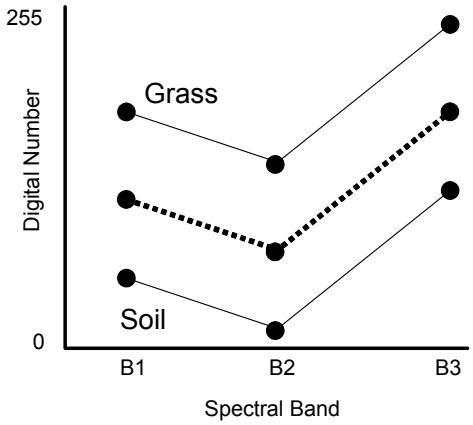

Figure 2.6 Hypothetical illustration of LSU (after Mather, 2004). The unknown pixel is a perfect combination of grass and soil (50/50).

The LSU algorithm is most effective when there are a few distinct cover types as it requires measurements (e.g. training data) for all cover types. Since LSU returns a proportion of a land cover type for each pixel it is viewed as a valuable tool for monitoring changes (e.g. increases/decreases) in established invasive plant populations and for quantifying the success of control activities over time (Lass et al., 2005). One of the benefits of LSU, when using the most common unconstrained approach, is the ability to obtain a residual error, which is essentially derived from the estimated mixture lying outside the range of 0 and 1 (known as undershoots and overshoots, respectively; Mather, 2004). This residual error, calculated for each pixel, can be used as a measure of uncertainty in class estimation, and thus the method can be used in an in-process classification assessment (IPCA) whereby pixels exhibiting unusually high residual errors can be located in the field to identify the cause. For example, there are usually three reasons why a pixel would have an unusually large residual error (Eastman, 2006):

i) the pixel contains a mixture of more basic categories;
ii) the pixel doesn't resemble any of the signatures provided; and
iii) the spectra of the target landcovers are too similar.

If the cause of the large residual error is due to insufficient training data (errors i and ii, above), the training set can be updated and the process re-run to improve results.

The main weakness of LSU is that for it to work properly the spectral reflectance of all existing land covers need to be known (Lass et al., 2005).

2.3.3.4.2 Matched-filtering and Mixture Tuned Matched Filtering

The main attraction of matched-filtering, unlike LSU, is that it does not require the spectral reflectance of all land covers. This is desirable in cases where it is not possible to sample all land covers or simply not desired. Matched Filtering (MF) allows for the relative abundance of a particular class to be determined without knowledge of the other classes found within the same scene (Aspinall et al., 2002; Harsanyi and Chang, 1994). Mixture tuned matched filtering (MTMF) is a related technique that produces an infeasibility image based on a pixels distance from the target species signature allowing pixels unlikely to represent the target species to be identified and masked out. This procedure is reported to be useful in studies aimed at keeping errors of commission low (Boardman, 1998). Both MF and MTMF are typically restricted to the processing of hyperspectral imagery.

2.3.3.4.3 Spectral angle mapper (SAM)

The SAM algorithm is typically used for processing hyperspectral imagery. The SAM algorithm treats each signature as a vector in a space with dimensionality equal to the number of bands. The algorithm then determines the spectral similarity between two spectra by calculating the angle between them and applying the coefficient of proportional similarity: cosine. If the line joining the unknown pixel to the origin was coincident to the "Class 1" signature (Figure 2.7) the angle would be zero. The cosine of zero is one, which indicates complete similarity. The maximum possible angle is 90^{o} ($\cos 90^{o}=0$), which implies complete dissimilarity. If the user chooses only to output the range of similarity [0-1], SAM is taken to be a soft classifier. However, this output is often 'hardened' by assigning an unknown pixel to the class that has the smallest angle between the signature vectors (Kruse et al., 1993; Mather, 2004; Eastman, 2006). For example, the unclassified pixel in Figure 2.7 is assigned to Class 1, since the angle it subtends with the unknown pixel (α) is smaller than with Class 2 (β). Users are generally required to enter the maximum angle that indicates the angle above which a class is likely to be too far from the characteristics of the signature vector to be considered a member of that class. In

general, a narrow angle will produce classified images with the highest likelihood of matching a pure population. As the angle is widened the classification includes deviations from the pure reflectance that contain a mixture of the target and spectral background (e.g. other species, soils, grasses) and can therefore increase errors of commission (see Section 2.3.4).

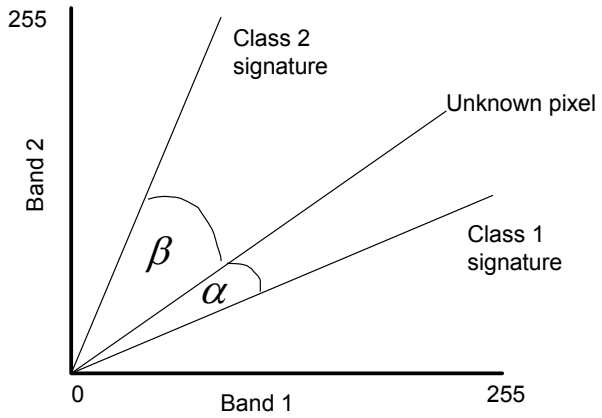

Figure 2.7 Conceptual rendition of the SAM algorithm (after Eastman, 2006). The unknown pixel will be assigned to Class 1, because the angle it subtends is smaller than the angle it subtends for Class 2 (see text).

2.3.3.5 Manual image interpretation

Manual image interpretation, in the context of invasive plant mapping, is the process of manually delineating patches or canopies by eye. The interpreter manually examines such criteria as shape, colour, texture, shadow and context to identify the different species present in the image. This is usually done using panchromatic, colour or colour infrared aerial photography. Interpretation is aided substantially if the imagery has been enhanced (e.g. filtering, histogram stretching) to improve sharpness (Richards and Jia, 1998). While manual image interpretation has some appeal (e.g. expert knowledge of the area over which the scene was acquired, and the ability of the human eye to recognise shapes far easier than traditional image processing routines) it has two major drawbacks (Kadmon and Harari-Kremer, 1999):

(i) interpretation may not be consistent between interpreters; and

(ii) interpretation is very time consuming and is therefore only practical over relatively small areas and/or where plant patch sizes are large.

2.3.3.6 Object-oriented (OO) classification

All of the previous methods introduced process imagery on a pixel-by-pixel basis. Object-oriented classifiers, by contrast, decompose the scene into many relatively homogenous image objects using a multi-resolution image segmentation process. Classification is then performed on those objects rather than single pixels (Rango et al., 2003; Hay et al., 2003; Burnett and Blaschke, 2003; Laliberte et al., 2004).

While OO classification may be considered a supervised classifier (it usually requires training data), by incorporating a range of parameters in its classification method, they represent something of a new paradigm in digital image processing. Other information included in the classification routine can include contextual information, colour, texture, shadow and geometric information such as shape. As such, OO classification can be viewed as an automated method to manual image interpretation (Laliberte et al., 2004; McGlynn and Okin, 2006).

e-Cognition, developed by Definiens Imaging, is one such software produce for performing OO classification. Esch et al. (2003) compare OO classification to the ML method and demonstrate its ability to achieve improved classification accuracy.

2.3.4 Step 4: Assessment of classification accuracy

No classification is complete until its accuracy is assessed (Tso and Mather, 2001). A basic accuracy assessment involves collecting testing data (or splitting the training data into two sets, of which only one is used for training the classifier) and computing a confusion or error matrix. Table 2.3 gives a simple conceptualisation. Most studies use this matrix to compute at least four measures of accuracy (e.g. overall accuracy, producer's accuracy, user's accuracy and overall Kappa). An additional method is also presented for cases where the accuracy of a specific class is desired that accounts for chance agreement (per-class Kappa).

2.3.4.1 Overall accuracy

Overall accuracy is the sum of correct predictions (shaded diagonal squares in Table 2.3) divided by the total number of observations (e.g. 1441). The overall accuracy should be treated with caution when the concern is the accuracy of only one land cover (e.g. the invasive plant). Numerous examples exist in the literature that give an

acceptable overall accuracy, yet map some classes poorly. If these poorly mapped classes happened to be the species of interest then the classification results would be deemed a failure. For example, Haara and Haarala (2002) attained a respectable overall accuracy of 77.5%, but with accuracy of individual species ranging from 59.2% to 85.4% (from a user's perspective, see Section 2.3.4.3). Similarly, Martin et al. (1998) obtained an overall accuracy of 77.5%, but with accuracy of individual species ranging from 16.6% to 100%. Therefore, it is important to describe accuracy for each class. The producer's accuracy, the user's accuracy and per-class Kappa are useful measures to this end, and are described hereafter.

Table 2.3 Illustration of an error matrix and associated statistics used for assessing the accuracy of a classification.

	Reference Data (Test Set)						
Classification	A	B	C	Totals	User's Accuracy (%)	Errors of Comission (%)	Per-class Kappa
A	928	8	38	974	95	5	0.86
B	12	97	13	122	80	20	0.78
C	4	4	337	345	98	2	0.97
Totals	944	109	388	1441			
Producer's Accuracy (%)	98	89	87				
Errors of Omission (%)	2	11	13				
Per-class Kappa	0.95	0.88	0.83				
Overall Accuracy				94.52			
Overall Kappa				0.88			

2.3.4.2 Producer's accuracy and errors of omission

Producer's accuracy is the proportion of the test set that is correctly assigned for each class. Its complement (1- producer's accuracy) is known as the error of omission. Errors of omission correspond to those pixels belonging to the class of interest that the classifier has failed to recognise (Richards and Jia, 1998). For example, a producer's accuracy of 98% equates to an omission error of 2% (see producer's accuracy of Class A in Table 2.3). This means that 2% of pixels were classed as either B or C by the classifier when they should have been assigned to Class A. In the context of invasive plant management, high omission errors can underestimate the extent of invasion and therefore management costs. Furthermore, invasive plants that are omitted from an eradication programme may expedite reinvasion.

2.3.4.3 User's accuracy and errors of commission

The user's accuracy shows the probability that the invasive plant is actually present. Its complement (1- user's accuracy) is known as the error of commission. Errors of commission are those that correspond to pixels from other classes that the classifier has labelled as belonging to the class of interest. For example, for a user's accuracy of 95%, there is a commission error of 5% (see user's accuracy of Class A in Table 2.3). In the context of invasive plant management, this means that 5% of the pixels classified as the invasive plant (assuming that is Class A) should have been classified as some other species (or land cover). High commission errors can be costly for management/control programmes, particularly in difficult to access sites because of the cost and time taken for transport of removal crews and equipment (Lass and Prather, 2004).

2.3.4.4 Overall Kappa

The overall Kappa statistic was developed by Cohen (1960). The basic idea behind the overall Kappa is that some of the apparent classification accuracy given by the three aforementioned measures could be due to chance. This is especially relevant when some classes are more likely to be encountered during field sampling than others. As a simple illustration, consider a map of just two classes where class A is mapped over 90% of the survey area and class B over the other 10%. This suggests that a randomly selected field sampling point would have a 90% chance (*a priori* probability) of being class A. The joint probability is then 0.81 of this point being correctly mapped as class A, strictly by chance. Similarly, for class B, the joint probability would be 0.01, suggesting that the map would be expected to have an overall accuracy of 82% simply by a chance assignment of ground truth points to mapped classes. This makes it hard to distinguish a good map from one that is simply "lucky". Furthermore, unlike the overall Kappa, the three aforementioned statistics are not appropriate for comparing between different classifications (Rossiter, 2004).

The overall Kappa uses all cells in the matrix and not just the diagonal cells (as done for calculating the overall accuracy). It can be calculated using Equation 2.1 (Stehman, 1999):

$$K = \frac{p_{ii} - \sum_{i=1}^{q} p_{i+}\ p_{+i}}{1 - \sum_{i=1}^{q} (p_{i+}\ p_{+i})} \tag{2.1}$$

where q is the number of land-cover categories;

p_{ii} = proportion of mapped data at row i, column i;

p_{i+}= proportion of mapped data in class (row) i;

p_{+i}= proportion of reference data in class (column) i.

Landis and Koch (1977) and have suggested the following ranges of agreement for the Kappa statistic:

(i) poor, K<0.4;
(ii) good, 0.4<K<0.75; and
(iii) excellent, K>0.75.

Monserud and Leemans (1992) later refined these ranges and suggested that Kappa can be interpreted as follows:

(i) no agreement, K<0.05;
(ii) very poor, 0.05<K<0.20;
(iii) poor, 0.20<K<0.40;
(iv) fair, 0.40<K<0.55;
(v) good, 0.55<K<0.70;
(vi) very good, 0.70<K<0.85;
(vii) excellent, 0.85<K<0.99; and
(viii) perfect, 0.99<K<1.

Negative values indicate extremely poor agreement. The overall kappa of 0.88 for the sample error matrix given in Table 2.3 suggests an excellent overall classification.

One of the drawbacks of overall Kappa is that, similar to the overall accuracy, if there are more than two classes being predicted, it gives no information on the

accuracy of one specific class of interest, and therefore may be of limited use when the aim is to optimise or report on the accuracy of one specific species. In such cases, the per-class Kappa can be used.

2.3.4.5 Per-class Kappa

As mentioned above, overall accuracy and overall kappa do not take into account the accuracy of a specific class and the producer's and user's accuracy measures cannot be used in map to map comparisons and are not adjusted to account for chance agreement (see Section 2.3.4.4). If such measures are desired, as they are in this research, per-class kappa (or conditional kappa) can be evaluated for each class from both the perspective of omission and commission errors. This allows the determination of which classes within the matrix are well mapped. Each entry in the error matrix is first divided by the number of pixels in the test set (e.g. 1441 in Table 2.3) to derive a proportion. The calculation then follows a similar logic to the overall Kappa, but is restricted to one row (Equation 2.2) or one column (Equation 2.3) of the error matrix at a time. These are known as per-class Kappa from a user's perspective and per-class Kappa from a producer's perspective, respectively (Rossiter, 2004):

$$\hat{\kappa}_{i+} = (p_{ii} - (p_{i+} \times p_{+i})) / (p_{i+} - (p_{i+} \times p_{+i}) \quad (2.2)$$

$$\hat{\kappa}_{+j} = (p_{jj} - (p_{+j} \times p_{j+})) / (p_{+j} - (p_{+j} \times p_{j+})) \quad (2.3)$$

where p_{ii} = proportion of mapped data at row i, column i;
p_{jj} = proportion of mapped data at row j, column j;
p_{i+} = proportion of mapped data in class (row) i;
p_{+i} = proportion of reference data in class (column) i;
p_{+j} = proportion of reference data in class (column) j; and
p_{j+} = proportion of mapped data in class (row) j.

The per-class Kappa values can be interpreted identically to overall Kappa, except they are relevant to only one class. Table 2.3 shows that Class C has the highest per-class Kappa from the user's perspective (0.97), but the poorest from the producer's perspective (0.83). As such, it is important that both measures be reported.

The variance of per-class Kappa for user's class i is calculated as (Congalton and Green, 1999):

$$s^2 = \frac{1}{n}\left\{\frac{p_{i+} - p_{ii}}{p_{i+}^3\ (1-p_{+i})^3}[([p_{i+} - p_{ii})((p_{i+})(p_{+i})\ (p_{ii})) + p_{ii}((1-(p_{i+})-(p_{+i})\ +(p_{ii}))]\right\} \qquad (2.4)$$

where n is the number of elements in the confusion matrix. All other parameters as described for Equations 2.2 and 2.3. For producer's class i, Equation 2.4 is permuted by interchanging the row (p_{i+}) and column (p_{+i}) summaries.

2.3.5 Review of the past success for mapping invasive plants

The following section summarises the success (e.g. accuracy achieved) of previous studies aimed at mapping invasive plants based on image type and classification method.

2.3.5.1 Panchromatic aerial photography

Panchromatic aerial photographs provide one of the longest records of remotely sensed imagery and are typically captured with high spatial resolution. However, invasive plants rarely have spectral characteristics that enable their discrimination from coexisting species using automated classification routines. At best, these methods have only been able to discriminate between trees and shrubs by, for example, introducing a size threshold post-classification (e.g. Kadmon and Harari-Kremer, 1999; Lahav-Ginot et al., 2001). This limitation has often led to researchers examining only small areas (typically less than 80 ha) where the plant has formed a monoculture (e.g. Goslee et al., 2003) or, where vegetation composition has been heterogeneous, discrimination has been achieved using manual photo interpretation (e.g. Fensham et al., 2002). However, the time consuming nature of interpreting and manually delineating the canopies of shrubs has limited analyses to only a small area, to sparsely vegetated areas or to the interpretation of relatively coarse vegetation units (Kadmon and Harari-Kremer, 1999).

2.3.5.2 Colour and colour-infrared aerial photography

Literature surveyed suggests that unsupervised classification routines (e.g. ISODATA) have been very popular techniques for mapping invasive species from colour or colour infrared (CIR) aerial photography (see Table 2.4). This is somewhat

surprising given its relative lack of sophistication compared to more complex supervised methods. Nonetheless, the majority of these studies emphasise the importance of mapping using knowledge of the invasive plants biological characteristics during the year (e.g. showy flowers). The accuracy of mapping different kinds of invasive plants with this imagery and different classification types can be seen in Table 2.4.

While unsupervised classification has been used with success, one problem with their use for species level mapping remains – it is not optimised to the specific requirements of the user (Lark, 1995). The underlying aim of most unsupervised methods (and indeed most supervised classification methods) is to optimise overall accuracy. However, in the case of mapping individual species the map user is really only interested in the accuracy of that particular species (e.g. high per class kappa from both perspectives as discussed in Section 2.3.4.5) and is not necessarily overly concerned with the accuracy of a different cover class or indeed the overall accuracy. For example, a map user interested in the precise location and distribution of mesquite may not be concerned if water, soil or other shrub species are correctly classified as long as the mesquite category is accurately classified.

Foody et al. (2005) uses a multi-stage classification approach to optimise the likelihood of correctly distinguishing sycamore (*Acer pseudoplatanus*) from coexisting species using 0.2 m resolution colour aerial photographs. They first extract the maximum and 80th percentile values from all shrub/tree crowns (patches) and then select the best variables (e.g. maximum, 80th percentile) using discriminant analysis in a pairwise fashion (e.g. sycamore v ash (*F. excelsior*), sycamore v lime (*Tilia cordata*), sycamore v oak (*Qercus robur* and *Q. petraea*) and sycamore v Douglas fir (*Pseudotsuga menziesii*)). Classification is performed using artificial neural networks (ANNs). A simple rule-based approach is then used to determine if a pixel is a member of the sycamore class or not (e.g. if fir or lime then non-sycamore and (if oak and ash then non-sycamore), else sycamore). An accuracy of 93.3% (number of sycamore shrubs correctly classified/number of sycamore shrubs known) was achieved using this method for the sycamore class. In comparison, using a standard approach, which seeks only to optimise overall accuracy (i.e., one

that does not utilise pairwise selection to identify the best separating variables), sycamore was classified with only 75% accuracy.

Table 2.4 Examples of the accuracy achieved in previous studies using various classification methods and either colour/colour infrared (CIR) aerial photography, airborne multispectral or satellite multispectral imagery.

Imagery Used	Invasive Plant Mapped	Classification Method(s)	Accuracy	Author
Colour aerial photographs	Sycamore (*Acer pseudoplatanus*)	ANN	Omission=17% Commission=7%	Foody et al. (2005)
	Various spp.	ANN	97% overall accuracy	Burks et al. (2005)
CIR aerial photographs	Chinese tallow (*Sapium sebiferum*)	Unsupervised	95% (number detected/number known)	Ramsey et al. (2002)
	Waterlettuce (*Pistia stratiotes*)	Unsupervised	Omission=20% Commission=14%	Everitt et al. (2003)
	Giant salvinia (*Salvinia molesta*)	Unsupervised	Omission=11% Commission=11%	Everitt et al. (2002)
	Redberry juniper (*Juniperus pinchottii*)	Unsupervised	Omission=0% Commission=6%	Everitt et al. (2001)
Airborne Multispectral	Yellow hawkweed (*Hieracuim pratense*)	Unsupervised	Kappa=0.76	Carson et al. (1995)
		ML	Kappa=0.8	
	Yellow starthistle (*Centaurea solstitialis*) and St. Johnswort (*Hypericum perforatum*)	Unsupervised	Down to 30% cover.	Lass et al. (1996)
	Balsim fir (*Abies balsamea)*	Linear Regression	51% to 91% (depending on the number of defoliated classes used	Leckie et al. (1992)
	Sicklepod (*Senna obtusifolia*) and horsenettle (*Solanum carolinense*)	Discriminant analysis	>75% accuracy	Medlin et al. (2000)
	Blackberry (*Rubus fruticosis*)	Various image enhancements/ transformations	Concluded omission confined to patches <5m^2	Ullah et al. (1989)
Satellite Multispectral	False Broomweed (*Encameria austrotexana*)	ML	Kappa=0.41	Anderson et al. (1993)
		MDM	Kappa=0.61	
	Various species	ML	Overall =86%	Carleer and Wolf (2004)

2.3.5.3 Airborne multispectral imagery

Various airborne acquisition systems have been used to capture imagery capable of successfully differentiating between species. One of the earliest uses of this kind of imagery was conducted by Ullah et al. (1989) who used the airborne thematic

mapper (ATM) for mapping blackberry invasions (*Rubus fruticosus*) (Ullah et al., 1989).

An airborne acquisition and registration system (ADAR) has been used for mapping yellow hawkweed (*Hieracieum pratense*) (Carson et al., 1995), St. Johns Wort (*Hypericum perforatum*) and yellow starthistle (*Centaurea solstitialis*) (Lass et al., 1996). Medlin et al. (2000) used a 4-band charged coupled device to discriminate the invasive plants sicklepod (*Senna obtusifolia*) and horsenettle (*Solanum carolinense*) from soybean (*Glycine Max*) crops (Medlin et al., 2000). The Multispectral Electro-optical Imaging Scanner (MEIS) has been used for mapping defoliated Balsim fir (*Abies balsamea)* populations (Leckie et al., 1992). See Table 2.4 for more details.

2.3.5.4 Satellite multispectral imagery

Wang et al. (2004) compared IKONOS-2 and QuickBird imagery to map mangrove forests using the maximum likelihood method. They concluded that the IKONOS-2 imagery provided the best spectral discrimination. This is somewhat surprising given that both satellites have very similar spectral resolutions and both have 11 bit quantisation. However, the authors suggest that even though IKONOS-2 has poorer spatial resolution (compared to QuickBird), it appeared to capture a richer, more detailed spectral reflectance for the same ground targets. They suggest that this finding can be related to a visual effect, that IKONOS-2 utilises more enriched colour and looks more vivid than the QuickBird image. Carleer and Wolff (2004) have also successfully discriminated various tree species using IKONOS-2 imagery and the maximum likelihood classification, reporting an overall accuracy of 86%.

Using a hand-held radiometer, set to approximate the wavelengths of Landsat, at a height of 2 m, Taylor (1990) demonstrated that this spectral resolution was sufficient to map bracken fern (*Pteridium aquilinum*). However, the relatively coarse spatial resolution of Landsat imagery has generally been considered inappropriate for species level mapping (Carson et al., 1995; Hunt et al., 2003), particularly where vegetation types within an area of interest exhibit small-scale heterogeneity. Plausibly, the main utility of Landsat (and “Landsat-like”) imagery for invasive plant management has been to identify the spatial distribution of the most rapid change in

woody vegetation as a whole (e.g. Gardiner et al. 1998). If differentiation between species is not required (e.g. *Acacia nilotica* has invaded previously treeless grasslands throughout the Mitchell grass plains in Queensland) then classifying woody vegetation in Landsat imagery equates to mapping the species under interest (Lawes and Wallace, 2006). However, such scenarios are rare in practice.

In an interesting study by Dewey et al. (1991), known locations of dyers woad (*Isatis tinctoria*) are overlayed on land types classified from Landsat imagery. This enabled quantification of the land types most strongly associated with dyers woad and suggested management should target the same highly suited areas that have not yet been invaded.

Anderson et al., (1993) present one of the few relatively successful studies that have used multispectral imagery with a spatial resolution of 20 m (SPOT-4) for invasive plant species differentiation (false broomweed (*Ericameria austrotexana*)) in a heterogenous environment. However, they were only able to map relatively large stands (e.g. >0.5 ha) and state that commission errors were high when false broomweed was mixed with dense brush or high amounts of herbaceous biomass. In addition, discrimination was only possible when grass cover was minimal. For example, at one particular time of the year, the confusion between grasses and false broomweed resulted in 1/3rd of the study area being classed as false broomweed, where there was no presence.

2.3.5.5 Hyperspectral imagery

While aerial photography and airborne multispectral imagery has typically been the main data source for providing timely information on the spatial location of invasive plant populations in the past, this kind of imagery, in general, has relatively poor spectral resolution and therefore its ability to successfully discriminate between individual species present within the same image relies heavily on the target species exhibiting obvious and unique phenological or structural characteristics at some opportune time of the year. However, this is not always the case and any spectral differences (e.g. key absorption features) between coexisting species may be masked by the broad spectral bands characteristic of these image acquisition systems. Hyperspectral imagery, with its large number of contiguous, narrow wavebands (e.g.

10 nm) over a wider spectral region (e.g. 400 to 2500 nm) may offer an enhanced potential for separating the subtle spectral differences between the target species and the coexisting species present within the same scene (Schmidt and Skidmore, 2003). Recently, the use of hyperspectral imagery to map various invasive plants has become more commonplace. The results of these studies are summarised in Table 2.5 and described in more detail below.

Table 2.5 Examples of the accuracy achieved in previous studies using various classification methods and hyperspectral imagery. Table is in ascending order of spatial resolution.

Imagery Used	Invasive plant Mapped	Classification Method(s)	Accuracy	Author
0.5 m resolution 120 band from Surface Optics Scanner	Tamarisk (*Tamarix* spp.)	Parallelepiped MTMF	Parallelepiped produced higher % agreement for all size classes tested	Hamada et al. (2007)
1 m resolution, 36 band from CASI-2	Yellow starthistle (*Centaurea solstitialis*)	LSU	Max. standard deviation=11%	Miao et al. (2006)
1.3 m resolution, 15 channel CASI-2	Several spp.	ANN VCNNC	Kappa=0.75 Kappa=0.87	Wang et al. (2007)
2 m resolution, 48 band – from CCD sensor	Spotted knapweed (*Centaurea maculosa*)	SAM	Omission=43.7% Commission=8.1%	Lass et al. (2005)
	Babysbreath (*Gypsophila paniculata*)	SAM	Omission=3.3% Commission=39%	
3 m resolution Hymap (126 bands)	Hoary cress (*Cardaria draba*)	MTMF	Omission=18% Commission=21%	Mundt et al. (2005)
3.5 m resolution Hymap (126 bands)	Blackberry (*Rubus fruticosis*)	SAM	Omission=29% Commission=42%	Dehaan et al. (2007)
		MF	Omission=39% Commission=47%	
		MTMF	Omission=19% Commission=9%	
3.5 m resolution Hymap (126 bands)	Leafy spurge (*Euphorbia esula*)	MTMF	Omission=30% Commission=32%	Glenn et al. (2005)
5 m resolution, 128 band - from Probe 1	Spotted knapweed (*Centaurea maculosa*)	SAM	Omission=3% Commission=3%	Lass et al. (2002)
5 m resolution, 128 band - from Probe 1	Brazilian Pepper (*Schinus terebinthifolius*)	SAM	Omission=10% Commission=12%	Lass and Prather (2004)
20 m resolution, 224 band AVIRIS	Leafy spurge (*Euphorbia esula*)	MTMF	R^2=0.69 R^2=0.79 (in prairie) R^2=0.57 in heterogenous cover	Parker-Williams and Hunt (2002)

2.3.5.5.1 Studies using SAM

Lass et al. (2002) collected hyperspectral imagery using the Probe 1 sensor, which records 128 spectral bands in 12 to 16 nm intervals ranging from 440 to 2,543 nm and, in their case, at a spatial resolution of 5 m. SAM was used to classify the imagery to detect infestations of spotted knapweed (*Centurea maculosa*). They found that large infestations could be detected regardless of the angle used in the SAM algorithm, but lowest overall errors were found when the angles ranged from 10^o to 11^o. Specific errors for the spotted knapweed class for the 10^o to 11^o angles showed that omission and commission errors were less than 3%, with areas with as little as 1 to 40% cover detected with an omission error of 1% and a commission error of 6%.

Lass and Prather (2004) used similar imagery from the Probe 1 sensor to detect Brazilian pepper (*Schinus terebinthifolius*) using the spectral angle mapper (SAM) algorithm with angles of 1^o to 5^o and 10^o. They concluded that pure Brazilian pepper pixels were accurately classified but mixed Brazilian pepper pixels and sparse populations were poorly classified. Poor access throughout their study site limited their tolerance for errors of commission (e.g. because of the cost and time for transport of removal crews and equipment). Therefore, the authors suggest using a low spectral angle to match a pure population and then applying buffering, which is hypothesised to improve the probability of finding another plant nearby, on the basis of seed morphology and dispersal mechanisms.

Lass et al. (2005) used a CCD to collect imagery in 48 bands between 415 and 953 nm with 12 nm increments and a spatial resolution of 2 m to map spotted knapweed (*Centaurea maculosa*) and babysbreath (*Gypsophila paniculata*). The SAM algorithm was utilised with angles of 1^o to 5^o and 10^o. They found that the most appropriate angle for spotted knapweed was 5^o, and for babysbreath an angle of 4^o gave the best accuracy.

2.3.5.5.2 Studies using LSU

Miao et al. (2006) implement LSU for mapping yellow starthistle (*Centaurea solstitialis*) using 36 band, 1 m resolution, CASI-2 imagery. Uncertainty is estimated through monte carlo simulation. The maximum standard deviation was

approximately 11%. The authors conclude that LSU could be used for mapping yellow starthistle for larger regional areas (Table 2.5).

2.3.5.5.3 Studies using MF or MTMF

Parker-Williams and Hunt (2002) used 20 m resolution, 224 band AVIRIS imagery to map leafy spurge (*Euphorbia esula*) using the MTMF algorithm. They found that overall performance for estimating percent cover of leafy spurge for all sites was adequate (R^2=0.69) with better performance in prairie areas (R^2=0.79) relative to sites of heterogeneous cover (R^2=0.57).

Glenn et al. (2005) obtained hyperspectral imagery from the HyMap sensor (126 bands) with a spatial resolution of 3.5 m. This sensor typically acquires imagery in 15 nm bandwidths across the electromagnetic spectrum from 450 to 2500 nm (visible to short wave infrared portions of the spectrum). They found that leafy spurge could be discriminated from coexisting species for patches around 5 m^2 (40% cover per pixel) when using the MTMF algorithm.

Similarly, Mundt et al. (2005) also obtained imagery from the HyMap sensor to map hoary cress (*Cardaria draba*) and obtained a producer's accuracy of 82% for hoary cress infestations with greater than 30% cover (patches greater than 2.7 m^2) when using either MTMF or SAM. Comparisons between SAM and MTMF by Deehan et al. (2007) suggested that the MTMF produced the highest agreement between known blackberry (*Rubus fruticosus* sp. agg) distributions, using 3.5 m spatial resolution hyperspectral imagery obtained from the HyMap sensor.

2.3.5.5.4 Studies using ANNs

Wang et al. (2007) implement ANNs for mapping mixed vegetation communities found in salt marshes using CASI imagery (15 channels) with a spatial resolution of 1.3 m. This study compares a traditional ANN with what they call a vegetation community based neural network classification (VCNNC). The main difference is that the VCNNC incorporates information of the relative abundance of vegetation types at the sub-pixel scale. The authors report a Kappa value of 0.75 for the traditional ANN and 0.87 for the VCNNC (Table 2.5).

2.3.5.5.5 Dealing with spectral redundancy

Because hyperspectral imagery is collected in many narrow contiguous bands there is significant spectral redundancy. Most studies using hyperspectral imagery attempt to reduce this redundancy in some way. Transformations exist to decorrelate and compact spectral information into fewer bands with decreasing data coherence (Lillesand and Kiefer, 2000). Principal components analysis (PCA) is perhaps the best known transformation method, which is a linear solution of the reflectance data projected on rotated orthogonal axes in n-dimensional space (Lillesand and Kiefer, 2000). Green et al. (1988) present the maximum noise fraction (MNF) transformation, which is effectively a two phase PCA. The first phase projects the mean correlated noise whitened data into its respective eigenvector space, and the second phase performs standard PCA on the resulting decorrelated matrix. MNF transforms have been documented to be more consistent in the arrangement of data by band coherence than PCA (Green et al., 1988). However, both methods have worked effectively in species discrimination studies (e.g. Mundt et al., 2005; Underwood et al., 2003).

Rather than using transformed results, bands may be selected by determining the distance between vegetation types in hyperspectral space. Such measures include the Bhattacharyya (BH) and transformed divergence (TD) distance measures (Schmidt and Skidmore, 2003; Martin et al., 1998). The best combination of bands from the original dataset using BH is found where its sum is the highest, whilst a TD value of 2000 suggests excellent between-class separation. Above 1900 provides good separation, while below 1700 is poor (Jensen, 1996). Formulae for these measures can also be found in Jensen (1996).

Discriminant analysis can also be used to select the discriminatory variables (bands) that best separate the groups of interest (e.g. shrub/tree or grass species). Bands which are not very different to the group means for the species of interest can be eliminated from the classification analysis. Additionally, bands that may be individually good discriminators may share the same discriminating information and can also be eliminated on the basis that they will likely weaken the classification (e.g. band redundancy). One way to eliminate redundant and other unnecessary

bands is by using a backward stepwise procedure. For example, all bands could be initially considered to be "in" and the worst one is cast out at each step. A useful measure at each step is the F-to-remove statistic, which tests for the significance of the decrease in discrimination should that band be removed from consideration. The band with the largest F-to-remove makes the greatest contribution to overall discrimination, the band with the second largest F-to-remove is the second most important and so forth (Klecka, 1980). Gong et al. (1997) and Foody et al. (2005) both use discriminant analysis to chose optimum bands and ancillary information when using hyperspectral or a combination of hyperspectral and multispectral imagery.

2. 4 Spatial and Temporal Assessment of Invasion

Assessments over time and space are essential in the study of plant invasions (Mack et al., 2000) and can have wide application. For example, previous researchers have examined rates of population increase over different land types to predict future patterns, determine the proximate causes of invasion and quantify the success of different control strategies (e.g. Scanlan and Archer, 1991; Brown and Carter, 1998; Goslee et al., 2003; Sharp and Bowman, 2004a,b). Since invasion of woody shrubs occurs over decades such studies have often utilised temporal sequences of historical aerial photography.

Knowledge of the rate of spread, proximate causes and habitat vulnerability facilitates the identification of areas at highest risk of invasion (Mullerova et al., 2005). For example, Brown and Carter (1998) have observed that the rate of *A. nilotica* invasion in the Mitchell grasslands of Queensland is far greater over riparian areas than upland areas. Sharp and Bowman (2004b) have demonstrated that proliferation of *Melaleuca minutifolia* in the Victoria River District (VRD) is primarily regulated by water drainage and secondarily, by soil characteristics, leading them to suggest that favourable climatic conditions in years with an extended wet season were most likely cause of recruitment. Similarly, Fensham and Fairfax (2003) report that substantial changes in canopy cover of various woody vegetation in the VRD is associated with soil type/geology and correlate vegetation thickening to increased precipitation since the 1970s. Eckhardt et al. (2000) observed woody cover increasing by 12% over granite substrates and decreasing by 64% over basalt

substrates, over 58 years in Kruger National Park, South Africa. They suggest that the proximate causes for the increase over granite areas were the result of decreased competition from grasses caused by overgrazing. Decreases over the basalt areas were attributed to short-interval, prescribed burning and higher levels of nutrients upon which grasses can rapidly recover after heavy grazing.

In southern Texas, Archer et al. (1988) and Archer (1989, 1995) concluded that mesquite invasion:

(i) has occurred relatively recently (50 to 100 years);
(ii) follows a process of high patch initiation followed by coalescence;
(iii) livestock, particularly cattle, have been the dominant source of spread;
(iv) has been regulated by different land types, with the highest rates of recruitment and coalescence occurring in the most mesic parts of the landscape; and
(v) facilitated the ingress and establishment of subordinate woody species from other habitats.

Laliberte et al. (2004) observed an increase in mesquite cover from 0.9% in 1937 to 13.1% in 2003 (0.2% per year) in southern New Mexico. Goslee et al (2003) also observed a net 0.2% increase in mesquite cover over 60 years (1936 to 1996) in this area. Laliberte et al. (2004) attributed the increases to more prolific grazing by cattle and subsequent dispersion of mesquite seeds and the ability of mesquite to out-compete grasses in periods of drought. By tracking individual mesquite patches on aerial photographs Goslee et al. (2003) were able to conclude that mesquite cover stabilised at 43% cover and 83 patches ha^{-1} and that individual patches were highly persistent (95% of the area occupied by patches in 1936 were still occupied in 1996). This high persistence suggests that drought has little effect on already established individuals. Patch shape complexity increased as adjacent shrubs merged, and then declined as those clusters filled in and became rounder. Spatial pattern was quantified using Ripley's K statistic and showed a distinct trend over time: strongly clustered in 1936 around dispersal foci, then random at all scales and by 1983 the pattern was regular at lag distances greater than 100 m, which may be related to increasing competition as shrubs mature.

Asner et al (2003) used a combination of aerial photographs and Landsat 7 (ETM+) imagery to study temporal mesquite invasion in northern Texas from 1937 to 1999 over a 400 km^2 region. As mesquite was the only species at the site, linear spectral unmixing was capable of extracting a percentage of mesquite cover from the Landsat imagery. That is, there was no possible confusion between other woody species and so LSU was able to discriminate between one woody species, bare soil and dry grass. Mesquite was extracted from the aerial photographs using a supervised classifier and then convolved to 30 x 30 m^2 cells to coincide with the spatial resolution of Landsat. They concluded that rangelands not targeted for brush management experienced cover increases of up to 500% in 63 years. Areas managed with herbicides, mechanical treatments or fire exhibited a wide range of woody cover changes relative to 1937 (-75% to +280%), depending on soil type and time since last management action. At the integrated regional scale, there was a 30% increase in woody plant cover over the 63 year period (average rate of 0.5%). Regional increases were greatest in riparian corridors (33%) and shallow clay uplands (26%) and least on upland clay loams (15%).

Also in northern Texas, Ansley et al. (2001) was able to study the effects of control programs by comparing the rate of mesquite encroachment over two areas: an uncontrolled area and one controlled 20 years prior with root-ploughing. They concluded that rates of increase were approximately twice as rapid on the uncontrolled area, and also suggest that net rates for their study area were higher than those attained in most studies due to higher than normal precipitation and more productive soils.

2. 5 Predicting the Suitability of a Region to Plant Invasion

Because of the impacts of plant invasions, the difficulty of eradicating an invasive plant once it has established, and the scarce resources available for controlling invasive populations, models have often been implemented to predict the suitability of regional areas to future invasion in an effort to prioritise management activities (e.g. where to survey, where to control). The underlying principle of these models is that there are areas within a landscape that are more prone to colonisation than others

and, theoretically, by integrating variables that have a cause and effect relationship with the invasive traits of the species under study these areas can be identified.

Models used to highlight the likelihood of a specific habitat meeting the requirements for invasion of a particular species can be broadly dichotomised into data-driven models and knowledge-driven models.

2.5.1 Data-driven models

Under a data-driven model, operations such as standardisation and, in some cases, variable importance (e.g. weight assignment) are achieved by examination of statistical relationships between data of evidence (e.g. where the species is present) and the evidential data layers (herein referred to as layers for brevity) (Bonham-Carter, 1994). The data-driven models used in ecological modelling can be further dichotomised into profile techniques and group discrimination techniques.

2.5.1.1 Profile techniques

Profile techniques use data on the presence of an invasive species to make predictions, effectively ignoring data on the absence of the species. A well known profile technique is the envelope model known as BIOCLIM (Busby, 1991). In their most basic form, envelope models standardise a range of climatic factors (e.g. frost duration, mean temperature of hottest and coldest month, mean annual precipitation, evaporation rates and altitude (Rouget et al., 2004; Robertson et al., 2004) to '1' where the species is known to survive and '0' for values outside this range (Boolean standardisation). For example, mean temperature will be coded with the value of '1' for all temperatures that can be tolerated by that species and 0 elsewhere. All layers are combined using a Boolean AND operation (multiplication of layers), thereby identifying the potential range as the intersection between all grid cells assigned '1'. While envelope models have been popular tools for species distribution modelling (Guisan and Zimmermann, 2000), several studies have identified that (Rouget et al., 2004; Roberston et al., 2004):

(i) while they may work adequately for some species, they perform poorly for others; and
(ii) they have several inherent weaknesses, including:

a. Boolean standardisation does not account for the fact that within the range of values assigned to '1' there will be areas more favourable than others;
b. layers that have a greater bearing on the distribution of a particular species are not attributed more weight in the final outcome; and
c. the use of a conservative operator (Boolean AND) to integrate the datasets does not allow layers to trade-off (e.g. only one layer need be '0' for the solution to be false, yet all other 'conditions' may be ideal).

2.5.1.2 Group discrimination techniques

Group discrimination techniques require both presence data and absence data. Arguably the most common type of group discrimination technique used in ecology/distribution modelling is logistic regression (e.g. Higgins et al., 1999; Collingham et al., 2000; Morisette et al., 2006; Stephenson et al., 2006). Logistic regression improves upon the basic envelope model by assigning a weight (coefficient) to each evidential layer according to their importance, and those that do not contribute significantly are simply removed from the model (Robertson et al., 2004). The ability of logistic regression to work with both continuous and categorical data makes it more flexible than many other data-driven models.

Logistic regression has been applied to model the potential distribution of a range of invasive plants including: Rhododendron (*R. ponticum*) (Stephenson et al., 2006), salt ceder (*Tamarix* spp.) (Morisette et al., 2006) and various species of Acacia (Higgins et al., 1999). Typical datasets used in these studies are flammability, soil moisture, soil nutrients, and land type.

2.5.2 Knowledge-driven models

Under knowledge-driven models, parameters such as weights, standardisation of layers and the appropriate layers to incorporate into the model are chosen on the basis of experts' opinions (Bonham-Carter, 1994), although standardisation may be partially assisted using data of evidence (e.g. Robertson et al., 2004). Knowledge-driven models have been used far less frequently than data-driven models in ecological applications, yet the potential to exploit their capabilities have been well established in many other fields. One exponent of a knowledge-driven model,

presented by Gillham et al. (2004), is the Weed Invasion Susceptibility Prediction (WISP) model.

2.5.2.1 The weed invasion susceptibility prediction (WISP) model

The WISP model uses a database to store nine parameters thought to assist in the successful invasion of several invasive plant species (e.g. black henbane (*Hyoscyamus niger*), perennial pepperweed (*Lepidium latifolium*), hoary cress (*Cardaria glabra*), spotted knapweed (*Centaurea maculosa*) and leafy spurge (*Euphoriba esula*)). These parameters were developed based on expert opinion or literature surveys and include preferences to soil texture, soil pH, distance from water sources, distance from disturbances, annual precipitation, associated land cover, elevation, slope and aspect. Similar to basic envelope models, the WISP model assigns a Boolean value of '1' if a raster grid cell represents a favourable area for invasion and a '0' elsewhere, and thus suffers from the disadvantage of not being able to assign degrees of favourability for each layer. Similarly, no consideration is given to weight layers relative to their importance in determining a species potential range. Instead, a subsequent and final step is used to tally all nine layers together. Grid cells receiving a value of '9' (all layers suggest favourability) are seen as the areas most prone to that particular species, and susceptibility predictions continue to decline down this 9-point scale.

2.5.2.2 Models incorporating fuzzy standardisation

The concept of fuzzy sets was first developed by Zadeh (1965). Unlike the crisp sets used in Boolean logic (e.g. envelope models), where a value can only be '0' or '1', fuzzy sets allow the transition between non-membership (0) and membership (1) to be gradual (Zadeh, 1965). This transition is governed by the use of fuzzy membership functions, which assign a possibility value between '0' and '1', to each cell in a layer.

A number of forms of membership can be used, such as sigmoidal (s-shaped) (Figure 2.8a), j-shaped (Figure 2.8b), linear (Figure 2.8c) or user defined (Figure 2.8d) (Eastman, 2006). Except for the user defined function which may have any number of control points, the shape of the membership function for the sigmoidal, j-shaped and linear functions is governed by four control points (Figure 2.8). For example, for

the monotonically increasing sigmoidal function (Figure 2.8a) point ‘a’ marks the location where the membership function begins to rise above zero and point ‘b’, ‘c’ and ‘d’ mark the point where values beyond this range are all equally likely to be favourable (Robertson et al., 2004; Eastman, 2006). It should be noted that the j-shaped function approaches ‘0’ but only reaches it at infinity. Thus the inflection point ‘d’ in Figure 2.8b indicates the point at which the function has a grade of membership of 0.5, rather than ‘0’ (Eastman, 2006). Although fuzzy membership functions appear to be similar to probability functions, these two concepts are quite different (Zadeh, 1965): fuzzy membership functions define possibility rather than probability (Zadeh, 1987).

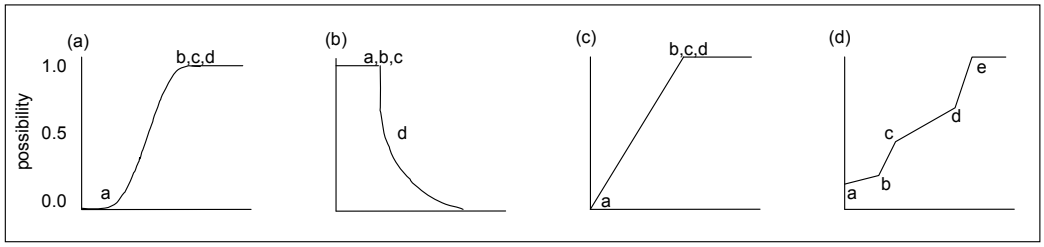

Figure 2.8 Examples of fuzzy membership functions (FMFs): (a) monotonically increasing sigmoidal (s-shaped) FMF; (b) monotonically decreasing j-shaped FMF; (c) user defined FMF; linear FMF. Control points are indicated by the letters a-e.

The parameters required to shape the fuzzy membership functions can be defined through expert judgement or through interpretation of how training data (if it exists) interacts with the layers of evidence. For example, training data for riparian weeds may be graphed against distance from the riparian zone to indicate at what distance suitability begins to decline.

After all layers are standardised, a choice needs to be made as to how to combine them. In traditional fuzzy set theory, this has been accomplished using fuzzy operators. A range of operators are available and can be used to combine different data layers together at intermediate stages (c.f. Bonham-Cater, 1994), before a final layer of habitat suitability is created. Fuzzy operators include the fuzzy OR (which returns the maximum value of each coincident cell for all cells in all layers) and the fuzzy AND (which returns the minimum value). The choice of operator very much

depends on the problem at hand, with the fuzzy AND being the most conservative fuzzy operator available and the fuzzy OR being the most liberal. For example, the fuzzy AND will return fewer areas of susceptibility, yet present a high likelihood that those areas are in fact susceptible to invasion. In addition, other fuzzy operators can be used where the output is a blend of coincident pixels for all layers. Briefly, the fuzzy algebraic product blends pixel scores so that the output is always smaller or equal to the smallest contributing pixel value, whereas the fuzzy algebraic sum blends pixel scores so that the output is always larger or equal to the largest contributing pixel value. Fuzzy gamma can be tuned to take on all possible combinations between the fuzzy algebraic product and the fuzzy algebraic sum, by adjusting an exponent (gamma parameter) towards 0 or 1, respectively. See Bonham-Carter (1994) provides formulae for these fuzzy operators.

Robertson et al. (2004) recognised that continuous variables are poorly represented by Boolean standardisation (as used in the envelope and WISP models) and therefore implemented fuzzy membership functions to define a grade of favourability for various layers (e.g. monthly potential evaporation, monthly minimum and maximum temperature, monthly rainfall, number of days of frost and altitude). Data on the presence of each species was collected to assist in identifying the most appropriate fuzzy membership function. This was achieved by plotting a frequency histogram for each variable (using the data on the presence of each species as a mask) and assessing its form (e.g. bell-shaped (normal), monotonically decreasing with distance). These standardised layers were then combined in a conservative fashion using a fuzzy AND operator. However, the Fuzzy AND operator was partially chosen to assist comparison between the results of an envelope model, which also uses the conservative Boolean AND operator. Such comparisons were based on models for various invasive plants (*Lantana camara*, *Ricinus communis* and *Solanum mauritianum*) and cicada species (*Platypleura capensis, Capicada decora* and *Platypleura deusta*)). Based on a threshold dependent measure (maximum Kappa; see Section 2.5.4.1) and due to the standardisation of layers using fuzzy membership functions, it was found that the models incorporating fuzzy membership functions generally performed better than those incorporating Boolean standardisation (envelope model), and never poorer.

2.5.3 Hutchinson's niche model – impact on model choice

Many of the models used to predict the vulnerability of a region to invasive plant species have a theoretical link with Hutchinson's niche model (Schoener, 1990), which recognises that there are a range of favourable environmental conditions that may dictate where a species may reproduce and survive (termed the fundamental niche). However, these areas are not always fully occupied for reasons such as competition between coexisting species or predation. This subset of the fundamental niche is termed the realised niche. Data-driven models assume that the species under study has reached its realised niche. However, populations that are still in an active phase of expansion have not yet expanded to the full capacity of this niche (Goslee et al., 2006), and this may therefore have important consequences on the decisions drawn from such models. When examining the effectiveness of a model, two imperative factors are likely to be (Robertson et al., 2004):

(i) the cost of the number of grid cells where the species is known to occur yet predicted to be absent (false negatives) versus the cost of grid cells where the species is predicted to occur yet presently does not (false positives); and
(ii) the resources available for management intervention.

In the case of identifying regions at risk from invasive species (especially those known to still be rapidly expanding) it may be more appropriate, particularly if management funds are sufficient, to over predict a species potential range (i.e. allow a certain percentage of false positives and attempt to minimise the percentage of false negatives). This will assist in management intervention before the species encroaches upon an area and is likely to be cheaper than post invasion detection and eradication (Rejmanek and Pitcairn, 2002; Robertson et al., 2004).

2.5.4 Model validation techniques

It is generally accepted that robust measures to validate the success of predictive models make use of independent data, i.e., data that have not been used to develop the parameters of the model (Fielding and Bell, 1997). These data are typically

referred to as validation or testing data. Two different techniques are often used for validation:

(i) the threshold dependent measure; and
(ii) the threshold independent measure.

Both measures are discussed in detail hereafter.

2.5.4.1 The threshold dependent measure

Threshold dependent measures use the validation or testing data to calculate a confusion matrix that cross-tabulate the observed and predicted presence/absence patterns. Four parameters are summarised in the confusion matrix:

(i) the number of true positives (number of cases predicted when actually present);
(ii) the number of false positives (number of cases predicted present when absent);
(iii) the number of false negatives (number of cases predicted absent when present); and
(iv) the number of true negatives (number of cases predicted absent when absent).

False positives are sometimes referred to as Type I errors whilst false negatives are sometimes referred as Type II errors. Table 2.6 gives a conceptual illustration of these errors.

Table 2.6 The various error types used to validate a prediction model.

		Actual Condition	
		Present	**Absent**
Test Result	**Positive**	Condition Present + Positive test result = **True Positive**	Condition Absent + Positive test result = **False Positive (Type I error)**
	Negative	Condition Present + Negative test result = **False Negative (Type II error)**	Condition Absent + Negative result = **True Negative**

Similar to the overall Kappa used for assessing the accuracy of classification from remotely sensed data, a version of Kappa can be calculated to assess the

effectiveness of a model. It is calculated as follows, and its ranges can be interpreted in the same manner as discussed in Section 2.3.4.4 (Fielding and Bell, 1997):

$$\kappa = [(a+d)-(((a+c)(a+b) + (b+d)(c+d))/N]/[N-(((a+c)(a+b)+(b+d)(c+d))/N] \quad (2.5)$$

where a = number of cases predicted when actually present (true positives);
b = number of cases predicted present when absent (false positives);
c = number of cases predicted absent when present (false negatives);
d = number of cases predicted absent when absent (true negatives); and
N = a+b+c+d.

2.5.4.2 The threshold independent measure

Threshold dependent measures fail to use all of the information available in a continuous model and choosing to arbitrarily select one particular threshold (e.g. testing for model accuracy for all values above 0.8, where the scale ranges from 0 to 1) can result in bias (Fielding and Bell, 1997; Altman et al., 1994). As such, they are usually only used for presence/absence models, not those that produce a range of suitability values. Instead model evaluation can be achieved using a threshold independent measure known as the receiver or relative operating characteristic (ROC) plot. ROC plots are considered to be more robust and more objective than threshold dependent measures (e.g. kappa statistics) since they do not rely on a single threshold, but rather plot the true positive fraction (TPF; equation 2.6) on the y-axis and the equivalent false positive fraction (FPF; equation 2.7) on the x-axis where (Figure 2.9) (Fielding and Bell, 1997):

$$TPF = a/(a+c) \quad (2.6)$$

$$FPF = 1-(d/(d+b) \quad (2.7)$$

where parameters a-d are the same as for Equation 2.5.

The area under the ROC curve (AUC) can then be calculated using the trapezoidal rule (Pontius and Schneider, 2001). An AUC of 0.5 indicates that the suitability values are assigned at random locations throughout the region. An AUC of 1 indicates a perfect model (Ayalew and Yamagishi, 2005). The ROC plot also makes

comparison between two or more models relatively straight-forward. For example, if one of the curves is consistently above the other then clearly that one is better because it minimises both false negatives and false positives (Zweig and Campbell, 1993; Fielding and Bell, 1997; Gorsevski et al., 2006)).

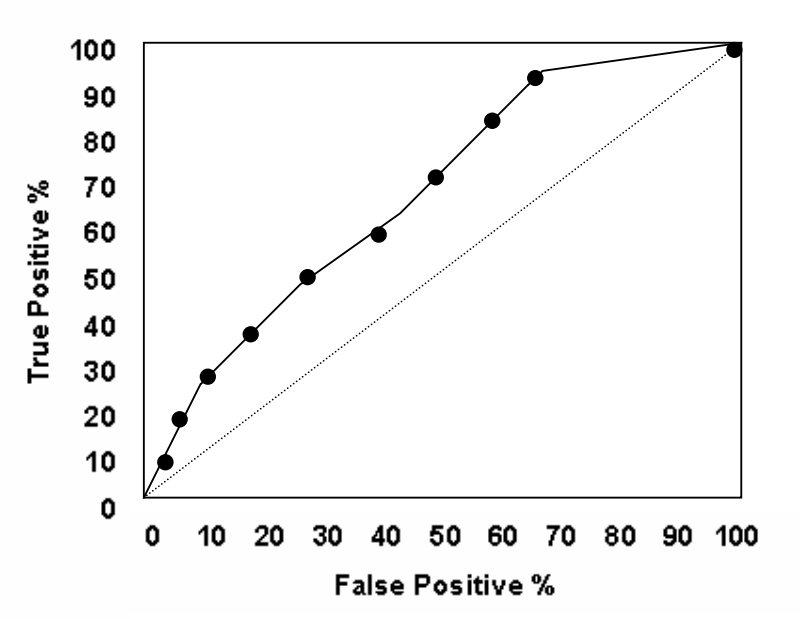

Figure 2.9 Illustration of a ROC plot. A point for each threshold is plotted with the percentage of true positives on the vertical axis and the percentage of false positives on the horizontal axis. The dashed diagonal line derives from an input image in which the locations of the image values were assigned at random (ROC=0.50).

2. 6 Summary

The use of remote sensing for mapping invasive plants relies on the target species exhibiting a unique spectral signature relative to the spectra of coexisting species. Some invasive plants have extremely obvious and unique biological traits that make them relatively easy targets to map with moderate spectral resolution imagery (e.g. colour or colour infrared aerial photographs) and comparatively simplistic classification methods. However, the biological traits of some invasive plants may not be quite as obvious. In these cases, hyperspectral imagery coupled with more advanced classification methods may be necessary.

Assessments of the spatial and temporal rates and patterns of weed invasion can reveal significant information for future management. This includes information on land type preferences, causes for accelerated invasion, life cycle processes, dispersal vectors and recruitment rates under different environmental conditions (e.g. periods of extended drought or rainfall).

The integration of the knowledge found from longitudinal studies of the spatial and temporal rates and patterns of invasion along with ground-based observations can be extrapolated over large areas to define areas representing various levels of susceptibility to invasion. Various spatial models were reviewed to this end. Clearly, a robust model requires the assignment of degrees of favourability to evidential layers (e.g. via fuzzy membership functions) as well as the ability to assign more importance to evidential layers that have more influence in determining the invasive species most suitable habitats. Methods to achieve this are explored in Chapter 5.

3 STUDY AREA AND DATASETS

3. 1 Introduction

This chapter describes the location and characteristics of the mesquite population under study. Reference is given to methods of control, most notably that of biological intervention. Climatic data are presented illustrating the arid to semi-arid environment of the study area. Remotely sensed datasets are presented and are used for multiple purposes:

(i) analysing the spatial and temporal patterns of mesquite invasion (aerial photographs) (Chapter 4);
(ii) modelling the suitability of the Pilbara Region to mesquite invasion (Chapter 5); and
(iii) assessing the accuracy and precision of discrimination between mesquite and versus coexisting species (digital multispectral imagery (DMSI) and hyperspectral imagery) (Chapter 6).

Finally, an overview of the main software used for various analyses throughout the thesis is given.

3. 2 Study Area

The studied mesquite population is located in the Pilbara Region of Western Australia. This population was initiated from intentional plantings in the 1930s to serve as drought fodder plants (pods) as well as for shade for livestock. It has been described as a hybrid swarm of *P. pallida*, *P. velutina* and *P. glandulosa* var *glandulosa* (van Klinken and Campbell, 2001). *P. pallida* belongs to the *P. juliflora-P. pallida* complex, which is native to southern Central America, the Caribbean and northern South America, while *P. velutina* and *P. glandulosa* are a complex native to USA and Mexico (Pasiecznick et al., 2001). All subspecies are referred to collectively throughout this thesis as *Prosopis* spp. or, simply, mesquite.

Currently, the population occupies approximately 150,000 ha, of which roughly 30,000 ha includes moderate to very dense stands (van Klinken and Campbell, 2001; Figure 3.1). The core of the invasion is located on the Mardie Pastoral Station

(herein referred to as Mardie unless differentiation between the lease and the homestead is needed), and is primarily to the north and east of the Mardie Station homestead (UTM Zone 50: 394188E, 7656247N), situated on the Fortescue River floodplain (Figure 3.1). Sheep were the main livestock on this lease from the late 1800s, but were replaced with cattle in 2000. Sheep and cattle have not been observed to browse on mesquite, although both consume mesquite pods and subsequently disperse seeds through their dung (Brown and Archer, 1987; Cox et al., 1993).

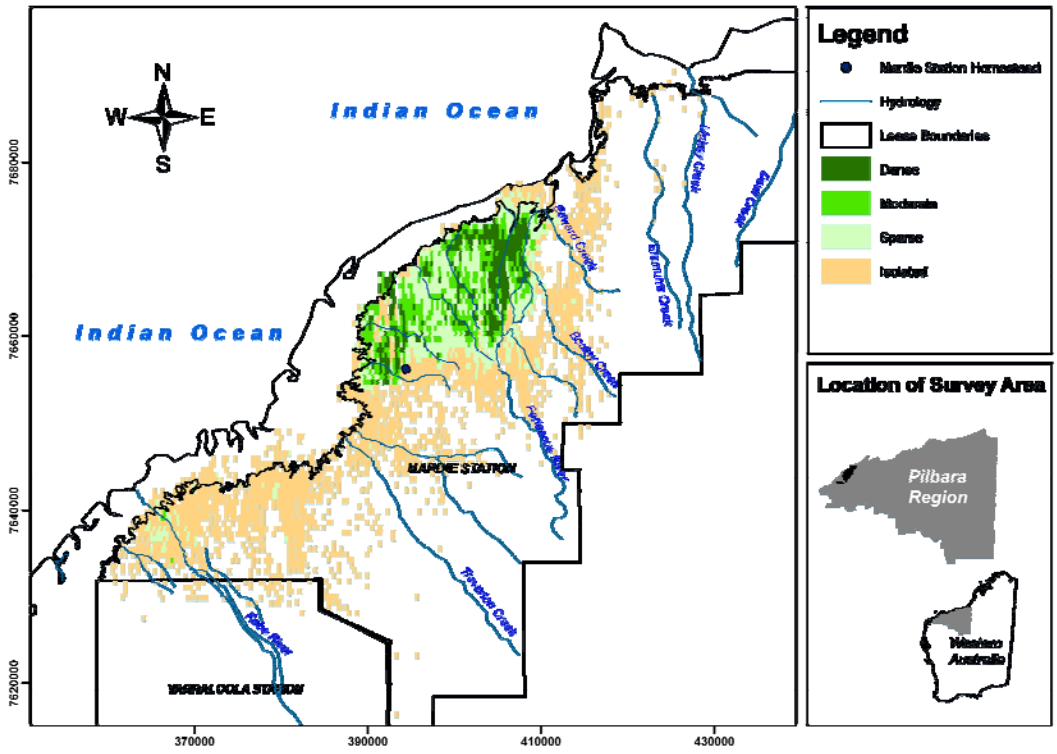

Figure 3.1 The distribution of mesquite by density class, as recorded visually from an airborne (helicopter) survey (see Section 3.3.1). Grid cells are 18.5 ha in size. The black dot represents the location of the Mardie Station homestead. The Mardie Station and Yarraloola Station labels represent respective lease boundaries.

3.2.1 Control methods

Control using both herbicides and the mechanical removal of trees (e.g. chain pulling) began in the early 1950s in the vicinity of the Mardie Station homestead. However, these control efforts have not succeeded in preventing its spread or

recovering substantial portions of land previously lost to it (Osmond et al., 2003). More recently (1998) biological control has been implemented in the form of a leaf-tying moth (Geleschiidae: *Evippe* sp. #1; Figure 3.2a). Activity from the leaf tier causes a distinctive yellowing of the leaves (Figure 3.2b). Persistent activity from the leaf tier results in wilting of its leaves/partial defoliation throughout the mesquite population (van Klinken et al., 2003). Since the leaf tier was released, there has been a significant reduction in pod production. While it is unlikely to result in large-scale mortality, a potential reduction in seed numbers is likely to slow recruitment.

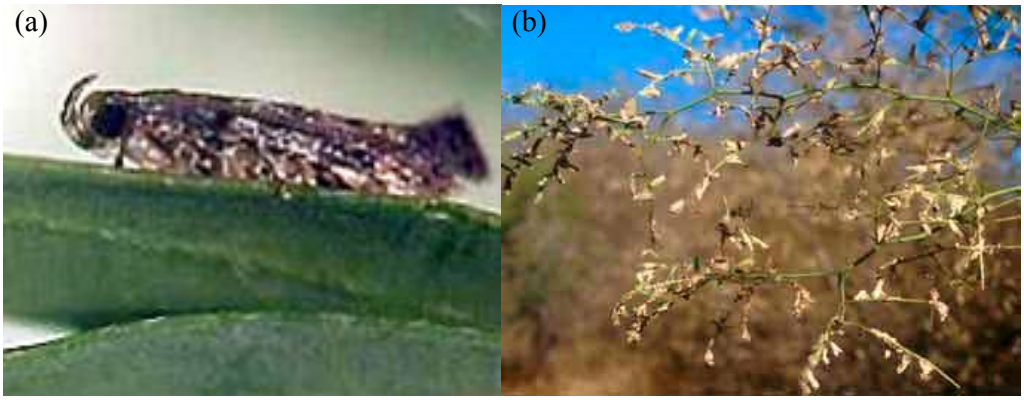

Figure 3.2 (a) Biological control, leaf tier (*Evippe* sp. #1); (b) Close up photograph showing the yellowing of the leaves and partial defolation of a mesquite shrub caused by the leaf tier.

Integrated control is also being trialled, which includes testing one or a combination of mechanical removal (which can work, but is expensive), biological control and fire. However, the mesquite population is relatively fire resistant (c.f. Wright et al., 1976) and only exceptionally hot fires will cause sufficient mortality. Patchy fuel loads make it difficult to carry hot fires, although the increased leaf litter from defoliation, coupled with pushing mesquite over with chains may increase this likelihood (Osmond et al., 2003).

3.2.2 Vegetation

Vegetation composition throughout the Pilbara is highly heterogeneous, varying with microtopography and soil type (Beard, 1975; Mitchell and Wilcox, 1994). The natural vegetation on Mardie is typical of the Pilbara Region, consisting predominantly of hummock grasslands and tall shrublands between eucalypt

dominated drainage channels (Beard, 1975). At the study sites where the aerial photographs, digital multispectral and hyperspectral imagery were acquired (see Sections 3.3.2 to 3.3.4), *Eucalyptus camaldulensis* (river red gum), *E. victrix* (coolibah) and the tussock grass *Eragrostis exerophilia* (knottybutt neverfail grass) dominate heavy clay and highly absorbent calcareous alluvium soils. On shallower soils and stony plains, the main woody vegetation is *Acacia xiphophylla* (snakewood), which is sparsely scattered amongst spinifex grasses, *Triodia wiseana* and *T. pungens*. The exotic *Cenchrus ciliaris* (buffel grass) is abundant on alluvial and shallow stony soils. Little or no vegetation grows on claypans and scalded soils, which are present throughout the floodplain (van Klinken et al., 2006). Mesquite has mixed into these existing vegetation communities, and is now the most dominant species in the area, including along riparian zones. Over time, there appears on most areas, to have been considerable in-fill of mesquite individuals, resulting in the formation of large, impenetrable thickets.

3.2.3 Climate

The climate of the Pilbara can be described as arid to semi-arid, with hot humid summers and warm winters in the north and hot dry summers and mild winters towards the southern boundary. Frosts occur very infrequently in the Pilbara. The right combination of saturated air and very low temperature is most likely to occur only in the lower south-east, and is therefore not an issue on the Mardie Pastoral Station (Van Vreeswyk et al., 2004).

3.2.3.1 Rainfall

The majority of the Pilbara Region is dominated by summer and early autumn rainfall (January – March). The convective nature of summer rain means that large amounts can be received in a single fall and such falls can be very localised. Winter rainfall (June – August) is usually much lower than summer and autumn, and only occurs, primarily, as a result of elongated southern latitude fronts. Spring rain throughout the Pilbara is extremely low and usually restricted to rain in November preceding the opening of the wet season in December.

Long-term annual rainfall, recorded on Mardie, averages 275 mm (CV=51%, n=74 years). On average, rainfall in summer and autumn are roughly equivalent, although

summer cyclones experienced at rainfall can be far more erratic, partially due to the number of tropical this time (Table 3.1; Figure 3.3). Both summer and autumn experience roughly the same number of rain days on average. Due to the relatively low frequency of rainfall (see mean number of rain days in Table 3.1), the area is viewed as highly to severely susceptible to drought (Van Vreeswyk et al., 2004).

Table 3.1 Summary of monthly rainfall data for Mardie (adapted from Van Vreeswyk et al., 2004)

Mardie	J	F	M	A	M	J	J	A	S	O	N	D
Mean monthly rainfall (mm)	37	59	49	18	39	39	14	8	1	1	1	9
Median monthly rainfall (mm)	8	30	17	1	16	20	5	0	0	0	0	0
Highest monthly rainfall (mm)	241	675	330	180	212	275	151	117	64	24	32	171
Mean number of rain Days	3	4	3	1	3	3	2	1	0	0	0	1

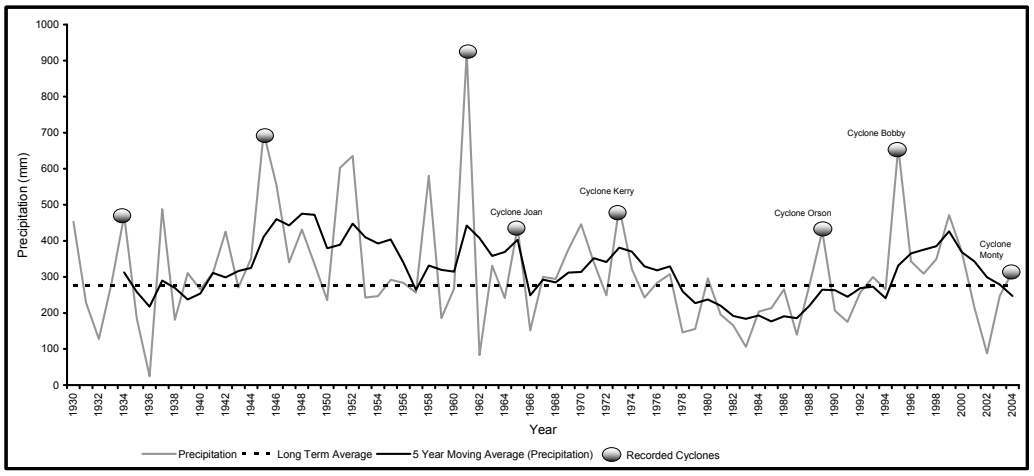

Figure 3.3 Annual rainfall for Mardie, WA, Australia, 1930-2004. *Note*: On average 2.5 cyclones per year cross the Pilbara coast (Van Vreeswyk et al., 2004). This figure only illustrates the major cyclones that resulted in substantial rainfall on Mardie as reported by the (Australian) Bureau of Meteorology (2006).

3.2.3.2 Temperature and humidity

Mean annual temperatures on Mardie are 26^{o}C (CV=18%, n=3307 records), with a mean minimum of 12^{o}C (CV=18%, n=263) in July and a mean maximum temperature of 38^{o}C (CV=6%, n=125) in January (Table 3.2). The mean maximum

in January is caused, in part, by weak onshore winds at this time. The highest maximum recorded in the Pilbara was recorded at Mardie (50°C, 19th February, 1998). Universally throughout the Pilbara the coldest month is July, however, Mardie averages 5.5 days with temperatures over 30°C during this period (Table 3.2). The coldest minimum temperature on Mardie also occurred in July (2.9°C, 10th July, 1967).

Table 3.2 Summary of monthly temperature data for Mardie (adapted from Van Vreeswyk et al., 2004)

Mardie	J	F	M	A	M	J	J	A	S	O	N	D
Mean daily max. temp. (°C)	38	38	38	36	31	28	28	29	32	35	36	38
Mean daily min. temp. (°C)	25	25	24	21	17	14	12	12	14	17	29	23
Mean No. days temp. >40°C	10	7	9	2	0	0	0	0	0	3	7	9
Mean No. days temp. >30°C	30	27	30	28	22	7	6	13	23	27	29	30
Mean daily 9 am rel. humidity (%)	52	61	56	50	51	57	51	46	39	35	37	43
Mean daily 3 pm rel. humidity (%)	44	50	43	35	36	38	33	30	28	31	34	39

]The 9 am relative humidity throughout the year varies between 35% and 61%. The lowest humidity is in spring, consistent with low rainfall for the same period. The highest humidity is during late summer and corresponds with the relatively high amount of rainfall received, coupled with extreme temperatures. The largest drop in humidity between 9 am and 3 pm occurs during the winter months (46.6% drop), and smallest drop occurs in summer (17.3%; Table 3.2).

3.2.4 Topography

The topography of the areas imaged by aerial photographs, digital multispectral and hyperspectral imagery is predominantly flat, sloping gently towards the northern coastline. The average height over the test area where aerial photographs were attained is 13.5 m (standard deviation = 2 m) and ranges from 10 m along the riparian corridor to 16 m in the east of the image. Average elevation for both the digital multispectral and hyperspectral imagery is at 10 m (standard deviation = 3 m), varying from 15 m at the southern most point to 3 m on the northern most point. Due to the relative flatness of the imaged areas, shadow effects resulting from topographic variation were minimal.

3. 3 Remotely Sensed Datasets

Several remotely sensed datasets were acquired for this study. A temporal sequence of aerial photographs was sourced to provide a historical record of the spatial and

temporal rates and patterns of mesquite invasion. DMSI and hyperspectral imagery were acquired to determine their effectiveness at accurately separating mesquite from all other land covers. An aerial survey of mesquite distribution is used for validation purposes (see Figure 3.1 and Section 3.3.1). These datasets are described in more detail hereafter.

3.3.1 Airborne survey

An airborne survey was conducted in 2004 using a R44 four-seater helicopter for work at low speed and altitude. Survey grid cells were fixed at 617.2 m long by 300 m wide (18.52 ha). Grid cell dimensions were largely determined by the flying height (60 m), flying speed (ca 110 km/hr), observation frequencies (ca 20 seconds, depending on conditions) and viewing width (300 m) that were determined as optimal for identifying and quantifying mesquite, while still allowing large areas to be surveyed.

Mesquite could be distinguished from other shrub species by its characteristic untidy appearance, the result of zig-zagged branches protruding beyond the main canopy (van Klinken and Campbell 2001), leaf colour, and by the high level of wilting/defoliation caused by the biological control agent (van Klinken et al., 2003). Observers recorded mesquite density or canopy cover for each grid cell. Mesquite was categorised as absent, isolated (up to 70 plants/grid cell) sparse (< 20% cover), moderate (20-50%, crowns separated) and dense (50-100%, crowns slightly separated, touching or overlapping). Photographs of the latter four classes, taken from the helicopter during the survey are shown in Figure 3.4. Observers also used Figure 3.5 to assist in these class definitions during the survey (McDonald et al., 1990).

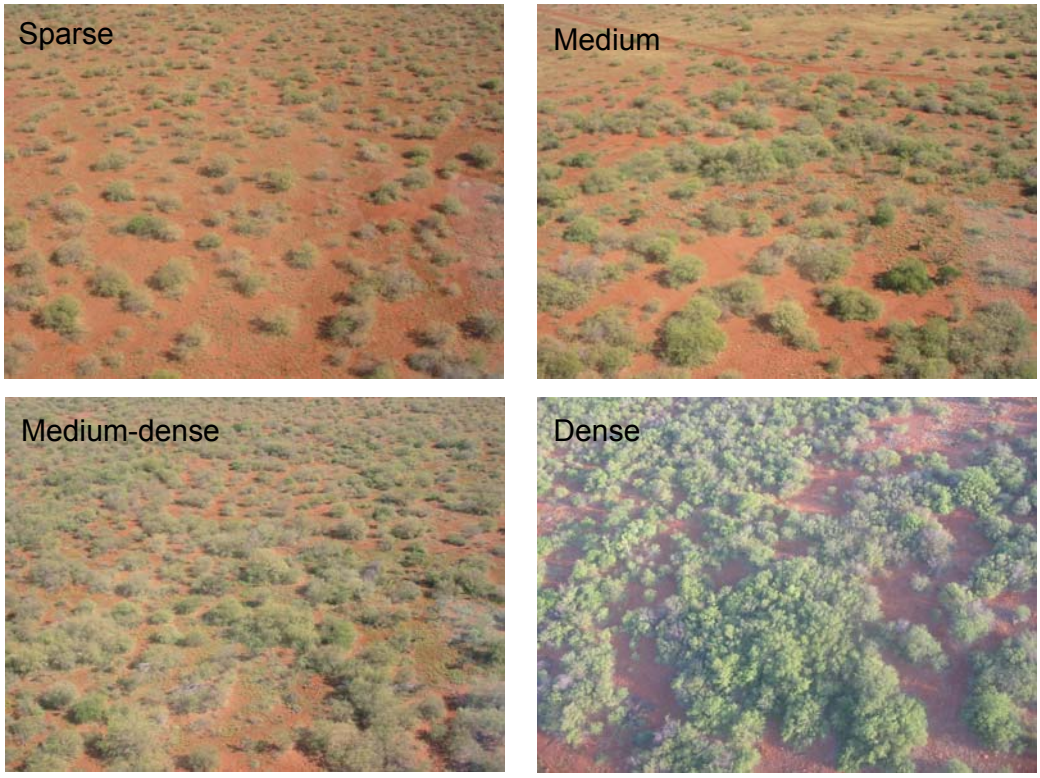

Figure 3.4 Overhead views of mesquite brush at different aerial cover values. Photographs were taken from the helicopter during the survey.

Results of the survey are presented in Figure 3.1 (page 55). The survey was found to be accurate at mapping very low densities of mesquite, but examination of overlapping portions of the survey conducted at different times showed it to be unreliable at quantifying cover levels (van Klinken et al., 2007)[1]. Further details of the survey can be found in van Klinken et al. (2007).

[1] The author was a coauthor on this paper.

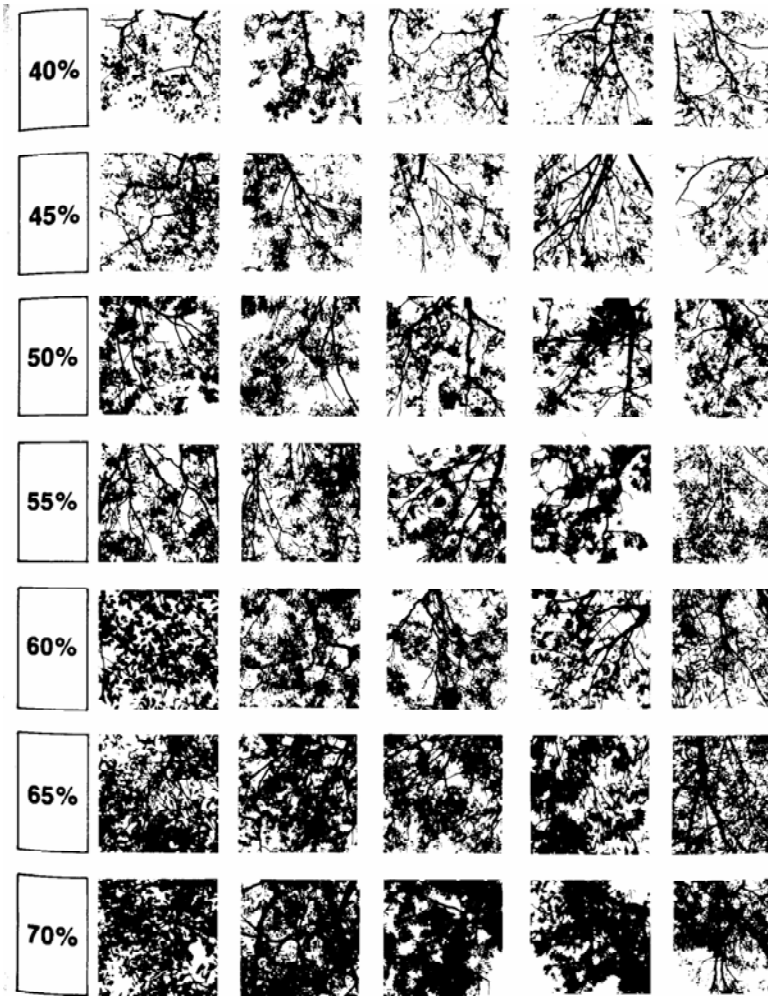

Figure 3.5 Typical shrub/tree densities used to categorise the percentage of mesquite canopy cover found within a surveyed grid cell into different class definitions (from McDonald et al., 1990).

3.3.2 Aerial photographs

A series of aerial photographs and flight line diagrams were examined prior to their acquisition in order to minimise seasonal fluctuations in mesquite's appearance and to assist in the selection of photographs without cloud interference. Two individual panchromatic aerial photographs were selected as temporal data points (August 1943, 1:30,000 and August 1970, 1:40,000). In addition, a true colour digital orthophoto was also selected, captured during September 2001 (1:25,000) (Figure 3.5).

There was no meta-data on the time imagery was acquired (e.g. solar azimuth), but visual inspection of hard copies showed them to be free from shadow effects. A test

area of 450 ha was pre-selected mainly because it has been the focus of other ground based studies on mesquite invasion (e.g. van Klinken et al., 2006). To enable digital processing, the two panchromatic aerial photographs were scanned from film at a resolution of 1200 dots per inch (dpi) using a photogrammetric scanner. Each image was georeferenced to the 2001 orthophoto using the georeferencing extension for ArcGIS 9. Root-mean-square-errors were recorded to be 1.4 m for the 1943 image and 1.3 m for the 1970 image. Because of the varying flight altitudes for each image, grain sizes ranged from 0.8 m (1943) to 0.86 m (1970). Both images were resampled to 1.4 m resolution, to coincide with the resolution of the 2001 orthophoto, using bilinear interpolation since an attempt to use the nearest neighbour algorithm resulted in images that appeared blocky (Mather, 2004). All images were clipped to the 450 ha test area (Figure 3.6). As this chosen area was located at the centre of the two panchromatic aerial photographs, the vignetting effect that commonly occurs at the edges of aerial photographs was avoided.

The 450 ha test area was located within a single, 3700 paddock ("home" paddock) in order to keep any disturbance and dispersal effects by livestock as consistent as possible. Anecdotal evidence suggests that mesquite was unlikely to have established over the test area prior to the wet season of 1945 (Meadly, 1962) with significant quantities of mesquite not observed north of the Mardie Station homestead prior to 1949 (T. Patterson, personal communication, 2004). However, mesquite is the dominant shrub/tree species in the area today. The water table is at approximately 8 m (Department of Environment, Western Australia, unpublished records) and therefore well within the reach of mesquite's taproot (Gibbens and Lenz, 2001; Gile et al., 1997; Stromberg et al., 1993). Records suggest that no control work was conducted in the chosen test area (Meadly, 1962). This is supported from a local pastoralist (T. Patterson, personal communication, 2004) who has been in the area since before control work commenced and by assessment of the historical aerial photographs.

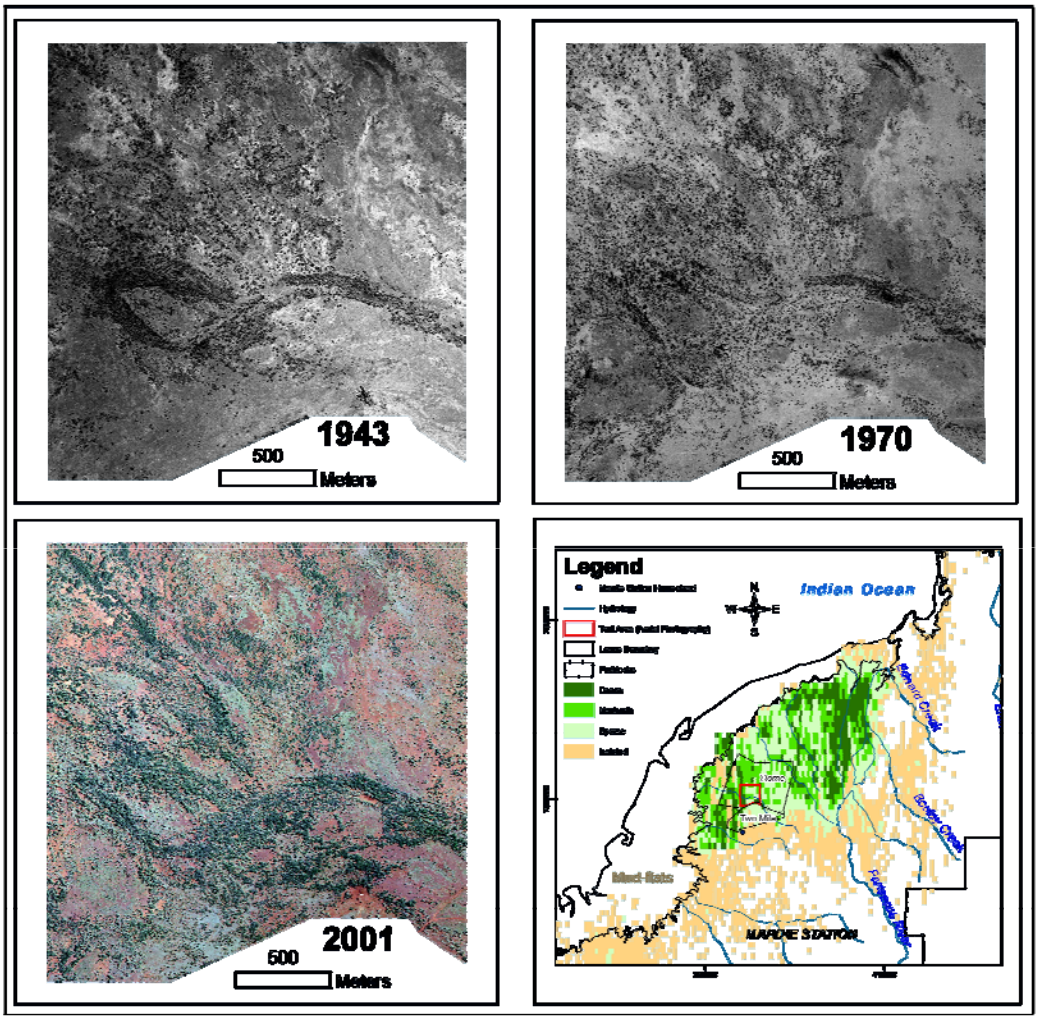

Figure 3.6 Location map and display of the chosen aerial photographs. The 450 ha test area is located approximately 3 km from the Mardie Station homestead.

3.3.3 Digital multispectral imagery (DMSI)

In November 2004, DMSI was acquired from a Cessna 182 flying at a height of 5500 ft. This altitude was used to ensure the imagery could be collected at 1 m resolution. The sensor comprises four individual CCD cameras recording 1024 pixels x 1024 pixels per array. Four interchangeable narrow band-pass interference filters were used to generate imagery in blue (450 nm), green (550 nm), red (675 nm) and near-infrared (780 nm) bands with a radiometric resolution of 12 bits. All imagery was georectified to the 2001 orthophoto mosaic (see Section 3.3.2) using a first order polynomial warping and bilinear resampling. Mosaicing was performed

using a technique based on a cut-line feathering over three pixels (PCI Geomatica, 2003). The radiometric correction was carried out using in-house developed software, based on inversion of the bidirectional reflectance model proposed by Roujean et al. (1992). Current corrections achieve a reduction of frame brightness of 20%, to less than 3% variation between individual frames (SpecTerra Services, 2003).

In total, an area of 4000 ha was acquired with dimensions 16 km long and 2.5 km wide (see Figure 3.7). These dimensions and the orientation of the imagery were chosen to minimise shadow effects, ensure tracks were included to assist ground truthing, maximise species variability and to enable the collection of an adequate sample size of the dominant vegetation types. Enlargements of the DMSI were used to collect training and validation data by marking each species encountered on the transect (Figures 3.6) and later digitising them into the GIS.

Imagery was acquired when the leaf tying moth was most active and abundant throughout the population causing a wilting and yellowing of the leaves (see Figure 3.2b). It was therefore envisaged that mesquite might be discernible from coexisting vegetation on the premise that: a) reflectance in the green portion of the spectrum will be low as pigments other than chlorophyll begin to dominate (see Section 2.3.1.4); b) reflectance in the near infrared region will decline due to a reduction in the plants ability to photosynthesise (see Section 2.3.1.6); and c) growth habit (thickets) may also assist in providing a uniquely identifiable spectral signature (see Section 2.3.1.5). Additionally, there was a desire to avoid early summer rain that might result in the regeneration of both grasses and mesquite shrubs.

Due to the absence of marked topographic variation (see Section 3.2.4), and the use of imagery acquired at a single date, near noon time, and at a low altitude with a clear desert-like atmosphere, no atmospheric correction of the imagery was deemed necessary (Foody 2001; Foody et al., 2005). In addition, since the minimum reflectance in the blue band was zero, atmospheric haze was expected to be negligible (Chavez, 1988).

3.3.4 Hyperspectral imagery

HyMap hyperspectral data were collected by HyVista in November, 2005 and flown so as to give 3 m spatial resolution with a width of approximately 1.5 km and a length of 20 km (Figure 3.7). The rationale for image timing is identical to those mentioned for the DMSI (see Section 3.3.3), and also roughly corresponds with the acquisition of DMSI a year earlier; hence, an attempt was made to keep the appearance and phenological characteristics of mesquite consistent between image acquisitions. The HyMap instrument collects 128 bands of data; however, the delivered data contains 126 bands because bands 1 and 32 are deleted in the preprocessing steps.

The sensor has four spectrometers (VIS, NIR, SWIR1, SWIR2) covering the spectral range of 400 to 2500 nm. Each spectrometer produces 32 spectral bands of imagery, which slightly overlap with an average spectral sampling interval of approximately 15 nm (Cocks et al,. 1998). Spectral and radiometric calibration of the HyMap sensor is accomplished prior to the survey and used to convert the raw digital number (DN) counts to radiance values in $\mu W/cm^2$ nm sr. Atmospheric correction is performed using the HyCorr package, which is a modified version of the ATmosphere REMoval (ATREM) software available from the University of Colorado, Boulder (Gao and Goetz, 1990; Gao et al., 1993). ATREM is a radiative transfer model based on MODTRAN for calibration to absolute reflectance that requires no ground-based measurements. Pixel-based estimates of water vapour are measured using a three channel ratioing technique of the 940 to 1140 nm atmospheric water vapour absorption bands (Gao et al., 1999). HyCorr then offers a second, more advanced level whereby spectra are also corrected for residual noise and any systematic errors involved in the ATREM pass using Empirical Flat Field Optimal bireflectance Transformation (EFFORT) software developed by Boardman (1998). Such preprocessing results in a high signal to noise ratio (e.g. >500:1), and thus mitigates the effect of most background noise (Cocks et al., 1998).

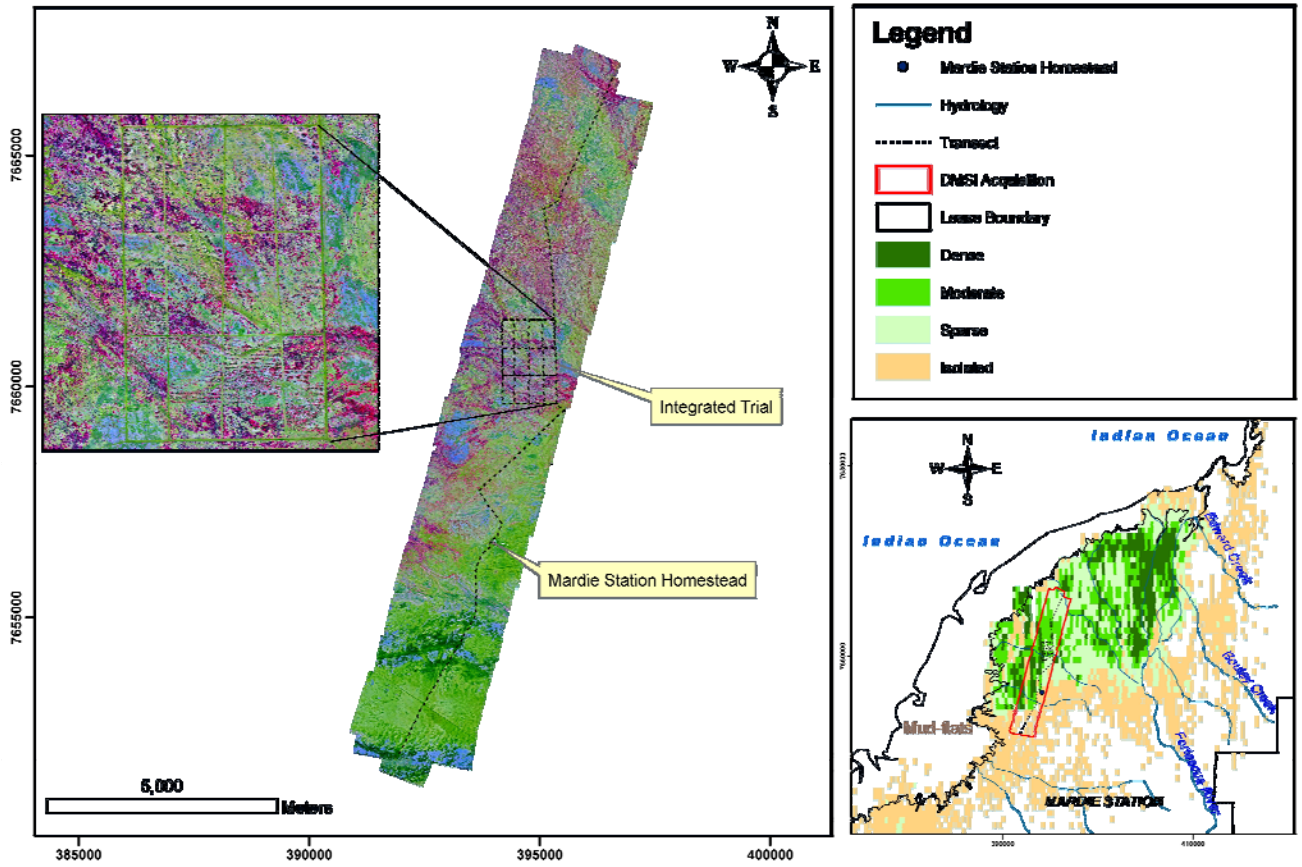

Figure 3.7 False colour composite (R=NIR, G=Red, B=Green) of the digital multispectral imagery (DMSI). The enlargement shows an aerial view of the integrated trial used to test the efficacy of various control methods (see Section 3.2.1) and roughly corresponds to the 450 ha test area shown in the aerial photographs (Section 3.3.2).

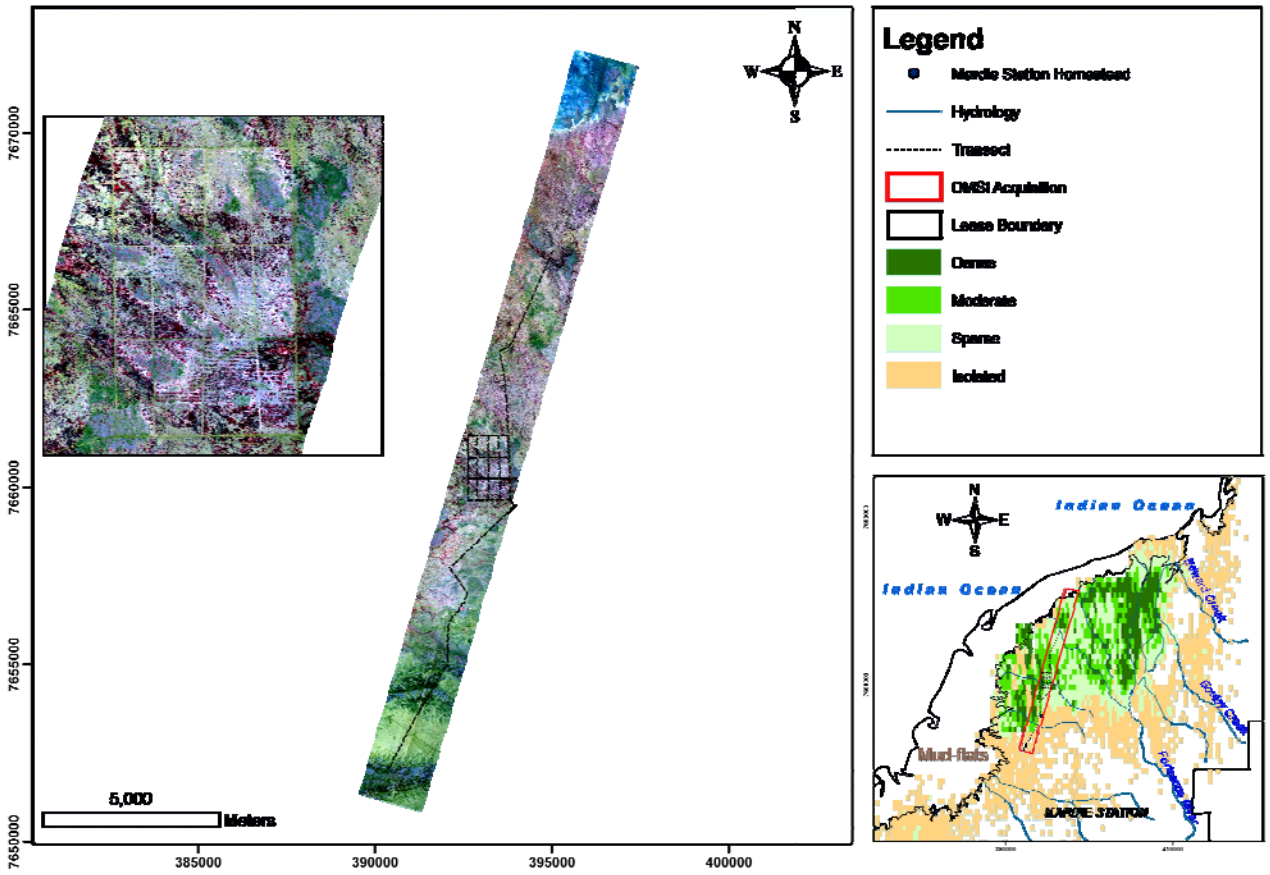

Figure 3.8 False colour composite (R=800nm, G=680nm, B=550nm) of the hyperspectral imagery acquired for this study. The enlargement shows an aerial view of the integrated trial used to test the efficacy of various control methods (see Section 3.2.1) and roughly corresponds to the 450 ha test area shown in the aerial photographs (Section 3.3.2).

The HyMap system is mounted on a Zeiss SM2000 gyro-stabilised platform that provides 5 degrees of pitch and roll correction and 8 degrees of yaw correction. High quality differentially corrected global positioning data coupled with a Boeing CMIGITS II GPS/INS inertial monitoring unit was used to provide sensor pointing data to precisely geo-reference the collected data (Cocks et al., 1998).

3. 4 Datasets to Predict Suitability for Mesquite Invasion

3.4.1 Land types of the Pilbara

As has been observed in previous studies, mesquite shows a definite preference to certain land types (Robinson et al., 2008; van Klinken et al., 2007), which is further explored in Chapter 4. Therefore, a mosaic of 20 diverse land types across the Pilbara Region was obtained from the Department of Agriculture and Food (Van Vreeswyk et al., 2004). Land types were mapped following a ground-based survey and grouped according to whether they represent erosional or depositional surfaces and secondly on soil genesis and drainage features (Leighton et al. 2004; van Vreeswyk et al 2004; Figure 3.9). Table 3.3 synthesises the proportions of the study area occupied for the mosaic of 20 land types surveyed.

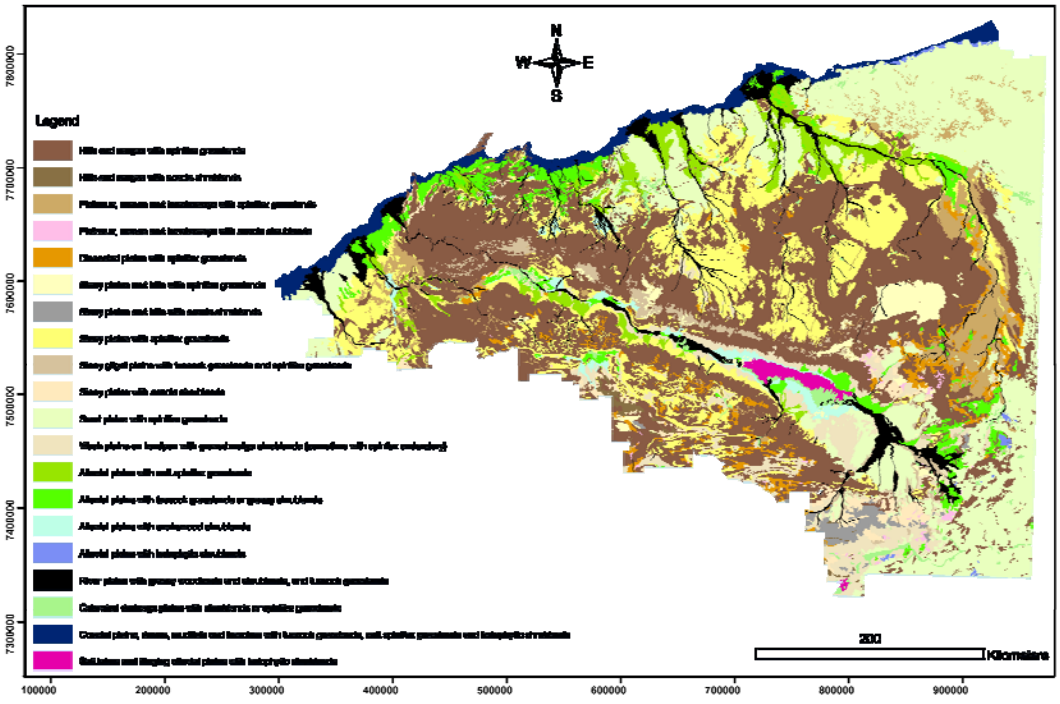

Figure 3.9 Map of the different land types throughout the Pilbara Region.

Table 3.3 Descriptions and proportions of the study area occupied for the mosaic of 20 land types surveyed.

Description[1]	Area (Km^2)	% of Study Area
Hills and ranges with spinifex grasslands	45093	40.0
Hills and ranges with acacia shrublands	527	0.5
Plateaux, mesas and breakaways with spinifex grasslands	1920	1.7
Plateaux, mesas and breakaways with acacia shrublands	81	0.1
Dissected plains with spinifex grasslands	2048	1.8
Stony plains and hills with spinifex grasslands	1028	0.9
Stony plains and low hills with acacia shrublands	705	0.6
Stony plains with spinifex grasslands	21160	18.8
Stony gilgai plains with tussock grasslands and spinifex grasslands	1896	1.7
Stony plains with acacia shrublands	1415	1.3
Sandplains with spinifex grasslands	9759	8.7
Wash plains on hardpan with groved mulga shrublands	5300	4.70
Alluvial plains with soft spinifex grasslands	3978	3.5
Alluvial plains with tussock grasslands or grassy shrublands	4004	3.6
Alluvial plains with snakewood shrublands	1989	1.8
Alluvial plains with halophytic shrublands	8	0.0
River plains with grassy woodlands and shrublands and tussock grasslands	6089	5.4
Calcreted drainage plains with shrublands or spinifex grasslands	1205	1.1
Coastal plains, dunes, mudflats and beaches with tussock grasslands, soft spinifex grasslands and halophytic shrublands	3469	3.1
Salt lakes and fringing alluvial plains with halophytic shrublands	977	0.9
Totals	112,649	100

[1]Land type descriptions are according to Van Vreeswyk et al. (2004)

3.4.2 Pastoral potential

The regional aerial survey (see Section 3.3.1) revealed a strong correlation with the above mentioned land types (and associated land systems) that had high pastoral potential (van Klinken et al., 2007). Pastoral potential is based on the number of hectares required to sustain the nutritional requirements of a unit of cattle (carrying capacity) based on the pasture type(s) found within each land system (Payne and Mitchell, 2002). Therefore, a layer of pastoral potential was also sourced to assist in the creation of a predictive model of suitability for mesquite invasion (Figure 3.10). Table 3.4 synthesises the area and percentage of each pastoral potential class. Only approximately 18% of the area shown has moderately-high to very high pastoral potential.

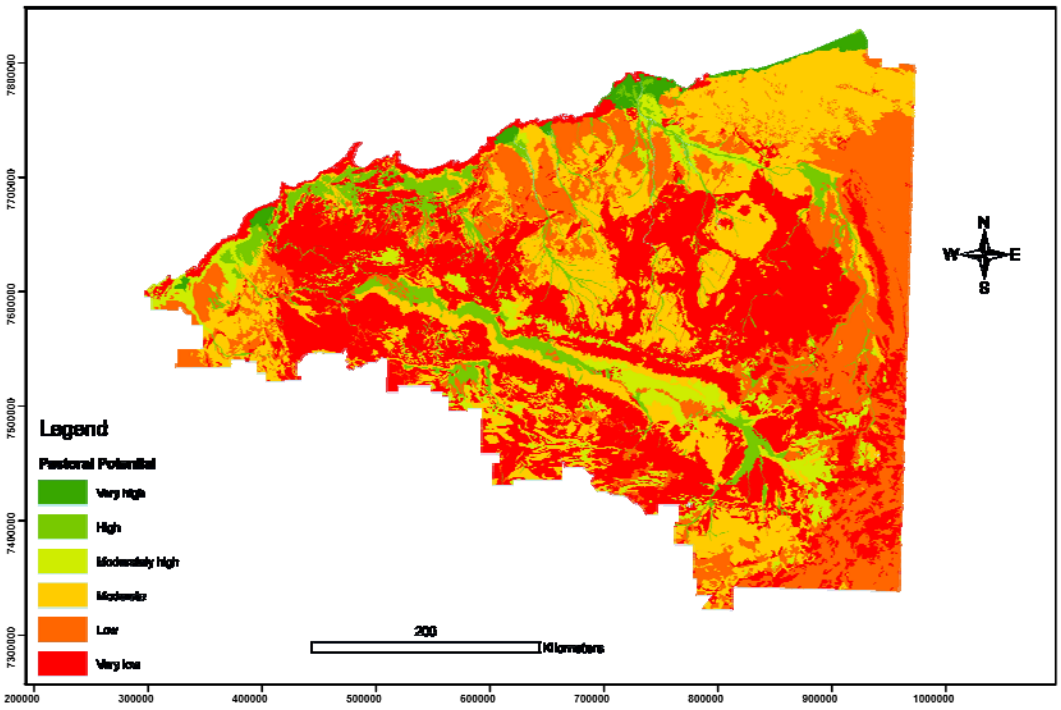

Figure 3.10 Map of the six classes of pastoral potential.

Table 3.4 Area and percentage of the 6 pastoral potential classes.

Pastoral Potential Class	Area (Km^2)	% of Study Area
Very Low	48350	42.9
Low	14080	12.5
Moderate	32260	28.6
Moderate-high	7250	6.4
High	9145	8.1
Very High	1564	1.4
Totals	112649	100

3.4.3 Land uses of the Pilbara

A layer of land use was obtained based on observed cause-and-effect relationships with land use and mesquite invasion (e.g. increased invasion rates on cattle stations; Brown and Archer, 1987; Robinson et al., 2008) and consisted of eight classes (Department of Environment, unpublished records). Figure 3.11 illustrates the spatial distribution of these land uses. Table 3.5 synthesises the proportions of the study area occupied for the eight land uses.

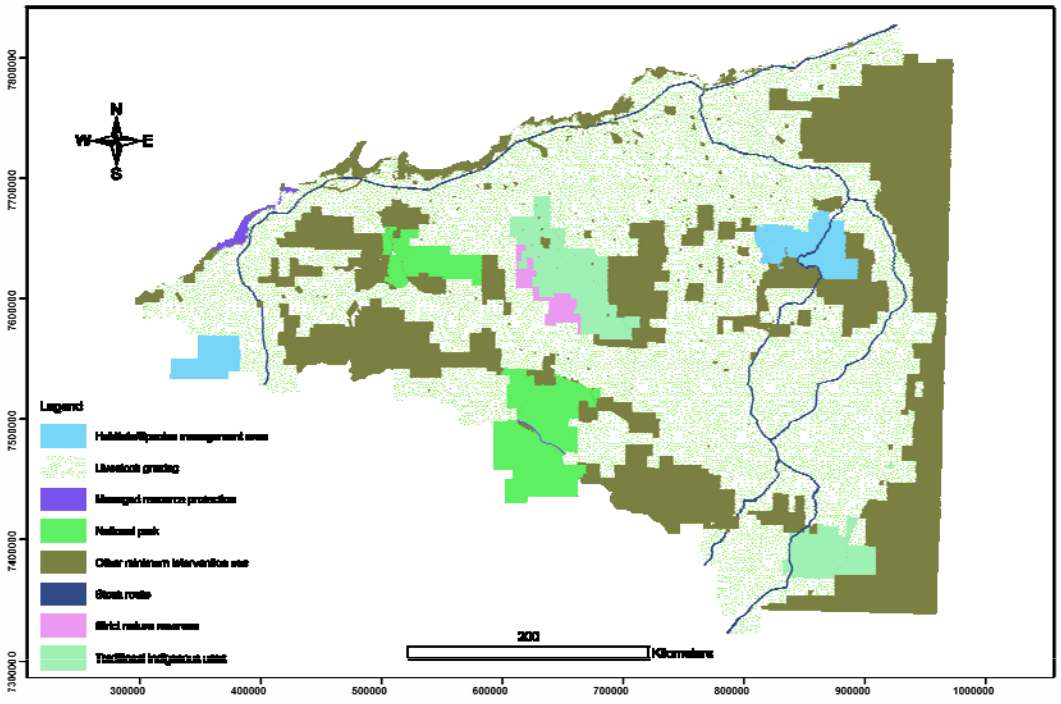

Figure 3.11 Map of the various land uses of the Pilbara Region.

Table 3.5 Descriptions and proportions of the study area occupied for the 8 land uses.

Description	Area (Km^2)	% of Study Area
Habitata/species management area	1499.1	1.3
Livestock grazing (cattle)	67868.3	60.2
Minimum intervention use	27227.3	24.2
Stock route	1040.2	0.9
Traditional indigenous uses	4968.0	4.4
Managed resource protection	408.9	0.4
National park	8578.8	7.6
Strict nature reserves	1058.4	0.9
Totals	112649	100

3.4.4 Digital elevation model

Based on knowledge that mesquite has a preference to the more mesic parts of the landscape (Robinson et al., 2008), existing spot-heights (point data) representing height above sea level and water network data were used to create an interpolated digital elevation model (DEM) at a resolution of 50 m using the ANUDEM algorithm (Figure 3.12). Areas with poor spot height coverage were removed from the DEM. As a consequence, this layer represented the spatial extents of the spatial

model produced. The DEM was used to create a steady state wetness model (CTI), which is presented in Chapter 5.

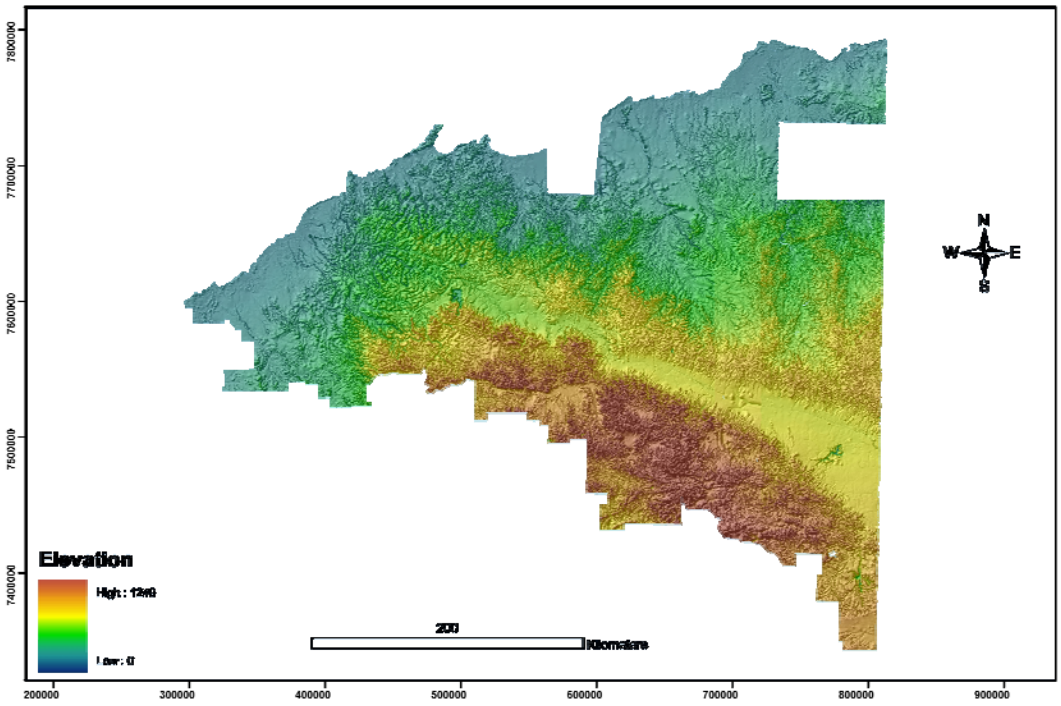

Figure 3.12 Digital Elevation Model (DEM) of the Pilbara Region.

3. 5 Software

ArcGIS (version 9.1; ESRI, 2004) was used to carry out the majority of GIS operations throughout this thesis. IDRISI Andes (Clark University, 2006) was used for all image processing/classification routines. Landscape metrics (e.g. distance to nearest neighbour patch and patch density) were performed in FRAGSTATS v. 3 (McGarigal et al., 2002). Brodgar (Highland Statistics Pty Ltd, 2006), an interface to R, was used for advanced statistical analyses (e.g. selecting the best discriminatory variables/bands using discriminant analysis). Microsoft Excel was used for data synthesis.

3. 6 Summary

In general terms, the study area is the Mardie Pastoral Station in the northwest Pilbara Region of Western Australia. Mesquite is predominantly isolated to this station, although small numbers exist on the adjacent Yarraloola Station. Mesquite currently has an extent of around 150,000 ha, of which ca 30,000 ha is dense.

Various forms of control have been attempted over the last 50 to 60 years; however, all have failed over the long term. Biological control was released in 1998 to curb further spread by limiting the energy available (via defoliation of the plants) to produce abundant numbers of pods.

A temporal series of aerial photographs were selected to study the invasion rates and patterns through both time and space. DMSI and hyperspectral imagery were acquired to test methods to accurately map the current distribution of mesquite. Other datasets (e.g. land types and land use, pastoral potential and a DEM) were obtained or created to assist modelling the suitability of the Pilbara Region to mesquite invasion.

4 EXAMINATION OF THE SPATIAL AND TEMPORAL RATES AND PATTERNS OF MESQUITE INVASION

4. 1 Introduction

Plant invasions pose one of the greatest threats to the world's ecosystems (Mack et al., 2000). A major challenge is to understand the processes underlying plant invasions, and thereby to identify opportunities for management intervention. Analysis of plant invasions at the landscape level has received considerable attention recently, because it is the scale at which spatial and temporal patterns of invasion can be linked to proximate causes, the rates and patterns of spread can be quantified and the efficacy of different management practices can be assessed (e.g. Brown and Carter, 1998; Ansley et al., 2001).

Historical archives of panchromatic aerial photography provide one of the few sources of long-term, temporal data at the resolution required to study historical invasion and its relationship with the landscape (Rango and Havstad, 2003). However, invasive plants rarely have spectral characteristics that enable their discrimination from coexisting species using panchromatic aerial photography and standard image processing techniques (e.g. Hutchinson et al., 2000; Lahav-Ginott et al., 2001; Manson et al., 2001; Kadmon and Harari-Kremer, 1999). Therefore, most studies aimed at examining the spatial and temporal rates and patterns of plant invasions have been restricted to small areas (typically less than 80 ha) where the plant has formed a virtual monoculture (e.g. Goslee et al., 2003) or, where vegetation composition has been heterogeneous, have relied on manual photo interpretation (e.g. Ansley et al., 2001; Fensham et al., 2002). However, as mentioned in Section 2.5.3.1, the time consuming nature of interpreting and manually delineating the canopies of a species of interest often limits analyses to only a small area, to sparsely vegetated areas, or to the interpretation of relatively coarse vegetation units (Kadmon and Harari-Kremer, 1999). Therefore, in this study, a combination of techniques is used in an attempt to overcome or partially overcome these limitations in order to extract the canopies of a mesquite population over a relatively large (450 ha) test site comprised of several shrub/tree species, from a temporal series of aerial photography. Results of the method are assessed quantitatively and the minimum

detectable mesquite crown area that can be resolved using the 1.4 m resolution imagery is identified.

Mesquite is recognised as a highly invasive plant in both its native (e.g. the Americas) and introduced range (Archer, 1995; van Klinken et al., 2006). Several studies have sought to describe the rates and patterns of mesquite invasion in its native range using aerial photography, long-term demographic studies and modelling (e.g. Archer, 1995; Scanlan and Archer, 1991; Ansley et al., 2001; Goslee et al., 2003). The core observations of these studies can be summarised as follows:

(i) the shift from grassland to mesquite shrubland has occurred relatively recently, typically in the past 50 to 100 years;
(ii) mesquite invasion generally follows a process of high patch initiation, followed by coalescence;
(iii) livestock, particularly cattle, are highly effective vectors of spread; and
(iv) rates of invasion have varied according to land type, with the greatest amount of recruitment and coalescence occurring in the most mesic parts of the landscape.

In this study, invasion rates and patterns are compared with those described at a smaller scale from its native range. Specifically, based on the abovementioned observations for mesquite in its native range, this study tested whether:

(i) mesquite invasion has been as rapid as that observed in its native range;
(ii) mesquite invasion follows a process of high patch initiation followed by coalescence;
(iii) dispersion is widespread soon after introduction, providing evidence of long distance dispersal vectors; and
(iv) certain land types are more resistant to mesquite invasion than others.

4. 2 Methodology

In order to study the spatial and temporal rates and patterns of mesquite invasion, mesquite first had to be extracted from the series of aerial photographs described in Section 3.3.2. The method used to accomplish this is described in Section 4.2.1. Secondly, in order to relate such measures to different land types, they were mapped (see Section 4.2.2) coincident to the collection of validation data used to corroborate the accuracy of the mesquite extraction technique (see Section 4.2.4) during the September 2005 field season. After the temporal database of mesquite canopies was established over the 450 ha test area, it was analysed to determine:

i) the major process or processes occurring on each of the different land types (e.g. high patch initiation from recruitment, coalescence or a combination of both) (Section 4.2.3.1);
ii) the overall rate of increase over the entire test area and over each land type (Section 4.2.3.2);
iii) the land type(s) experiencing the greatest change in cover to determine which land types were more resilient to invasion and which were more susceptible (Section 4.2.3.2);
iv) whether there is more presence/absence of mesquite on certain land types (Section 4.2.3.3); and
v) whether, as an extension of (iv), canopy cover is higher (over time) over certain land types where it is known to be present (Section 4.2.3.3).

4.2.1 Image classification and construction of vegetation layers

The high density of vegetation and relatively large test area demanded a semi-automated technique for extracting the canopies of mesquite shrubs/trees while removing all other vegetation. Figure 4.1 illustrates the algorithm used to accomplish this. Firstly, all images were processed using an iterative self-organising clustering procedure (ISODATA). This method begins by assigning pixel values to a set of arbitrary cluster means. The arbitrary cluster means are recalculated at iteration and as the number of iterations increase, the mean class values gravitate towards natural breaks in the distribution of image pixels (Mather, 2004). Figure 4.2 gives a simple illustration of the ISODATA process for two iterations and two arbitrary cluster means.

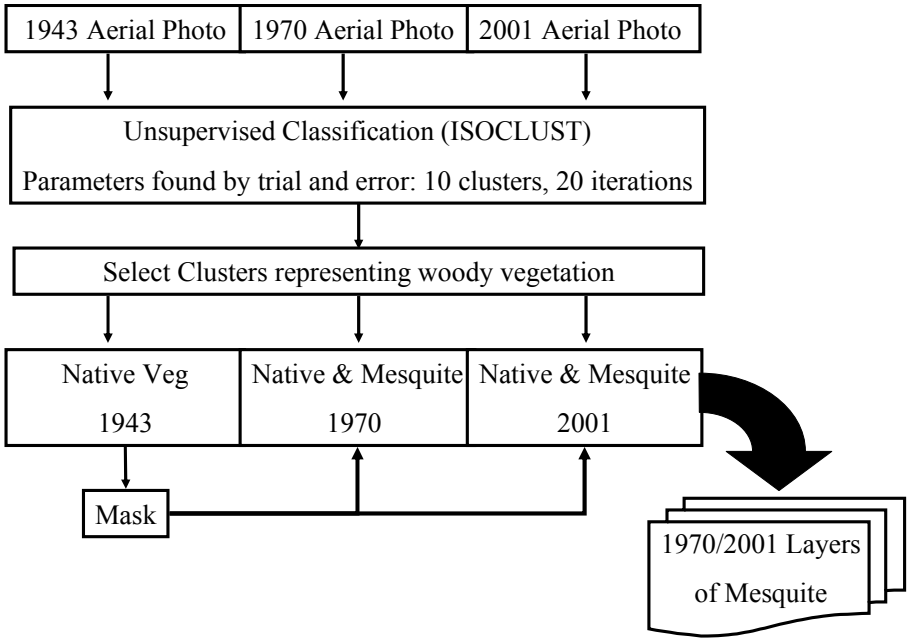

Figure 4.1 Flowchart of the algorithm used to extract the mesquite canopies from the aerial photography.

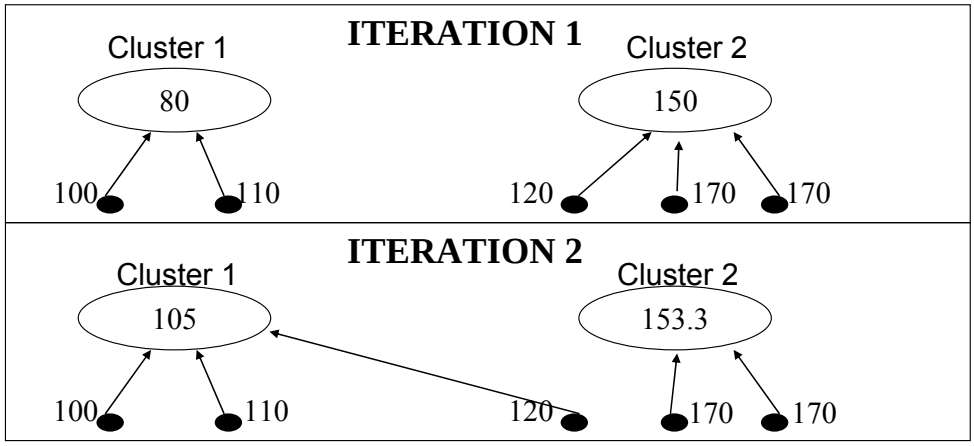

Figure 4.2 Illustration of how the ISODATA technique assigns pixels to different clusters. In this example, the pixel with a digital number of 120 has been reassigned to cluster 1 at iteration 2 because it is closer to 105 than to 153.3.

The required parameters of the ISODATA routine were found heuristically (20 iterations, five clusters). As expected, discrimination between vegetation types was not achieved during this step, although it did adequately distinguish between woody vegetation and other background landcovers.

The cluster representing woody vegetation was extracted to form four new raster layers; one for each of the time steps considered (1943, 1970, 2001 and 2004). A subsequent step was required to remove native vegetation from the 1970, 2001 and 2004 images. This was achieved by masking out all patches of vegetation present in the 1943 image, which were assumed to be native (Meadly, 1962; T. Patterson, pers. comm.) from all subsequent imagery using the editing tools in ArcGIS 9 (ESRI, 2004).

4.2.2 Mapping land types

GIS overlays of hydrography showed an obvious association between thick vegetation (both native shrubs and trees and mesquite) and drainage lines. For this study, the riparian zone was defined as an area within 50 m of hydrography, based on the work by Grice et al. (2000) and Bowman et al. (2001). The remainder was defined as uplands. The riparian zone was not subclassified by soil type, but it was primarily red loamy soil. Uplands were differentiated based on their edaphic characteristics, into two categories: stony flats (which comprised of all crusted soils, including hard pans and clay pans) and red loamy soils. These land types were mapped using a false colour composite (near infrared, red, green) of the DMSI and corroborated in the field. Stony flats were easily differentiated from red-loamy soils using this band combination. Stony flats appeared as dark green areas often associated with Spinifex (*Triodia wiseana* C. Gardner and *Triodia pungens* R. Br.), which appeared blue under this combination. Red loamy soils appeared as light green under this combination.

4.2.3 Analysis of mesquite cover and temporal change

Three methods of comparison were used to assess the relationship between mesquite canopy cover and the three land types (riparian zone, red loamy soils and stony flats). These methods are described hereafter.

4.2.3.1 Patch dynamics

Four processes have been reported to influence changes in mesquite cover: recruitment of new mesquite plants or patches; coalescence of expanding mesquite patches; a combination of recruitment and coalescence of mesquite patches; and mortality of mesquite plants (Ansley et al., 2001). To assist identification of the

process that was dominant for each time-frame studied, over the entire test area or for each land type, two landscape metrics were computed: (i) mean distance to the nearest patch (m), calculated as the average Euclidean distance to the nearest neighbouring patch, from cell centre to cell center; and (ii) patch density, calculated as the average number of patches per unit area (ha) (McGarigal et al., 2002). In addition, histograms were prepared showing the size class distribution of mesquite patches in 1970 and 2001 for each land type.

4.2.3.2 Change detection

A 20 x 20 m lattice of 11 250 quadrats was placed over the 1970 and 2001 images representing mesquite canopy cover and the percentage of cover for each quadrat was calculated within the GIS. The appropriate quadrat size for change detection (20 x 20 m) was determined by plotting the variance of estimated mesquite cover (%) against a range of quadrat sizes and identifying the point at which it became stable (Figure 4.3; Papanastasis, 1977; Greig-Smith, 1983). Image differencing (subtraction of earlier image from later image) was used to detect change in mesquite cover for all coincident quadrats between years. To visualise significant change throughout the test area, a threshold value was derived (using all quadrats) from the mean difference between images plus one standard deviation (Jensen, 1996).

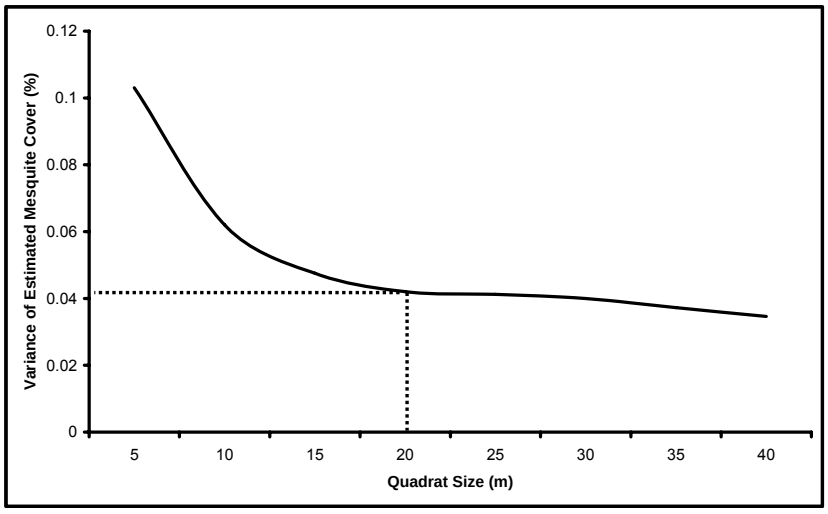

Figure 4.3 Relationship between the variance of estimated mesquite cover (%) and quadrat size.

4.2.3.3 Analysis of cover

Two tests were performed on both the 1970 and 2001 images to determine if certain land types are more resistant to mesquite invasion than others. The first test aimed to determine if mesquite *presence* was dependent on land type. Quadrats were converted to presence/absence and a random sample (N=200) was taken for each of the three land types. The interaction of mesquite presence/absence within the different land types was tested using one-way between subjects ANOVA, followed by Tukey's Honestly Significantly Different (HSD) test (Hair et al., 2006). A second test was carried out to determine if canopy cover was *higher* over certain land types, where it was *present*. To this end, a random sample of 200 quadrats from each land type were tested using one-way between subjects ANOVA on quadrats that had more than 0% cover. Tukey's HSD test was used to assess the differences in canopy cover between land types.

4.2.4 Field verification of image processing

To substantiate the accuracy of the semi-automated technique used to extract mesquite canopies from the aerial photographs, field verification was undertaken in September 2005. As shrubs may have grown between the last aerial photograph acquisition and the time of ground truthing, the mesquite canopy extractions from the DMSI (acquired in November 2004) was used to support ground verification.

Fifteen quadrats were randomly selected for each of the following cover classes: zero cover (0%); low cover (>0% and ≤30%); moderate cover (>30% and ≤90%) and high cover (>90%). To assist accessibility, only quadrats within 200 m of existing tracks were candidates for random selection. The 15 quadrats within the zero cover class were incorporated into the validation scheme to estimate the size of shrubs that were not reliably detectable from the spatial resolution (1.4 m) of the aerial imagery.

Each of the 60 quadrats were located in the field with the aid of a Magellan eXplorist (100) global positioning system (GPS) and enlarged false colour composites of the DMSI and delineated with measuring tape. To estimate the surface area of a mesquite shrub, the longest diameter of an individual shrub was first measured. This length was then divided into ten equal sized segments running perpendicular to the longest diameter. The length of these perpendicular segments were then recorded

and the surface area was then computed using Simpson's Rule of approximate integration (Stewart, 1995). The surface area of all individual shrubs within a randomly sampled quadrat were computed in this way. Canopy cover of mesquite within each quadrat was converted to a percentage by dividing the sum of the surface areas by 400m^2 (the size of an individual quadrat). Where mesquite had formed a thicket, a quadrat was divided into twenty, 1 m intervals and depending on which was easier in the field, either the surface area of the thicket or that of bare soil was then calculated using Simpson's Rule of approximate integration as before. If bare soil was used in the calculation it was inverted. As before, these calculations were converted to a percentage of canopy cover by dividing by the area of the quadrat. All mesquite shrubs that were less than 1.4 m in diameter were ignored since they were technically not detectable using 1.4 m resolution imagery. Additionally, for the same reason, shrub clumps closer than 1.4 m were measured as one unit (Goslee et al., 2003). Quadrats containing clustered stands of mesquite, which were common in the moderate and high cover classes, were divided into 1 m intervals and the area of bare earth was measured, also using Simpson's Rule of approximate integration. All field calculations were summed and converted to a percentage of mesquite canopy cover per quadrat and compared to the percentage of mesquite cover per quadrat calculated within the GIS.

4. 3 Results

4.3.1 Analysis of mesquite cover and temporal change

Table 4.1 shows the relative proportions of the test area attributed to each of the three land types. Native vegetation in 1943 was highest in the riparian zone and was low in the stony flats. By 2001 there was considerably more mesquite over all land types when compared with native vegetation found in the 1943 image.

Table 4.1 Statistical breakdown of the canopy cover changes for the 1943, 1970 and 2001 images over the three land types.

Land Type	Area (ha)	1943	1970				2001			
		Non-mesquite cover (%)	Mesquite Cover (%)	Rate of change[1] (% year^{-1})[2]	Patches ha^{-1}	Distance to Nearest Patch (m)	Mesquite Cover (%)	Rate of change[1] (% year^{-1})[2]	Patches ha^{-1}	Distance to Nearest Patch (m)
Riparian	70	15.7	3.0	0.11a	44	6.5	36.0	1.16a	72	4.1
Red loamy soils	324	10.2	2.6	0.10a	34	7.7	24.2	0.78b	81	4.4
Stony flats	56	2.7	0.4	0.02b	7	17.7	11.1	0.36c	101	4.5
Total	450	10.1	2.4	0.09			24.4	0.71		

[1]Calculated as linear increase in canopy cover from 1943 (0% cover) and 1973 respectively;
[2]Different letters within a column represent differences in rates of change.

4.3.2 Patch dynamics

The total number of mesquite patches over the test area increased from 13 950 to 31 704 over the 31-year period from 1970 to 2001. Stony flats had a relatively low patch density, and a relatively high mean distance to nearest neighbour, compared to the riparian zone and red loamy soils in 1970, which were roughly comparable (Table 4.1). Mesquite patches greater than 6 m^2 were uncommon on stony flats in 1970 suggesting that coalescence was rare (Figure 4.4a).

The number of patches increased substantially between 1970 and 2001 in all size classes in all land types, demonstrating continued patch recruitment (Figure 4.4; Table 4.1). The distance between patches was similar in each land type. However, stony flats had a higher density of patches overall (Table 4.1), as well as in each of the smaller size classes, especially patches less than 6 m^2 in size (Figure 4.4a).

Patch density was slightly higher in red loamy soils than in the riparian zone, although the size distribution was similar in both land types. Patches were up to 4.7 ha in size (Table 4.2). Patches larger than 100 m^2 were relatively common in both the riparian zone and red loamy soils in 2001 (Figure 4.4b,c; Table 4.2) and would have been partly the result of smaller patches coalescing to form dense thickets. Average and median patch size was largest in the riparian zone (Table 4.2), and is likely to be the main factor responsible for mesquite cover (%) being higher over this land type than over red loamy soils (Table 4.1).

Table 4.2 Summary statistics for patches greater than 100m^2 in 2001, broken down by land type.

Land Type	Number of Patches	Patches ha^{-1}	Median (m^2)	Average (m^2)[1]	Standard Deviation (m^2)	Maximum (m^2)
Riparian	280	4.0	194	789 (216)	3614	47717
Red loamy soils	1168	3.6	180	432 (37)	1270	29572
Stony flats	55	1.0	158	180 (12)	91	619

[1]Values given in brackets represent the standard error.

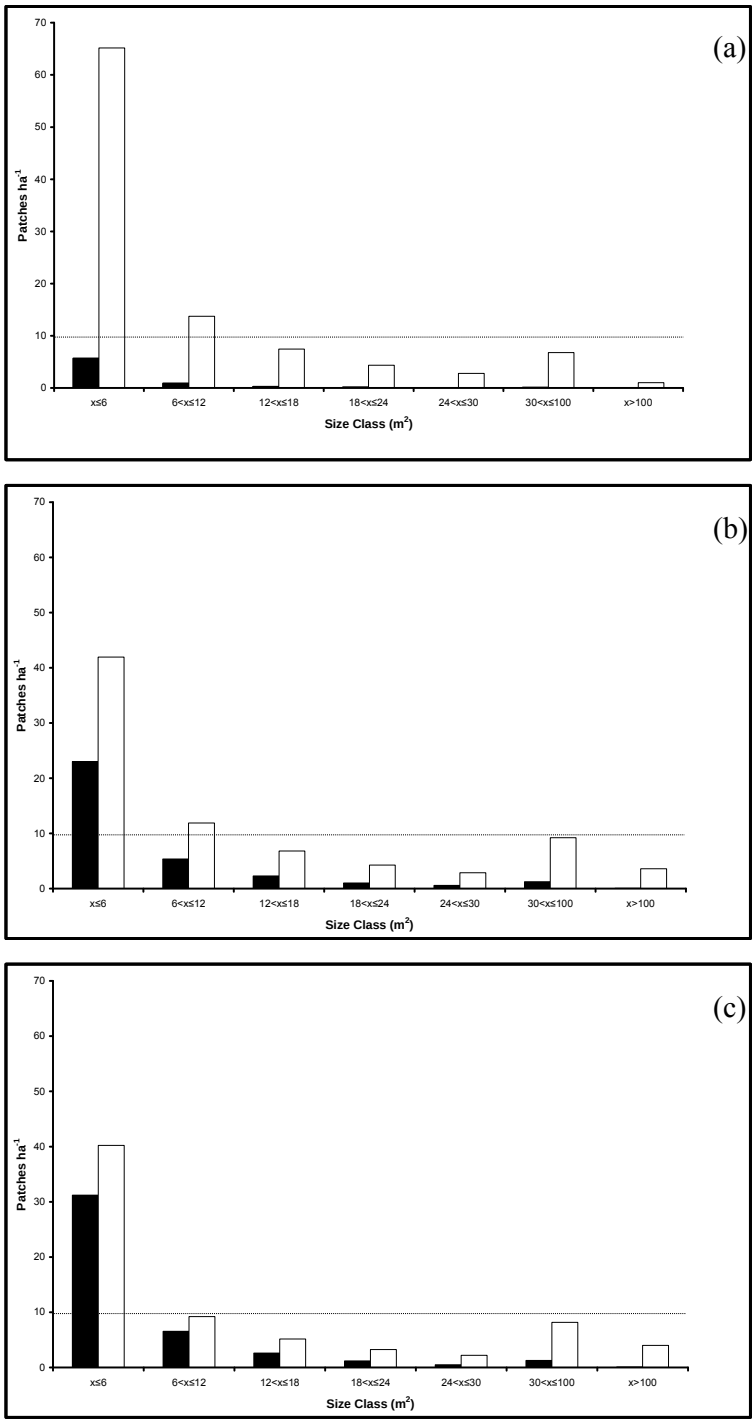

Figure 4.4 Density of mesquite patches by size class for 1970 (black bars) and 2001 (open bars): (a) stony flats, (b) red loamy soils, (c) riparian zone.

4.3.3 Change detection

Mesquite canopy cover occupied 2.4% (10.7 ha) of the test area by 1970 (Table 4.1), and was already highly dispersed through the test area (Figure 4.5a). Canopy cover was not uniform throughout the test area, being much higher in the riparian zone and red loamy soils (Table 4.1). Furthermore, the percentage of quadrats where canopy cover increased faster than the change threshold (>6.3% increase in canopy cover) was similar over both the riparian zone and the red-loamy soils in 1970 (15% and 13% respectively). In contrast, few quadrats showed a significant amount of change over the stony flats (0.3%).

Total mesquite canopy cover in 2001 was 24.4% (109.9 ha); representing an increase in canopy cover of approximately 0.71% $year^{-1}$, assuming a linear increase from 1970. This was almost eight times the rate of increase observed prior to 1970. Again, rates of increase in canopy cover varied with land type over this period (Table 4.1). The most rapid change was over the riparian zone (Figure 4.5b), with approximately 40% of quadrats increasing faster than the change threshold (>40.1% increase in canopy cover). This was followed by the red loamy soils (18.1%) and stony flats (1.8%).

4.3.4 Analysis of cover

The interaction between the presence of mesquite and each of the three land types was highly significant in both 1970 ($F_{(2,597)} = 70.9$, $P<0.01$) and 2001 ($F_{(2,597)} = 33.4$, $P<0.01$). Based on Tukey's HSD it was found that, in 1970, quadrats over the riparian zone were more likely to be occupied by mesquite than those over red loamy soils ($Q = 4.7$, $P<0.01$) or stony flats ($Q = 16.4$, $P<0.01$) and more likely to be occupied over red loamy soils than stony flats ($Q = 11.6$, $P<0.01$). In 2001, there was no statistical difference between quadrats occupied by mesquite over the riparian zone or red loamy soils ($Q = 2.5$, $P>0.01$); however there were fewer quadrats occupied over stony flats than over the riparian zone ($Q = 11.0$, $P<0.01$) or red loamy soils ($Q = 8.5$, $P<0.01$).

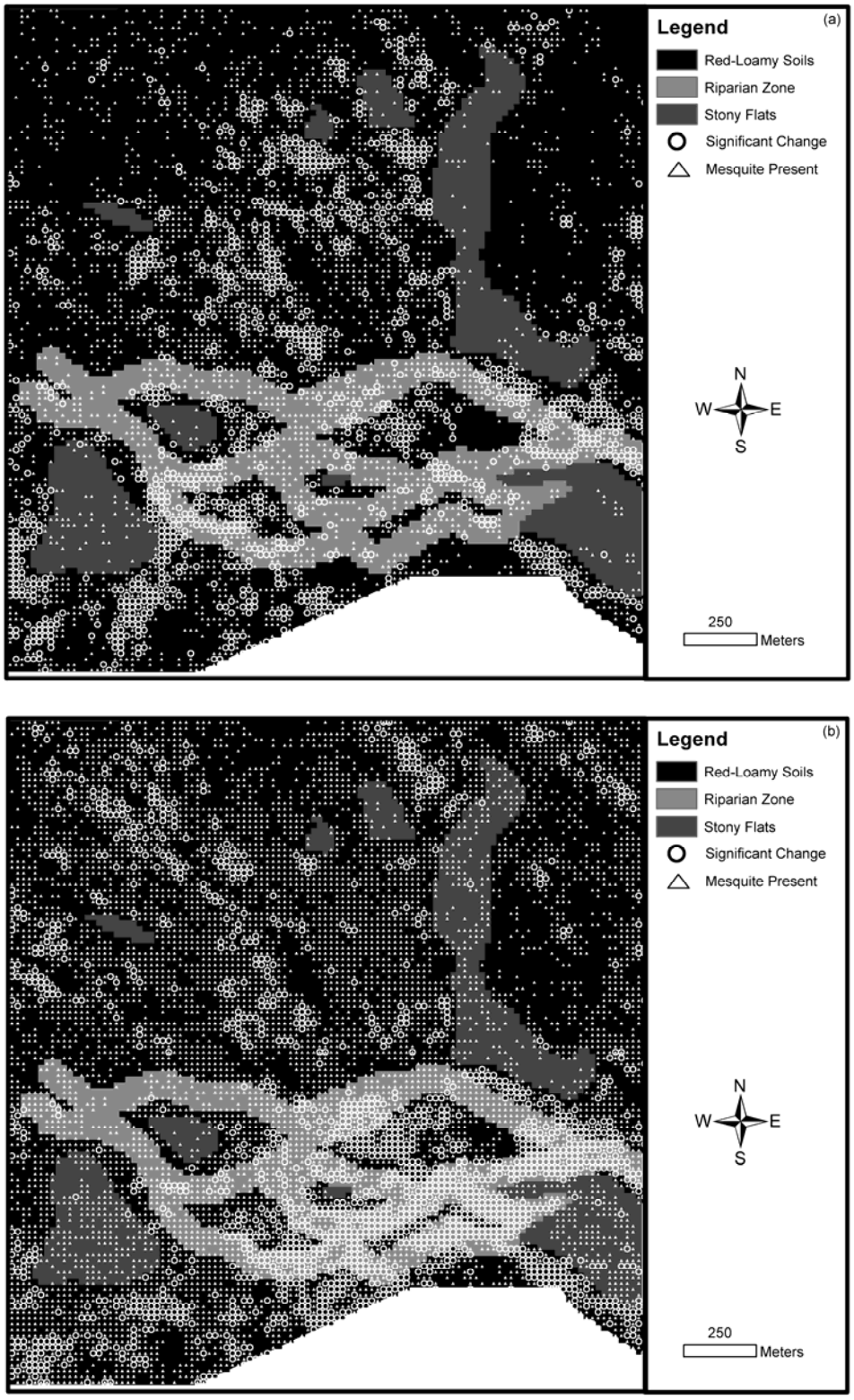

Figure 4.5 The distribution of land type and mesquite across the test area showing presence of mesquite (circles and triangles) and increase in mesquite cover within a quadrat above the change threshold (circles) in (a) 1970 and (b) 2001.

As might be expected from both the change analysis (Figure 4.5) and total canopy cover in each land type (Table 4.1), the interaction between mesquite canopy cover in quadrats in which mesquite occurred and the three land types was highly significant in both 1970 ($F_{(2,597)} = 33.0$, $P<0.01$) and 2001 ($F_{(2,597)} = 110.9$, $P<0.01$). In 1970, Tukey's HSD test showed that, when compared to the stony flats there was significantly higher mesquite cover in the riparian zone ($Q = 10.3$, $P<0.01$) and red loamy soils ($Q = 9.2$, $P<0.01$) but no difference between the former two land types ($Q = 1.2$, $P>0.01$). In 2001, there was considerably higher mesquite canopy cover over the riparian zone than the stony flats ($Q = 20.5$, $P<0.01$) and red loamy soils ($Q = 14.5$, $P<0.01$) and considerably more cover on red loamy soils than on stony flats ($Q = 5.9$, $P<0.01$) (Table 4.1).

4.3.5 Ground verification of canopy cover densities within quadrats

The relationship between mesquite canopy cover per quadrat (%) observed in the field and that estimated from image processing within the 60 ground truthing quadrats was found to have a strong linear relationship ($R^2 = 0.98$; Figure 4.6). The strongest correlation was found within the low density class ($R^2 = 0.95$), which is important as over 69% of quadrats had such canopy cover in the 2004 image. Canopy cover in the high cover class (>90%) were well matched in the field ($R^2=0.55$), however, this correlation is stymied by the fact that image processing results showing >95% could only be identified as 100% cover in the field. This class made up <1% of quadrats in the 2004 image, as much of the high cover had been removed by control methods by this time. The correlation in the moderate density class was also high ($R^2=0.74$). However, after results were compiled it was found that a large gap existed between 60-90% cover. The cause of this gap was a direct result of randomly sampling quadrats within such a wide class (30-90%) as there were more quadrats potentially selectable in the 30-60% range (14% of test area) than the 60-90% range (4% of test area). A more robust approach would, therefore, be to select an additional 15 quadrats in the 60-90% range. Certainty of correctly calculating cover from image processing in the 60-90% range can only be assumed to be similar to the quadrats sampled in the 30-60% range.

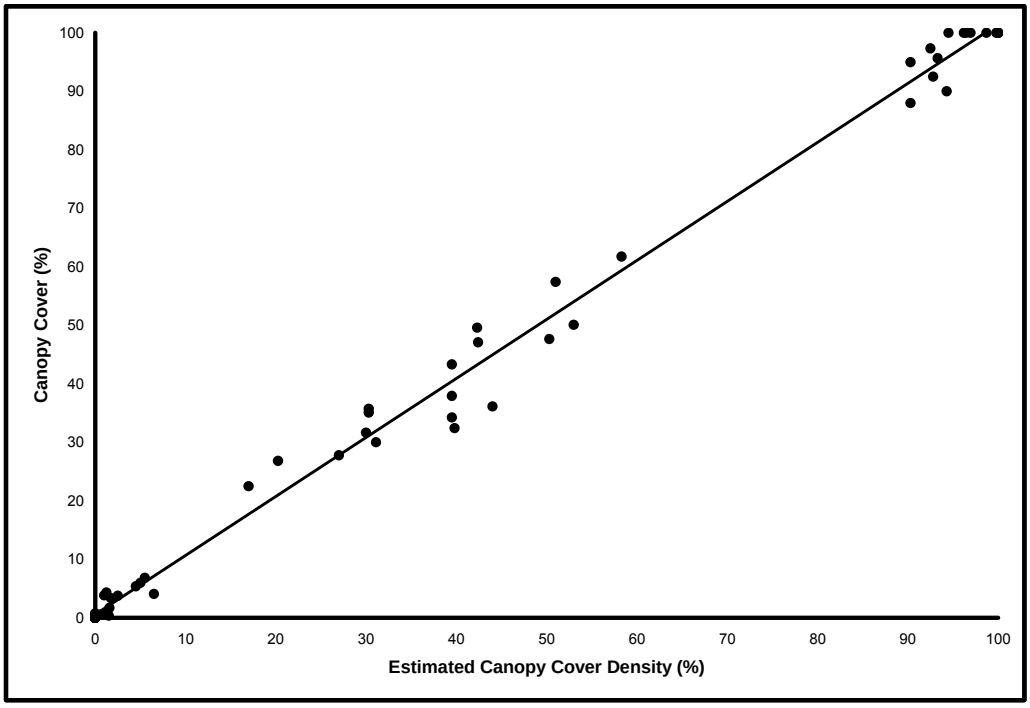

Figure 4.6 Field measurements of canopy cover plotted against estimates of canopy cover found from image processing within 60 randomly selected 20 x 20 (400 m^2) quadrats ($Y = 1.01x + 1.25$, $R^2 = 0.98$, $P<0.001$).

Estimates of canopy cover in the zero cover class were perfect except for two quadrats containing one individual mesquite shrub each. Approximately 12% of quadrats in 2004 were in this class. The largest mesquite shrub found within this class in the field that was not detected from image processing had a canopy diameter of 2 m and a surface area of 2.95 m^2. Furthermore, the smallest shrub that was detected from image processing and corroborated in the field had a surface area of 3.3 m^2, with the longest diameter spanning 3 m with a diameter perpendicular to it of 2 m. Therefore, the minimum detectable canopy size, using 1.4 m resolution imagery, appears to be within the range of approximately 2.95 m^2 and 3.3 m^2.

4. 4 Discussion

Longitudinal studies using aerial photographs to monitor mesquite cover in its native range have indicated rates of increase between 0.4% $year^{-1}$ and 1.2% $year^{-1}$. For example, rates between 0.4 and 1.2% $year^{-1}$ have been observed in South Texas (Archer et al., 1988); 0.7 to 1.1% $year^{-1}$ in New Mexico (Warren et al., 1996; Goslee et al., 2003); and 0.6% $year^{-1}$ in Arizona (Glendening, 1952). Differences in reported

rates of mesquite cover increases are the results of differences in initial canopy cover, soils, precipitation (Ansley et al., 2001), availability of dispersal agents, and the time it took for initial mesquite plants to reach detectable sizes. However, from these reports it can be assumed that long-term increases in mesquite cover in its native range rarely exceeds 1% $year^{-1}$ (Ansley et al., 2001). In this study, rates of increase became more rapid between the two periods examined (0.09 to 0.71% $year^{-1}$). Rates of increase observed in the second period (0.36 to 1.16% $year^{-1}$, depending on land type) were, thus, comparable with those observed for native range mesquite populations (Ansley et al., 2001).

Mesquite showed a strong preference for riparian and red loamy soils over stony flats, as reflected by a higher rate of initial colonisation by patches, higher rate of increase in canopy cover and the formation of larger patches. This could be due to both higher propagule pressure and higher recruitment, although it is not possible to differentiate these mechanisms using the data extracted from the aerial photographs. Stony flats have low grass cover (van Klinken et al. 2006), and herbivores are therefore likely to spend less time grazing, and will consequently deposit fewer seeds there (Andrew, 1988; Brown and Carter, 1998). Also, stony flats present a harsh environment for the establishment and growth of young plants, as indicated by the low densities of perennial grasses and shrubs found there (van Klinken et al. 2006), and is a likely explanation for the relatively slow increases in patch sizes. Nonetheless, patch number and size did increase dramatically over stony flats in the period from 1970 to 2001, supporting conclusions based on demographic data that suggests that mesquite densities will continue to increase over all land types (van Klinken et al. 2006).

Mesquite had already spread throughout the 450 ha site by 1970, including into areas that would rarely, if ever, have been inundated (e.g. stony flats), within approximately 35 years of being introduced to the area. In the following 31 years patch formation continued, and existing patches increased in size. This invasion pattern is therefore consistent with dispersal occurring primarily through the gut of animals, rather than by extreme flood events. An important ecological difference between invasive mesquite populations in its native range and the study population in Western Australia is the dispersal agents. A wide range of animal species consume

mesquite pods and subsequently disperse viable seed in both the native and introduced ranges (van Klinken and Campbell 2001; Pasiecznick, 2001). The introduction of cattle is considered to be responsible for the rapid spread of mesquite within its native range from riparian zones into uplands in historical times (Brown and Archer, 1987). An important factor is that a high proportion of seeds survive the passage through the digestive system of cattle, ca 60% (Brown and Archer, 1987). In contrast, the study property in Australia had sheep through the twentieth century (Van Vreeswyk et al., 2004; T. Patterson pers. comm. 2004), and the most abundant dispersers were therefore sheep and macropods. Sheep grind their food, and as a result seed survival through to the dung is very low (ca 13%; Cox et al., 1993). Seed survival through macropods is not known, but they grind their food in a similar manner to sheep (Griffiths and Barker, 1966). Much higher rates of patch formation may therefore be expected in this region with the recent introduction of cattle.

The invasion process mirrors the early phase of mesquite invasion in its native range, at least in the riparian zone and red loamy soils where coalescence of patches was common. However, in its native range, Archer (1995) observed that as mesquite plants matured they often served as nursery sites for native shrubs, facilitating the ingress and establishment of subordinate woody species from other habitats. These subordinate species may ultimately replace mesquite, resulting in successional change from grassland to mesquite shrubland to native non-mesquite shrubland (Archer, 1995). Individual mesquite patches were not tracked in this study; however, no decline in mesquite density was recorded in any 20 x 20 m quadrat, suggesting that mesquite is relatively long-lived (or the study period is too short to detect mortality) or that dying plants are being replaced by mesquite. Also, field based studies have found no evidence that mesquite is passively facilitating the ingress of native shrubs throughout the population studied (van Klinken et al. 2006). Thus, in the current context, successional change beyond mesquite shrubland seems unlikely.

Mesquite could not be discriminated from native background shrubs and trees using aerial photography due to the poor spectral resolution of the aerial photographs. Access to an image prior to invasion by mesquite assisted in overcoming this constraint, although it does assume that mesquite did not replace native vegetation,

mesquite did not reside in the understorey of native vegetation, and that there was no subsequent change in native vegetation cover. However, native vegetation that was removed had a similar shape and size for all subsequent years, suggesting it was not mesquite. Mesquite has been introduced to several areas throughout the world, and in many cases after the commencement of aerial photography (e.g. Harding and Bate, 1991). Therefore, the methods used for mesquite extraction in this study may have wide application. Notwithstanding, recent advances in object oriented image processing software has assisted discrimination between species in panchromatic imagery, typically by including such variables as shape, size, scale and colour, coupled with user defined membership functions such as mean brightness values and relationships between layers segmented at different scales (e.g. Laliberte et al., 2004; McGlynn and Okin, 2006). As the three main woody vegetation types in this study exhibit a unique shape and the canopy size of native vegetation is consistent, this software may be appropriate for future studies, particularly one aimed at broad scale mapping of mesquite from panchromatic and other very high resolution imagery.

The required spatial resolution for mapping weed patches has been estimated as less than one-quarter of the smallest patches that need to be mapped (Hunt et al., 2005). In this research it was determined that the spatial resolution of the aerial photography was sufficient to reliably detect individual small adults with a canopy of approximately 3 m^2. This suggests that a spatial resolution of approximately one-half the size of the shrub requiring detection may be adequate for mapping mesquite. Current panchromatic satellite imagery provides higher spatial resolution than most historical aerial photography (e.g. IKONOS-2, 1 m; CartoSat-2, 0.8 m; QuickBird, 0.61 m), and therefore may be able to detect shrubs with canopies smaller than 3 m^2. However, the most promising options for effectively detecting and differentiating isolated mesquite plants from other species clearly requires similar resolution to that obtainable from current high resolution panchromatic imagery, but with greater spectral information, which is the focus of Chapter 6.

4. 5 Summary

Historical archives of aerial photography provide a rare data source for quantifying rates and characterising patterns of plant invasions. Canopies of a ca 70 year old exotic mesquite population in Western Australia were extracted from a temporal

series of panchromatic aerial photography over an area of 450 ha using unsupervised classification. Non-mesquite trees and shrubs could not be differentiated from mesquite, and so were masked out using an image acquired prior to invasion. The accuracy of this technique was corroborated in the field and found to be high (R^2 = 0.98, P<0.001); however, accuracy varied between classes. The strongest correlation was found within the low density class (R^2 = 0.95), which is important as over 69% of quadrats had such canopy cover in the 2004 image. Canopy cover in the high cover class (>90%) were well matched in the field (R^2=0.55), however, this correlation is stymied by the fact that image processing results showing >95% could only be identified as 100% cover in the field. This class made up <1% of quadrats in the 2004 image, as much of the high cover had been removed by control methods by this time. The correlation in the moderate density class was also high (R^2=0.74). However, there were no samples taken in the 60-90% cover class. This was a direct result of randomly sampling quadrats within such a wide class (30-90%) as there were more quadrats potentially selectable in the 30-60% range (14% of test area) than the 60-90% range (4% of test area). A more robust approach would, therefore, be to select an additional 15 quadrats in the 60-90% range. Certainty of correctly calculating cover from image processing in the 60-90% range can only be assumed to be similar to the quadrats sampled in the 30-60% range. Only shrubs >3 m^2 could be reliably detected with the 1.4 m spatial resolution of the imagery used. Rates and patterns of invasion were compared to mesquite invasions where it is native. It was determined that: (i) the shift from grass to mesquite domination has been rapid, with rates of increase in canopy cover comparable to invasive populations in its native range; (ii) rate of patch recruitment was high in all land types, including stony flats, but patch expansion and coalescence primarily occurred in the riparian zone and red loamy soils; (iii) sheep and macropods have been the main vectors of spread; and (iv) early successional patterns, such as high patch initiation followed by coalescence of existing stands, are similar to those where mesquite is native, but patch mortality was not observed.

5 MODELLING THE SUITABILITY OF THE PILBARA REGION TO MESQUITE INVASION

5. 1 Introduction

Numerous modelling approaches have been applied to identify suitable habitats for a variety of purposes, including conservation (e.g. Loiselle et al., 2003) and invasive species management (e.g. Robertson et al., 2004). An important criterion governing the adoption of any one particular model is the amount of conservatism planners or land managers are willing to accept and how the model's predictions are going to be applied. For example, Loiselle et al. (2003) compared several models for conservation planning and concluded that some consistently produce more conservative estimates than others. They argued that in conservation planning, a conservative prediction (e.g. few false positives) will ensure that the site selected to protect the species is highly likely to be suitable for that species and therefore, the models that produced the more conservative estimates were most applicable. In contrast, when models are used to identify regions at risk from invasive plants, false positives may be viewed as less costly than false negatives (Fielding and Bell, 1997). This is because a more conservative estimate may omit areas that are actually suitable and therefore only be detected when the invasive species is well established (Robertson et al., 2004). At this stage it is often too late and too expensive to implement effective eradication programmes (Rejmanek and Pitcairn, 2002).

BIOCLIM (Busby, 1991) is a common profile model that may be viewed as conservative because it integrates evidence using a conservative Boolean AND operator. For example, if most conditions thought to promote invasion are ideal, yet one condition is standardised to '0', it is removed from consideration. Group discrimination techniques, such as logistic regression, may also render conservative estimates because they assume that existing sites represent the entire range that can be occupied by the target species. If the range of the species is still actively expanding, this is unlikely to be a valid assumption (Goslee et al., 2006). By assigning those areas as absent (or pseudo-absent), logistic regression models may exclude potentially suitable sites in its prediction. Some models have used a tally system to avoid excluding areas failing only one or a small proportion of conditions. For example, the Weed Invasion Susceptibility Prediction (WISP) model (Gillham et

al., 2004) sums binary predictor variables together to form a rating of suitability. If for example, only 8 out of 9 conditions are present, the result is 8, not 0.

Boolean standardisation has commonly been used to standardise predictor variables. For example, the BIOCLIM model identifies the minimum and maximum value of each predictor variable from distribution records and assigns to this range the value of 1. Values outside this range are coded 0. At least three major problems can be identified with such an approach:

(i) the assumption that this standardisation reflects the limits (climatic or otherwise) of the target species may be invalid for invasive species that have not yet occupied all suitable sites;

(ii) Boolean standardisation does not incorporate the notion that within the range identified, there is likely to be a scale of favourability; and

(iii) the crisp nature of Boolean standardisation means that pixels outside of the suitability range are excluded. For example, if a species can survive temperatures ranging from 10^{o}C to 40^{o}C, is it appropriate to exclude areas exhibiting temperatures of 9.9^{o}C or 40.1^{o}C?

A further deficiency of many models used throughout the literature is that they do not assign greater importance to predictor variables that are likely to have more impact in defining the areas suitable for invasion. For example, climatic models (e.g. BIOCLIM) assume that all climatic variables are equally important. Likewise, the WISP model assumes that all predefined variables have the same impact on predicting the suitability ranges of the target species.

In this chapter, ordered weighted averaging (OWA) is introduced to the field of ecological modelling for identifying the suitability ranges of mesquite. OWA represents an alternative to simply implementing models that generally return cautious results (as might be appropriate for conservation planning) or those that return broader potential areas of suitability (as might be appropriate for modelling the suitability of a region to biological invasion). This is achieved by altering the decision strategy space through a set of ordered weights and can produce models that

characterise locations by their worst quality (strongly conservative), their middle-most quality (intermediately conservative), or by their best quality. In fact, ordered weighted averaging can also produce any possibility in-between these three reference points. The disadvantages of crisp sets (e.g. Boolean standardisation), particularly in the standardisation of continuous variables, are avoided in this study through the use of fuzzy membership functions, which have been shown to produce better results when applied to model the suitability of areas to invasion from plants and insects (e.g. Robertson et al., 2004). A weighting method is used (pairwise comparison) to assign more importance to variables likely to have greater influence in dictating the suitability ranges of mesquite. These techniques directly incorporate the knowledge derived from Chapter 4, which identified that:

(i) mesquite prefers to establish in certain land types than others;
(ii) mesquite prefers the more mesic parts of the landscape; and
(iii) rapid invasion (including thicket formation) is the result of dispersion through the dung of vertebrate herbivores, particularly cattle; however, to a lesser extent, seedlings have also been observed to grow out of the excrement of sheep, emus and wallaroos (Osmond et al., 2003).

Recent literature has generally advocated the use of relative operating characteristic (ROC) plots for model evaluation, over more traditional measures such as the maximum Kappa (e.g. Fielding and Bell, 1997; Pontius and Schneider, 2001; Liu et al., 2005). However, the maximum Kappa method is still commonly used for evaluation (e.g. Robertson et al., 2003; 2004). Therefore, an additional aim of this study was to investigate whether the choice of one technique over the other would affect the final prediction of areas identified to be suitable for mesquite invasion.

5. 2 Description of Techniques

The following section describes the theory behind the modelling techniques used in this study.

5.2.1 Weighted linear combination (WLC)

WLC is a common technique that involves the integration of multiple criteria (layers) to arrive at a solution. Each layer is first standardised to a common numeric range

(e.g. via fuzzy sets; see Section 2.5.2.2) and multiplied by a weight based on its relative importance to the solution. Weights must be chosen so that their sum is equal to '1', and can be derived using pairwise comparison (Saaty, 1990; see Section 5.2.3). All weighted layers are then summed over all coincident pixels. In the context of predicting the suitability of a region for invasion, the pixels receiving the highest overall score (maximum = 1; minimum = 0) represent the highest suitability. Values less than 1 and greater than 0 represent a continuum of suitability that requires interpretation based on its magnitude.

5.2.2 Standardisation of categorical maps

The main *raison d'être* for standardising categorical maps is to assign importance to each of the categories on a scale of 0 to 1. Essentially, this is identical to weighting each of the categories, except that most weighting schemes (e.g. pairwise comparison) assign weights so that their sum equals 1. Normalisation of the derived weights can transform these weights to values within the range of 0 to 1, where 1 represents the most favourable conditions and 0 the least. One weighting method that can be transformed in this manner is known as the ranking, whereby each category is ranked in order of perceived importance. Once the ranking is established, the rank exponent method can be utilised according to the following formula (Malczewski, 1999):

$$w_j=(n-r_j+1)^p \tag{5.1}$$

where: w_j= the weight for the jth criterion;

n= the number of criteria (layers) under consideration;

r_j= the rank position of the criterion (layer); and

p = the exponent value. As p increases, the less weight is given to lower ranked factors.

The weights derived from equation 5.1 can then be divided by the highest w_j to derive a standardised score (normalisation).

Continuous layers can be standardised using fuzzy membership functions and the reader is directed to Section 2.5.2.2 for a discussion on their use.

5.2.3 Pairwise comparison for weight estimation

Pairwise comparison can be used to assign values of importance (weights) to each of the layers in the model. This method was developed by Saaty (1977) in the context of the decision making process known as the Analytic Hierarchy Process (AHP) (Malczewski, 1999). Each layer is compared to each other in turn using a nine point scale (Table 5.1) based on their suitability for the stated objective. For example, where the objective is identifying areas most susceptible for weed invasion, soil moisture may be compared to land types. If soil moisture is considered to be very strongly more important than land types, then one would enter 7 in the pairwise matrix.

Table 5.1 The fundamental scale on which pairwise comparisons are based.

Intensity of importance on absolute scale[1]	Definition	Explanation
1	Equal Importance	Two layers contribute equally to the objective
3	Moderate importance of one over another	Experience and judgement modertately favour one over another
5	Strong importance	Experience and judgement strongly favour one over another
7	Very strong importance	Experience and judgement very strongly favour one over another
9	Extreme importance	Experience and judgement extremely favour one over another - highest affirmation
2,4,6,8	Intermediate values between two adjacent judgements	When compromise is needed
Ricprocals	If layer *i* has one of the above numbers assigned to it when compared to *j*, then *j* has the reciprocal assigned to it when compared with *i*	

[1]If the layers being compared are closer together than integer numbers given, then decimals can be given.
Table adapted from Saaty (1987).

Once all candidate layers have been compared and relevant values have been entered into the matrix, weights can be calculated using the following operations: (a) sum the values in each column of the pairwise comparison matrix; (b) create a normalised pairwise comparison matrix by dividing each element in the matrix by its column total; and (c) sum the elements in each row of the normalised matrix and divide by the number of layers (Malczewski, 1999).

A measure can also be devised to determine if the comparisons have been made consistently throughout the matrix. This is necessary, because the matrix is constructed from expert opinion and therefore it is possible for a decision maker's judgement to change throughout (Saaty, 1977). It involves the following operations:

(a) determine the weighted sum vectors using matrix multiplication of the weights (presented in one column) by original pairwise comparison matrix; (b) divide each weighted sum vector by its respective layer weight determined previously to obtain α; and (c) sum all α values together and divide by the number of layers (n) to derive λ. The consistency index, which is a measure of departure from consistency, can then be calculated using:

$$CI = (\lambda - n)/(n - 1) \quad (5.2)$$

Finally, the consistency ratio can be calculated using:

$$CR = CI/RI \quad (5.3)$$

where: RI is the random index, the consistency index of a randomly generated pairwise comparison matrix (see Table 5.2). A CR<0.1 indicates a reasonable level of consistency, whereas a CR>0.1 indicates the original matrix should be revised.

Table 5.2 Random Inconsistency Index (RI) for n= 1,2,…,15 (adapted from Saaty, 1990).

n	RI	*n*	RI	*n*	RI
1	0.00	6	1.24	11	1.51
2	0.00	7	1.32	12	1.48
3	0.58	8	1.41	13	1.56
4	0.90	9	1.45	14	1.57
5	1.12	19	1.49	15	1.59

5.2.4 Trade-off and risk

Models that use the Boolean AND operator (e.g. profile techniques such as BIOCLIM (Busby, 1991)) do not allow poor qualities in one layer to be compensated for ("traded-off") by excellent qualities in another layer. The output of the Boolean AND operator is governed by its worst quality at each coincident pixel. Therefore, it is regarded as a low risk operator, with no potential for trade-off (see Figure 5.1). For the final prediction to be suitable, all criteria must also be considered suitable. For example, if all criteria at an arbitrarily defined pixel are considered highly suitable for invasion, yet one is deemed to be unsuitable, that pixel will be considered to be unsuitable. In terms of risk, this is considered to be a conservative solution. As mentioned in the introduction, in conservation planning this would be an acceptable approach as only areas found to be highly suitable over all criteria

would be considered for species protection, and therefore represents areas with a high likelihood of survival. However, in invasive species management, such an approach may underestimate potentially suitable sites, where one poor quality may not be sufficient to exclude the potential for invasion. Hence, in this context, a conservative approach that does not allow poor qualities to be traded-off may jeopardise invasive species management and early detection.

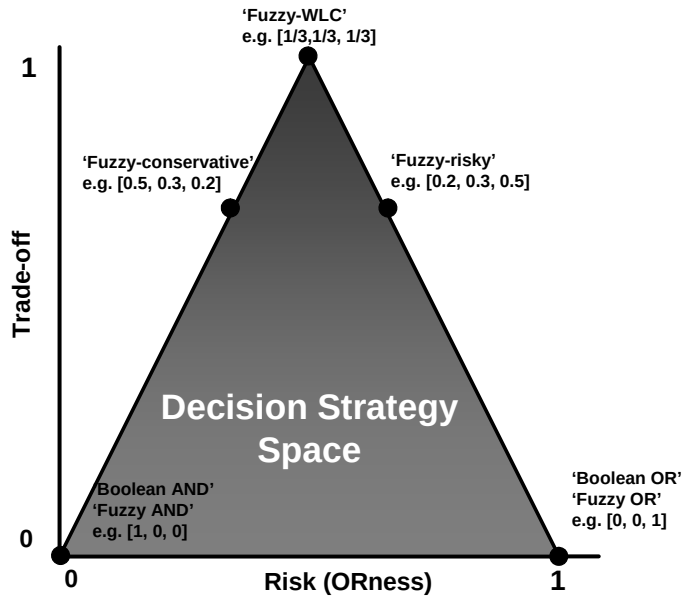

Figure 5.1 Conceptual depiction of the relationship between risk and trade-off. Order weights can be used to produce a solution at any point on the decision strategy space triangle.

On the opposite end of the risk scale, the Boolean OR operator treats each layer as sufficient evidence to solve the objective under consideration, because only one pixel need be suitable over all coincident pixels for that pixel to represent high suitability; however, like the Boolean AND does not permit layers to trade-off (see Figure 5.1). This operator is therefore considered risky because the poorer qualities are ignored in the prediction. This is likely to be inappropriate for conservation planning, but, depending on the criterion that is considered highly suitable, may highlight the worst possible distribution of an invasive species. For example, a high level of suitability for just one criterion may be sufficient to enable invasion.

Under WLC, the assignment of weights to each standardised layer allows them to fully trade-off against each other and therefore neither considers layers as necessary

or sufficient (Figure 5.1). Poorer qualities are not ignored but rather can be compensated for by layers with greater perceived importance for increasing the suitability of an area to invasion. Thus, WLC provides a solution that falls exactly in the middle of the Boolean AND operation and the Boolean OR operation (Eastman, 2006; Figure 5.1).

5.2.5 Manipulating trade-off and risk using ordered weighted averaging (OWA)

The theory of OWA was first established by Yager (1988). This technique can be used to augment WLC to allow solutions to fall anywhere along the risk/trade-off scale (Figure 5.1) and therefore the amount of risk can be directly tailored to the application of the model (e.g. conservation planning or invasive species management). Order weights do not apply to a specific layer, but rather are applied on a cell-by-cell basis as determined by their rank ordering across all layers. Order weight '1' is assigned to the lowest ranked layer for a particular pixel, order weight '2' to the next lowest ranked layer at the same location and so on until all pixels have been assigned an order weight for all layers (Eastman, 2006). The number of ordered weights used must be equal to the number of layers used in the model and must also sum to '1'.

Since each cell is ordered from lowest to highest, selecting values for the ordered weights that when graphed would present a right-skewed histogram produces a more risk adverse solution than WLC and vice versa. For example, for three layers, ordered weights of [0.5, 0.3, 0.2] would produce a more risk adverse solution than ordered weights of [0.2, 0.3, 0.5] (Figure 5.1). Ordered weights can also be chosen to create an image identical to WLC, the fuzzy AND or the fuzzy OR. They take w=[1/n, 1/n, …, 1/n], w=[w_1, w_2, …, w_n]=[1, 0, …, 0] and w=[w_1, w_2, …, w_n]=[0, 0, …, 1], respectively, where w is the weight vector comprising n weights, where n corresponds to the number of layers under consideration. The fuzzy AND is equivalent to the Boolean AND, except that it returns the minimum value of coincident pixels for all layers that have been standardised to a grade of favourability. Likewise, the fuzzy OR is the equivalent of the Boolean OR for layers standardised to a continuous scale of favourability whereby the maximum value of coincident pixels amongst all layers considered is returned.

The set of chosen ordered weights can be classified with respect to their position between AND and OR (Figure 5.1) by using measures known as ANDness, ORness and trade-off, as follows (Yager, 1988; Malczewski, 1999):

$$ANDness = \frac{1}{n-1}\sum_r (n-r)w_r \tag{5.4}$$

$$ORness = 1 - ANDness \tag{5.5}$$

$$Tradeoff = 1 - \left[\frac{n\sum_r (w_r - 1/n)^2}{n-1}\right]^{0.5} \tag{5.6}$$

where: n is the number of layers;

r is the order of the layers; and

w_r is the order weight for the layer of the r^{th} order.

5. 3 Model Design

A six step process was used to model the suitability of the Pilbara region to mesquite invasion. These steps are described in more detail hereafter.

5.3.1 Step 1: Define layers

Temporal analyses of aerial photographs (Chapter 4) quantified habitat associations of mesquite at a local scale. In particular, mesquite showed a strong preference to alluvial soils than to stony/crusted soils. The regional aerial survey provided further evidence of these habitat associations, revealing a strong correlation with land systems that had high pastoral potential (van Klinken et al., 2007). Pastoral potential is based on the number of hectares required to sustain the nutritional requirements of a unit of cattle (carrying capacity) based on the pasture type(s) found within each land system (Payne and Mitchell, 2002). Therefore, a layer of pastoral potential was sourced from the Department of Agriculture and Food, Western Australia (DAFWA) for this study (see Section 3.4.2 for a description and summary of this layer).

Chapter 4 also provided evidence that mesquite is dispersed through the dung of vertebrate herbivores, including livestock such as sheep and cattle. Native herbivores (e.g. emus and wallaroos) are also likely dispersers. The combination of

cattle browsing in high pastoral potential areas is likely to be a factor underlying the association between pastoral potential and high mesquite cover. Thus, there appears to be a synergistic effect between these two factors (van Klinken et al., 2007). Therefore, a layer depicting land use throughout the Pilbara Region was used in this study (see Section 3.4.2).

While high pastoral potential and the presence of a highly effective dispersal mechanism may enhance suitability, they are not necessarily sufficient. For instance, areas with high pastoral potential and the presence of cattle showed a very strong association with some habitats (especially flood plains and river deltas) but not others (e.g. gilgaied clay plains). This was identified in chapter 4, which demonstrated that soil moisture is a further requirement governing the suitability of an area for mesquite invasion. Therefore, a compound topographic index (CTI), which is a steady state wetness index, was derived from the digital elevation model (described in Section 3.4.4) for this study using the following formula (Gessler et al., 1995):

$$CTI=\ln(\alpha/\tan(\beta)) \tag{5.7}$$

where: α = upstream area calculated as (flow accumulation +1)*(pixel area in m^2)

β = slope expressed in radians.

Flow accumulation is calculated from a flow direction grid, which determines the water flow as the direction of steepest descent. Flow accumulation then records the number of cells that drain into an individual cell in the grid and is thus measured in units of grid cells (Olivera et al., 2002). Slope, in radians (β), was derived from the digital elevation model using the tools in ArcGIS (ESRI, 2004). The CTI derived for the Pilbara area studied is shown in Figure 5.2.

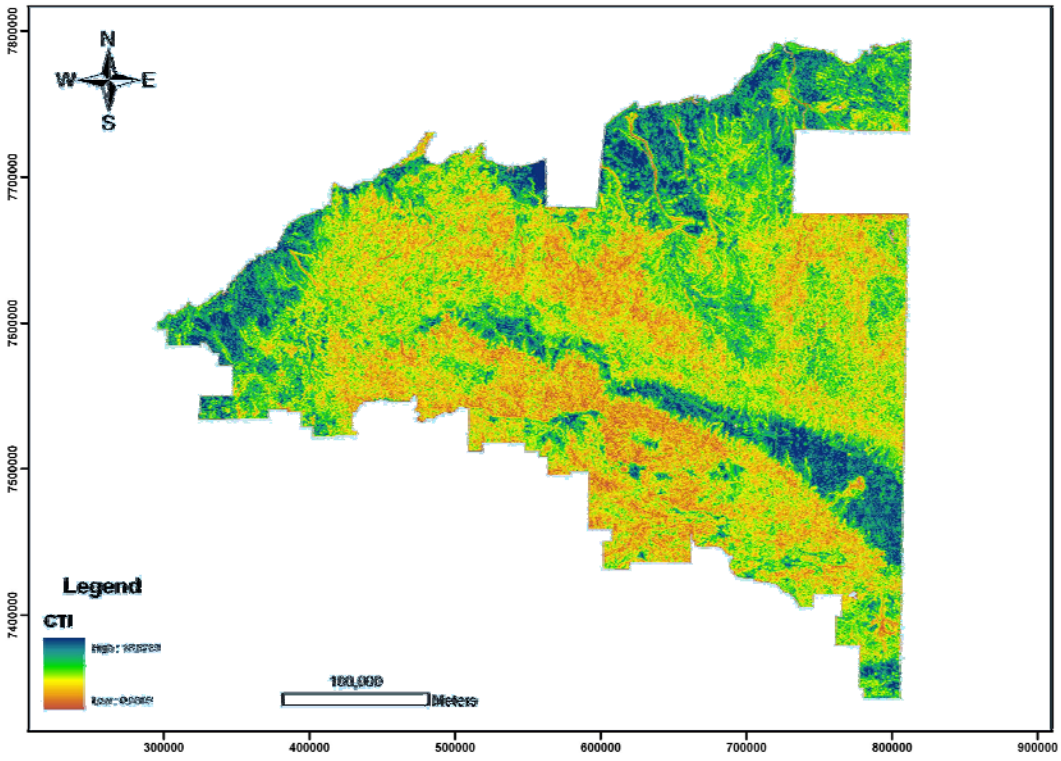

Figure 5.2 Compound Topographic Index (CTI) derived for the Pilbara Region.

5.3.2 Step 2: Standardise layers

The rank exponent method using an exponent of 2 was trialled as a standardisation tool in this study. The weights derived from this method were normalised, as described in Section 5.2.2. This technique was used to standardise both land systems (according to pastoral potential) and land uses. Pastoral potentials were ranked from 1 to 6, with 1 representing very high pastoral potential and 6 very low (Payne and Mitchell, 2002). The standardised values assigned to each of the pastoral potential ratings are shown in Figure 5.3.

Land uses were ranked according to their likelihood for promoting mesquite invasion, with the presence of cattle receiving the highest rank, based on the hypothesis that cattle are necessary, yet not sufficient, to generate extensive mesquite populations. It was deemed inappropriate to assign the other land uses to '0', since it would not account for other dispersal vectors (e.g. wallaroos and emus), which can also result in mesquite invasion and thicket formation, and would not allow the presence of other favourable criteria to compensate for the absence of cattle.

Therefore, all other land uses were ranked second. Consequently, land uses were standardised to '1' (representing the presence of cattle) and '0.25' (representing all other land uses) based on the rank exponent method (exponent=2) (Figure 5.4). The stock route (see Figure 3.11) was essentially ignored by assigning it to a contiguous class.

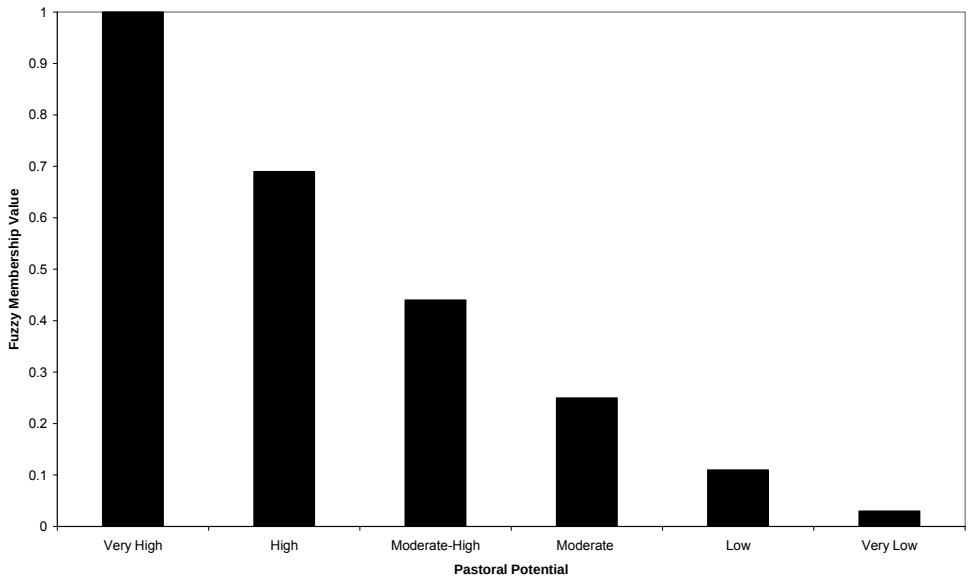

Figure 5.3 Fuzzy membership values assigned to each of the pastoral potential ratings.

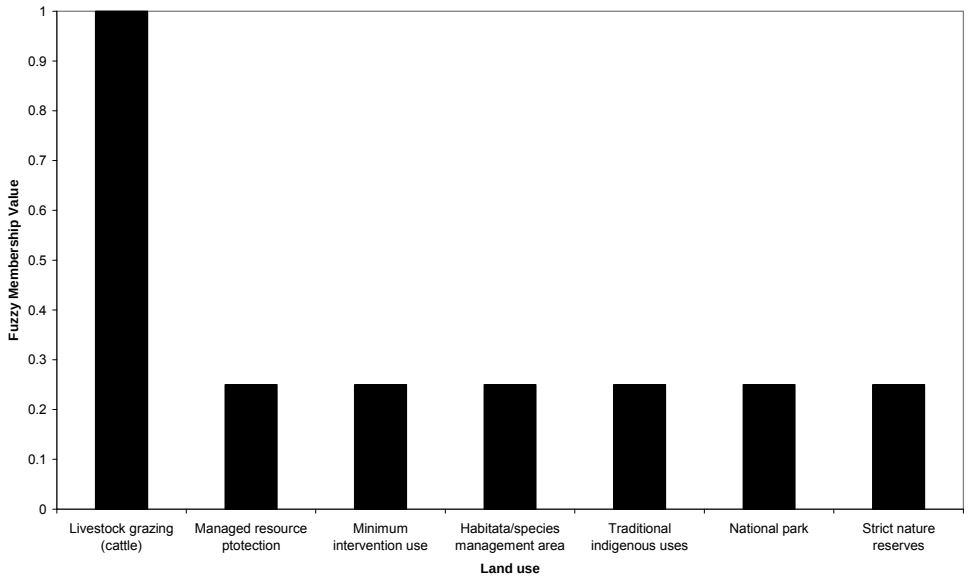

Figure 5.4 Fuzzy membership values assigned to each of the land uses.

A frequency histogram was constructed using 500 presence data (not used for validation) to assist in the identification of the required parameters to construct a fuzzy membership function to standardise the CTI. A right skewed distribution was found, with a minimum of 5.5, and a median of 9.4. A monotonically increasing sigmoidal function is considered appropriate for right-skewed data, where the minimum marks the point at which the membership function begins to rise above zero, and the median represents the point at which all values greater are assigned a value of one (Robertson et al., 2004). Therefore, the CTI layer was standardised using a monotonically increasing sigmoidal function (see Figure 5.5) using the following formula and parameters (Eastman, 2006):

$$\mu = \cos^2 \alpha \tag{5.8}$$

$$\alpha = (x - po\,\mathrm{int}\,a)/(po\,\mathrm{int}\,b - po\,\mathrm{int}\,a) * \pi / 2 \tag{5.9}$$

$$\text{if } x > point\ b,\ \mu = 1 \tag{5.10}$$

where: x=CTI of a pixel;

point a=5.5; and

point b=9.4;

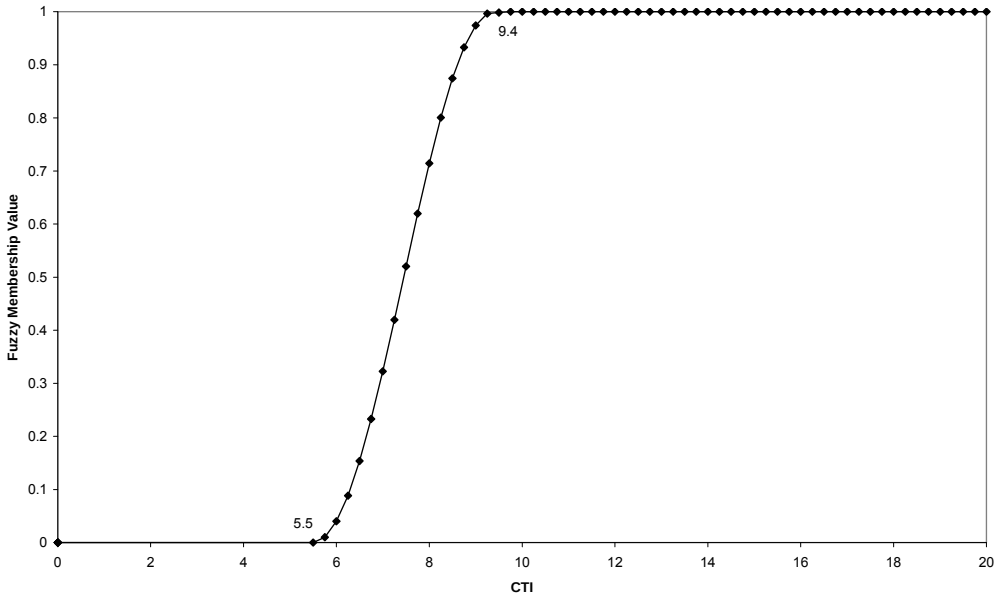

Figure 5.5 Fuzzy membership values assigned to the CTI layer.

5.3.3 Step 3: Derive and apply weights

Weights were derived using the pairwise comparison method as described in Section 5.2.3. The pairwise comparison matrix, derived weights and consistency ratio are shown in Table 5.3. Soil moisture (CTI) was considered slightly more important than pastoral potential (derived from land systems) based on the findings from Chapter 4 that showed that mesquite colonised and increased significantly more rapidly in the riparian zone than over the red loamy soils, even though both had the same soil type. Soil moisture was deemed to be moderately more important than land use because, although mesquite is successfully dispersed via livestock, with poor soil moisture it is less likely to survive. Pastoral potential was deemed to be slightly more important than land use for a similar reason: while seeds may be widely dispersed by livestock, they are unlikely to survive in harsh and poorly fertile soil.

Table 5.3 Pairwise comparison matrix used to weight each individual layer prior to assigning order weights.

	CTI	Pastoral potential	Land use	Weight
CTI	1	2	3	0.54
Pastoral potential	1/2	1	2	0.30
Land use	1/3	1/2	1	0.16

Consistency ratio = 0.01 (consistent)

5.3.4 Step 4: Apply ordered weights

OWA was used to create three outputs representing the suitability of the Pilbara area to mesquite invasion. Each model successively incorporated more risk, thereby also altering the level of trade-off in the final solution. Table 5.4 lists the model names assigned to each of the three model outputs along with the order weights applied. The degree of ANDness, ORess (risk) and trade-off inherent in the models is computed using Equations 5.4, 5.5 and 5.6 respectively. Figure 5.1 also illustrates these parameters graphically.

Table 5.4 Order weights used to control the risk-trade-off continuum for the three knowledge driven models computed.

Model Name	Order Weights	ANDness	ORness	Trade-off
Fuzzy Conservative	[0.5, 0.3, 0.2]	0.65	0.35	0.73
Fuzzy WLC	[1/3, 1/3, 1/3]	0.5	0.5	1
Fuzzy Risky	[0.2, 0.3, 0.5]	0.35	0.65	0.73

5.3.5 Step 5: Validate model

In order to reduce the impact of spatial dependency and bias in the observations, an arbitrary 500 samples were randomly selected from the aerial survey for both presence and absence of mesquite (1000 samples in total; see Figure 5.6) (Huberty, 1994; Fielding and Bell, 1997). It is a necessary assumption that these samples represent true presences and absences; however, evidence suggests that mesquite is still rapidly expanding, so has unlikely reached its full distribution (van Klinken et al., 2007; Robinson et al., 2008). These validation data were then used to construct a relative operating characteristic (ROC) plot, which plots the false positive fraction (FPF; 1-(true negatives/(true negatives + false positives))) against the true positive fraction (TPF; ((true positives/true positives) + false negatives)) for a set number of thresholds (see Section 2.5.4.2). The area under the curve (AUC) was calculated using the trapezoidal rule, as follows (Pontius and Schneider, 2001):

$$AUC = \sum_{i=1}^{n} [x_{i+1} - x_i][y_i + y_{i+1} - y_i / 2] \tag{5.11}$$

where: x_i is the false positive fraction at threshold *i*;

x_{i+1} is the false positive fraction at threshold *i+1*;

y_i is the true positive fraction at threshold *i*; and

y_{i+1} is the true positive fraction at threshold *i+1*;

An AUC of 0.5 indicates that the suitability values are assigned at random locations throughout the region and an AUC of 1 indicates a perfect model (Ayalew and Yamagishi, 2005). AUC values can be interpreted as indicating the probability that, when a presence site and an absence site are drawn at random from the population,

the first will have a higher predicted value than the second (Elith et al., 2006). In this study, each model was 'sliced' 100 times by ranking the highest 1% of suitability at slice '1' and assigning these cells to '1' and the other 99% to '0', the highest 2% at slice '2' until slice '100' had all pixels assigned '1'. The TPF and FPF were determined at each slice, allowing the AUC to be calculated based on 100 data for each model. The ROC plot and AUC was then used to compare the models to determine which was the most accurate. For example, a model with a higher AUC and a ROC plot that consistently outperforms other models is deemed the most accurate, because it minimises both false negatives (mesquite present, but model fails to predict it) and false positives (mesquite absent, but model predicts it as present) (Zweig and Campbell, 1993; Fielding and Bell, 1997).

5.3.6 Step 6: Examine optimal cut-points

Cut-points are often used to transform the results of suitability models derived on a continuous scale to one representing predicted presences/absences (Liu et al., 2005). Two approaches were examined in this study. The first approach was based on selecting the point on the ROC curve that is closest to the upper left corner (0,100%) since that point represents a perfect classification (Cantor et al., 1999; Liu et al., 2005). The second approach was based on the Kappa statistic. The equation for its calculation is shown in Section 2.5.4.1. This statistic is dependent on a single threshold to distinguish predicted presence from predicted absence (Fielding and Bell, 1997). Therefore, to identify the most reliable cut-point it needs to be calculated for all possible thresholds and the maximum value of Kappa chosen as the model most representative of the validation data (e.g. Robertson et al., 2003; 2004).

5. 4 Results

All three models produced on a continuous scale generally agree that the highest suitability of the Pilbara region to mesquite invasion predominantly occurs in relatively contiguous areas on the northern coastline (Figure 5.6). A narrow inland band of suitability is also prominent south-east of Pannawonica to just north of Newman.

In general, there is a good visual agreement between the presence data and the suitability values produced for the three models (Figure 5.6). However, while

average suitability is higher for presence data, suitability values for absent data are significantly greater than zero for all three models (Table 5.5).

Table 5.5 Average (and standard deviation) suitability values for presence and absence records for the three models implemented.

		Fuzzy Conservative	Fuzzy WLC	Fuzzy Risky
Average Suitability	Presence	0.71 ± 0.19	0.72 ± 0.14	0.79 ± 0.09
	Absence	0.43 ± 0.22	0.47 ± 0.19	0.57 ± 0.14

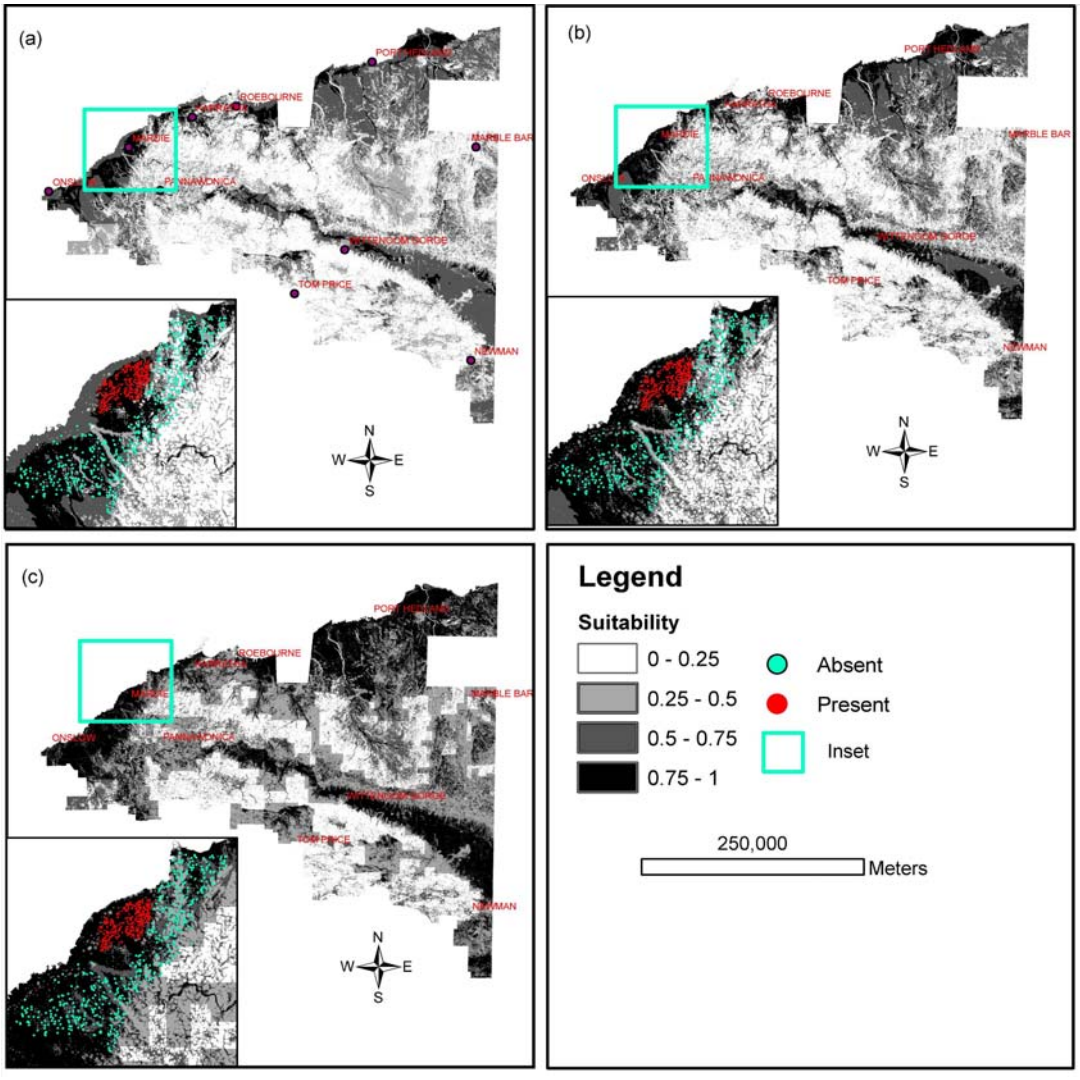

Figure 5.6 Model outputs illustrating the suitability of the study area to mesquite invasion: (a) Fuzzy Conservative; (b) Fuzzy WLC; and (c) Fuzzy Risky. Note the wider levels of suitability predicted between models.

Figure 5.7 shows the ROC curves for each of the three models. As can be seen from these curves, the 'fuzzy risky' model is deemed the most representative of the three, producing a higher true positive fraction, which corresponded with a lower false positive fraction for the majority of thresholds on which it was calculated. The AUC for this model was calculated to be 0.87, which was higher than the 'fuzzy conservative' model (AUC=0.80) and the 'fuzzy WLC' model (AUC=0.83). Figure 5.7 also illustrates the point at which the ROC curves are closest to the top left corner (0,100%), considered as the optimal cut-point as suggested by Cantor et al. (1999) and Liu et al. (2005). This was found to be the top 10% of ranked pixels for the 'fuzzy risky' model and corresponds to a TPF of 92% and a FPF of 23.4%. The top 15% of pixels were found to be the optimal cut-points for both 'fuzzy WLC' model (TPF=93.4%; FPF=36.2%) and the 'fuzzy conservative' model (TPF=88.6%; FPF=38.8%).

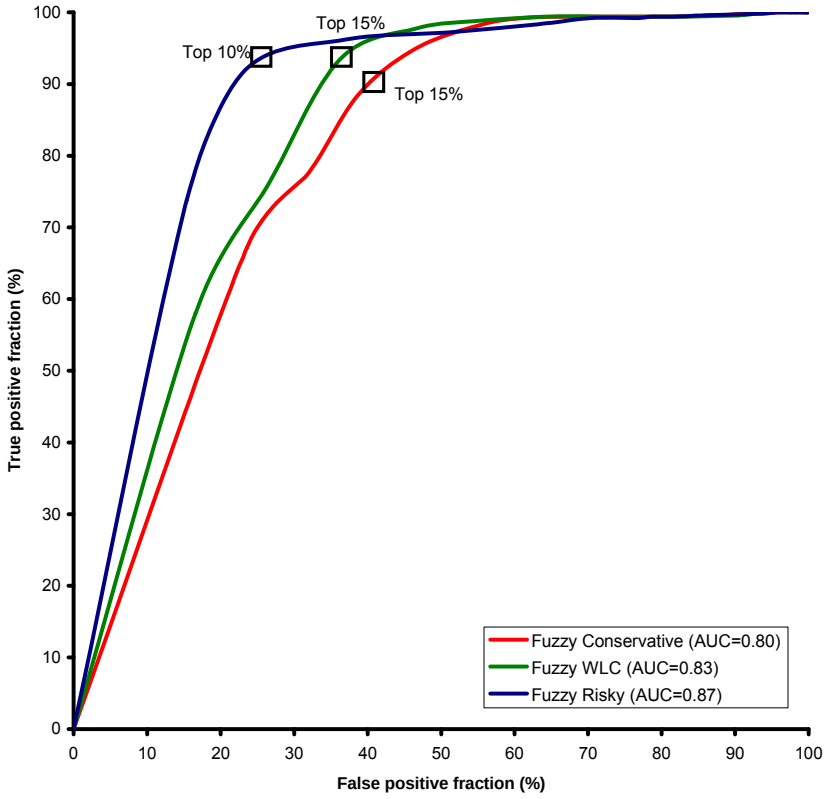

Figure 5.7 Relative Operating Receiver (ROC) plots for the three models implemented. Squares represent the closest point to the top left corner (optimal cut-points). Adjacent captions represent the percentage of ranked pixels (in descending order) that make up the optimal cut-point.

The maximum value of Kappa for all three models provided further confirmatory evidence that the 'fuzzy risky' model was the most representative of the presence/absence data. A maximum Kappa of 0.686 was found for the 'fuzzy risky' model, which can be described as a good to very good agreement with the presence/absence data using the ranges proposed by Monserud and Leemans (1992). As with the optimal cut-point method used on the ROC curves, the maximum Kappa was also found to be the top 10% of ranked pixels. The error matrix from which this value was calculated can be seen in Table 5.6 and shows that 92% of observed present data are predicted as being present and 77% of observed absence data are predicted as absent. The maximum value of Kappa for the 'fuzzy conservative' model was found to be 0.516, which can be described as a fair representation of the presence/absence data. The maximum Kappa method highlighted the top 18% of ranked pixels as the most representative of the presence/absence data, whereas the ROC plot highlighted the top 15%. The maximum value of Kappa for the 'fuzzy WLC' model was found to be 0.572 and can be described as having good agreement with the validation data. Maximum Kappa for this model was associated with the top 15% of ranked pixels and, therefore, coincided perfectly with that found from the ROC plot.

Table 5.6 Error matrix representing the number of pixels observed versus the number predicted from the 'fuzzy risky' model for the top 10% of pixels (Kappa = 0.686).

		Observed	
Predicted		Presence	Absence
	Presence	460	117
	Absence	40	383
	Totals	500	500
	Agreement	92%	77%

The optimal threshold obtained from both the ROC method (and corresponding Kappa maximum method) was used to create a Boolean image of suitability (Figure 5.8). The top 10% of pixels (blue pixels) represent tracts of land that have similar environmental attributes to those found where mesquite is currently present. Pixels ranked lower than the top 10% were assigned to '0' and represent areas less suitable to mesquite invasion (light brown/orange pixels).

Figure 5.8 shows that large pockets of the northern coastline, often associated with drainage features, are highly suitable for invasion by mesquite. In total, approximately 12,000 km^2 of the coastal areas (or 10% of the area modelled) are considered highly suitable. This also represents the concerns reported by Kendrick and Stanley (2001) who have identified permanent pools within 40 km of the coast on the Turner, Yule, Sherlock, Fortescue and Maitland Rivers as highly suitable for mesquite (and parkinsonia) invasion. Furthermore, they have also recognised that riparian zone vegetation along the Fortescue, Maitland, Turner, De Grey, George and Sherlock Rivers are prime habitats for mesquite invasion to occur, which have also been highlighted in this study (Figure 5.8). The relatively contiguous inland band of suitability is comprised of an area of roughly 6400 km^2 (5% of the area modelled). Thus, in total approximately 15% of the Pilbara region studied is considered to be highly suitable for invasion.

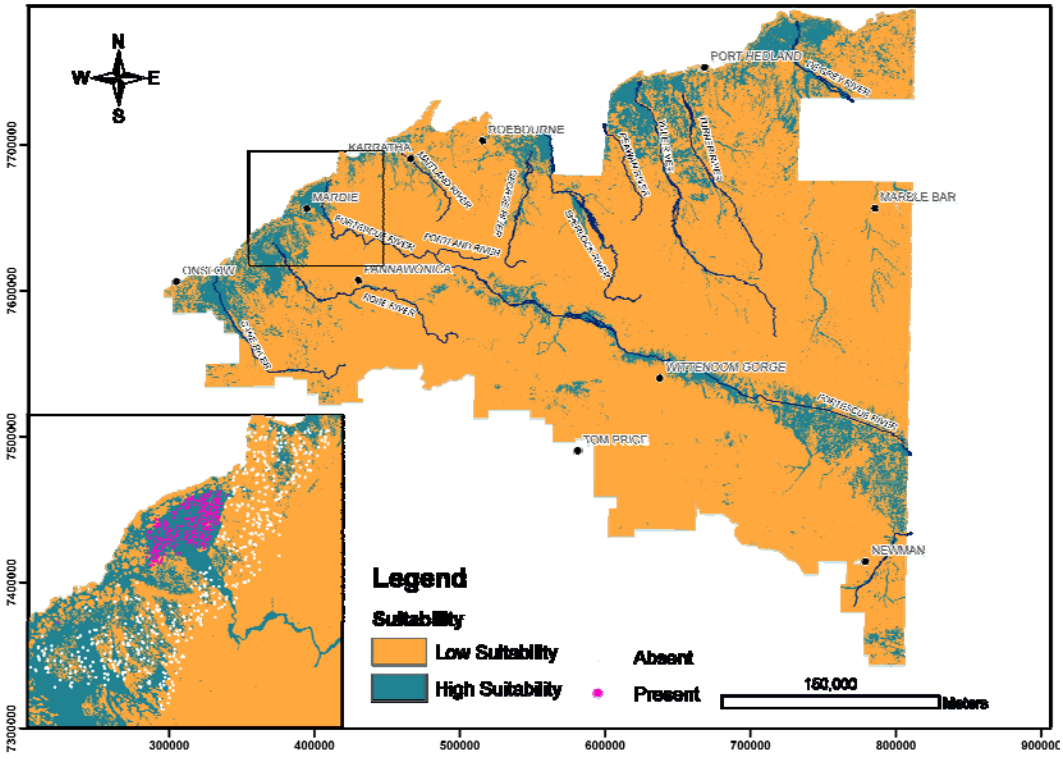

Figure 5.8 Map showing the suitability of the Pilbara to mesquite invasion split into two classes. Note the high suitability along the drainage systems and river mouths along the northern coastline.

5. 5 Discussion

In contrast to correlative models, the modelling techniques presented here do not rely on (direct or indirect) statistical correlations between the invasive species and environmental variables but rather incorporate existing *knowledge* of a particular species response to various environmental attributes. In this study such knowledge was incorporated using fuzzy membership functions (FMFs), which offer a flexible procedure for expressing the response of the target species to a particular environmental variable. In particular, FMFs are able to incorporate the notion that some conditions are more favourable than others and the differences are continuous. In addition, unlike correlative models, fuzzy membership functions can be developed without the need for presence/absence records and hence can be used for very isolated or recent introductions where the parameters for invasion are relatively well understood or where such records are difficult to obtain (e.g. remote rangelands) and/or too expensive to collect. While this is considered an advantage of such models, the somewhat subjective manner in which the FMFs are constructed can also be viewed as a weakness when compared to correlative models (e.g. logistic regression) where the shape of the response curves to environmental attributes are defined by the data in a more direct fashion (Robertson et al., 2004). However, to define such curves a sufficient sample size needs to be collected over all areas, which may rely on the generation of pseudo-absence records (random points throughout the study area assuming no presence or no likely presence of the target species) over areas where the species may not have had a chance to colonise. Such a process also has inherent risks.

The continuous representation of the suitability of a region to invasion from the models produced indicates to the map user a level of uncertainty in the prediction (Heuvelink and Burrough, 1993). These models show that while invasion may be unlikely in certain areas, the map user can identify as to what extent it is unlikely on a scale from ‘0’ to ‘1’, and thus can be interpreted as a continuum of suitability. For example, an area with a value of 0.5 may be somewhat unlikely for invasion, yet more likely than an area with a value of 0.1. Therefore, by incorporating and displaying the uncertainty of the input data used to create the model, these outputs attempt to optimise generality. By defining the optimal cut-points as the last stage of the analysis, the model is effectively transformed to optimise accuracy. While

valuable information is lost during this phase, the potential for favourable information to compensate for less favourable information has still been achieved. This is not true of crisply standardised models (e.g. basic profile techniques), where valuable information is discarded in the Boolean standardisation process at the first step of model building.

OWA enabled the production of three outputs, which represent different risk/trade-off scenarios. The best model was produced by assigning more importance to pixels ranked higher out of the three layers used. This is considered more risky than assigning equal ordered weights, or more importance to poorer ranked layers, because it considers favourable evidence as being more sufficient for enabling invasion, than just necessary. The fact that the conservative and WLC models performed poorer than the risky model suggests that assigning more importance to pixels with higher suitability increases the true positive fraction at a rate faster than the false negative fraction and, therefore, favourable evidence does not occur in tandem over many of the areas where absence data has been recorded.

This study demonstrated that the amount of risk inherent in each model can be directly altered through the manipulation of ordered weights. Suitability predictions can therefore be developed at any point on the risk/trade-off scale, so that predictions can be based on the poorest ranked ecological variable, the best ranked ecological variable or any ranking in between these two extremes. This is likely to be a desirable quality for a range of users of suitability maps, and therefore, may have wide application. For example, conservation planners may choose a conservative set of ordered weights, while managers of invasion species may adopt a more liberal set.

The level of detail at which the layers were mapped for this study is reasonably coarse and as such may result in overestimation, through generalisation, of the potential areas for invasion (Hulme, 2003; Collingham et al., 2000). This is because coarse resolution datasets tend to homogenise the landscape, while higher resolution datasets will define the subtleties of the landscape (Ball, 1994). As a result, management responses must remain equally generalised. For example, within a mapped land system there is known to be greater heterogeneity that was not captured at this regional level of mapping (Beard, 1975; Mitchell and Wilcox, 1994). This is

confirmed by examination of aerial photographs (1.4 m resolution) of the area and by field work (unpublished data). Additionally, while the areas where cattle are present are known, there is also likely to be substantial variation in their numbers at a paddock scale. Therefore, finer resolution datasets, including fine scale elevation records, which could be used to further refine the CTI, could be collected over areas of greatest interest and the techniques described in this chapter could be reapplied. This would be an advantageous way to highlight the applicability of each of the models employed in this study. Additionally, this would enable the derivation of relationships between density recordings (from the aerial survey) and the continuous outputs of the local model so that a series of cut-points could be constructed. Such an approach was used to reclassify continuous maps of potential distribution predictions for a number of biocontrol agents (insects) for the control of *Lantana camara* based on the level of damage caused to the invader and the abundance of these agents (Baars, 2002).

Model evaluation relies on the assumption that absence records represent an underlying reason for the invasive species to have avoided such areas, which may not be true for many alien species whose distributions are still relatively young and/or still expanding. Both conditions are true in the case of the mesquite population studied here, which is approximately 70 years old and still rapidly expanding (van Klinken et al., 2007; Robinson et al., 2008). Repeat sampling and model refinement through iteration is thus required (Hulme, 2003). These additional samples would be most advantageous over a range of different environmental conditions, to ensure that data currently used to describe mesquite as being absent actually represents conditions precluding mesquite invasion, not simply that mesquite has not had sufficient time to invade there. This is particularly relevant to this study because, while the models were able to predict a very high number of presence data, it could not exclude all absence data suggesting that either these areas are somewhat suitable (and that mesquite has not had sufficient time to invade there) or, as mentioned above, the scale of the data is too aggregated. For example, the previous chapter showed, at a more local scale, that although mesquite prefers the more mesic parts of the landscape, over time and given the opportunity (e.g. the presence an effective dispersal) even more resilient land types may be suitable sites for invasion (Robinson

et al., 2008). Therefore, standardised values (and, potentially, layer weights) may need to be revised if the modeller becomes aware that invasion is still highly probable in these areas.

Utilising error measures that take into account the spatial configuration of the data may also be justified for model assessment. For example, false positives in close proximity to true positives may be less serious than false positives distant from real positives (Fielding and Bell, 1997; Collingham et al., 2000). This is simply because false positives near true positives are likely to require inspection and management intervention by virtue of their proximity (spatial autocorrelation). False positives at some distance from true positives pose less of a threat. Additionally, if resources are available, the cut-points can be inflated to maximise the true positive fraction, at the cost of including a higher proportion of false positives (Fielding and Bell, 1997). In other words, the cost of controlling invasive species once they become colonised may be mitigated by spending more on ensuring they do not invade by monitoring a wider than expected potential range. These areas may be included as a third class in the final model that represents the uncertainty given by the continuous outputs, similar in fashion to the marginal range given by the BIOCLIM model.

Many recent studies have advocated the use of ROC plots over the maximum Kappa method for model evaluation because it uses a range of thresholds, which are less likely to introduce distortions (e.g. Fielding and Bell, 1997; Pontius and Shneider, 2001; Liu et al., 2005). However, in this research, the two methods suggested identical or nearly identical cut-points for all models. This may be explained by using evaluation data with a prevalence of 50% – that is, an identical number of presence and absence data were used (500 each). Liu et al. (2005) suggests in such a case that most methods converge on the same solution. However, the ROC method has one deficiency – the AUC is difficult to interpret. For example, the difference between the three models was only 0.07 (0.87-0.8), yet the ranges proposed by Monerud and Leemans (1992) for Kappa statistics suggest that the poorest model ('fuzzy conservative') returned only a fair representation of the dataset, while the best model ('fuzzy risky') provided a good to very good representation of the dataset. Elith et al. (2006) suggest that this is because the ROC method is a rank-based statistic and therefore the prediction at the presence site can be higher than the

prediction at the absent site by a small or large amount, and the value of the statistic will be the same. Therefore, it would seem appropriate to use more than one evaluation statistic, particularly if the researcher is able to use data with a prevalence of 50%, when examining the effectiveness of model outputs.

5. 6 Summary

This chapter implemented a knowledge driven model for predicting the suitability of mesquite invasion in the Pilbara region. Layers were standardised on a scale of suitability from 0 to 1 and thus represents an improvement on crisply defined models (e.g. profile techniques). This was achieved through the use of fuzzy membership functions (continuous layers) or a modification of the rank exponent method (categorical layers). Layers were weighted based on their perceived importance for enhancing suitability using pairwise comparison and combined using weighted linear combination (WLC). Ordered weighted averaging (OWA) was used to augment WLC to provide three outputs that differ in the amount of risk and trade-off assumed. Models were evaluated using both the area under the curves produced from ROC analyses and by the maximum Kappa procedure. Both techniques agreed that the model most representative of the validation data was the one assuming the greatest risk (‘fuzzy risky’). Optimal cut-points were derived using the point closest to the top left hand corner of the ROC plots and by the maximum Kappa method. Both methods suggested similar or identical cut-points. The highest AUC was found to be 0.87 and, based on the maximum Kappa method, can be described as a good to very good agreement with the validation records used.

6 ASSESSMENT OF HIGH SPATIAL RESOLUTION MULTISPECTRAL AND HYPERSPECTRAL IMAGERY FOR DISCRIMINATING BETWEEN MESQUITE AND OTHER WOODY SPECIES

6. 1 Introduction

Encroachment of invasive plants into grasslands poses a significant threat to biodiversity (Gibbens et al., 1992) and ecosystem functioning (Schlesinger et al., 1990) and is an issue of concern worldwide (Mack et al., 2000). Knowledge of both the location and areal extent of such species are perhaps the most crucial information required to assist both land managers and policy makers in the crafting of management strategies. A robust and repeatable tool is thus required to enable monitoring at regular time intervals in order to track changes, quantify the effectiveness of control interventions and reassess management strategies. These kinds of assessments from ground surveys are costly and extremely difficult for broad-scale invasions, particularly in inaccessible rangelands. However, remotely sensed imagery is a potential data source for this information that is less labour intensive than ground surveys and can provide timely information over large and inaccessible areas (Underwood et al., 2003).

Remote mapping of invasive plants with high spatial resolution (e.g. <5 m) multispectral (e.g. three to four band) airborne imagery has typically been limited to species that exhibit a highly discernible biological trait such as a unique flower, fruit or bract colour (e.g. Everitt and Villarreal, 1987), erectophile canopy architecture (e.g. Everitt et al., 1992b), seasonal changes in colour (e.g. Everitt and DeLoach, 1990 and Everitt et al., 1996), defoliation (e.g. Everitt et al., 1999) and/or unique growth habits such as thicket formation (e.g. Frazier, 1998; Everitt et al., 2004). The presence of one or more of these traits may provide sufficient spectral separation to enable their detection using high spatial resolution yet low spectral resolution imagery and relatively unsophisticated image processing techniques such as the unsupervised ISODATA algorithm (e.g. Ramsey et al., 2002; Everitt et al., 2001; 2002; 2003) or the maximum likelihood algorithm (e.g. Carson et al., 1995).

In many other cases, the biological traits of invasive plants may not be sufficiently unique to provide an adequate spectral dissimilarity from coexisting species to enable discrimination with the use of multispectral imagery. Therefore, there has been a

tendency to advocate the use of hyperspectral imagery for these more challenging species in order to isolate spectral differences that may be masked by the broad band widths of multispectral imagery (Schmidt and Skidmore, 2003). While studies have shown that hyperspectral imagery is capable of mapping invasive plants (e.g. Parker-Williams and Hunt, 2002; Lass et al., 2002; Underwood et al., 2003; Lass and Prather, 2004; Mundt et al., 2005; Glenn et al., 2005; Lass et al., 2005; Lawerence et al., 2006; Miao et al., 2006; Deehan et al., 2007; and Hamada et al., 2007) few have made a quantitative comparison of the two media for particular species. Moreover, in many cases, multispectral imagery has already been shown to be sufficient for mapping the target species. Such species include blackberry (e.g. Ullah et al., 1989; Frazier, 1998; and Dehaan et al., 2007), tamarix species (e.g. Everitt and DeLoach, 1990; Everitt et al., 1996; and Hamada et al., 2007), yellow starthistle (e.g. Lass et al., 1996; and Miao et al., 2006) and leafy spurge (e.g. Everitt et al., 1995; and Glenn et al., 2005). Hence, it is difficult to gauge whether these species represent a real test for hyperspectral imagery or how much better hyperspectral imagery has been at mapping these species. Selecting one medium over another depends on several factors, including accuracy requirements and parsimony in terms of cost, processing time and ease of image processing and its potential for automation.

Studies have shown that, when mapping woody species, the high spatial resolution of airborne multispectral imagery can assist in the exploitation of the spectral information available through the use of various statistics (herein referred to as patch statistics) assigned to their crowns or woody assemblages (e.g. thickets; herein collectively referred to as patches) of the various species present within the same scene (e.g. Brandtberg, 2002; Haara and Haarala, 2002; Erikson, 2004; Foody et al., 2005; Hamada et al., 2007). However, this has rarely been done in studies designed to map invasive plants and needs further exploration in this field. For example, the maximum response from all pixels representing a highly vigorous shrub is likely to be higher in the near infrared portion of the spectrum, than a shrub with erect leaves or undergoing defoliation. However, this can be masked by variable illumination conditions caused by shrubs of different heights (e.g. shadow effects) and structure (e.g. Gong et al., 1997) if the spectral response per pixel is used as the only information on which to classify. In such a case, the variation may be so great that pixels representing the same plant may be incorrectly classed as multiple species.

An additional method that can be used to focus on a single class of interest, which has rarely been considered in weed mapping studies, is the selection of variables (e.g. bands, patch statistics or other ancillary data) that best separate the target species from *each* of the coexisting species in turn. Instead, most studies have chosen variables that exploit differences between *all* species in their classification routine. The ultimate aim of these methods is to optimise overall accuracy. However, when the map user is only interested in the accuracy of one class (e.g. plant species), Lark (1995) demonstrates that, through judicious selection of appropriate variables, it might be possible to optimise the accuracy for only that class. Foody et al. (2005) provide an application of this concept and demonstrate the improvement in accuracy when selecting variables that focus on the class of interest (the invasive sycamore tree (*Acer pseudoplatanus*)) versus each coexisting species in turn, over attempting to optimise overall accuracy. They then combine these outputs using Boolean logic operators (e.g. Boolean OR and the Boolean AND).

A robust monitoring tool should also disclose the reliability of mapping patches of various sizes. For example, small and isolated patches can challenge detection and often go unnoticed. These satellite populations can result in the colonisation of new areas or range expansion of the existing population (Moody and Mack, 1988). Additionally, such knowledge can assist in how the outputs are used for management. For example, it is unlikely to be appropriate to monitor an invasion front if the imagery and associated classification techniques can only reliably detect large patches (e.g. thickets).

Currently, efforts to directly map and monitor the distribution of mesquite are rare using either multispectral or hyperspectral imagery and, therefore, little guidance is available for choosing between the two mediums. In this study, several well known (e.g. mean, maximum, minimum, standard deviation) and novel patch statistics (e.g. majority, variety) are derived from 1 m resolution, 4 band, digital multispectral imagery (DMSI) in an attempt to derive greater information to assist in the discrimination of mesquite from coexisting species. Results are compared to just the mean patch statistic (average spectral response of a patch) extracted from the crowns of 3 m resolution, 126 band, hyperspectral imagery. Two approaches are taken in the

selection of the most suitable patch statistics to use for training the classifier: those that best separate all species (referred to as overall separation) and those that could best discriminate between mesquite and each of the other species in a pairwise fashion (e.g. mesquite versus snakewood; mesquite versus eucalyptus). This approach is referred to as pairwise separation herein. To identify the reliability of classifying mesquite shrubs of various sizes, they are grouped into size-classes and their accuracy defined for both datasets. Artificial neural networks (ANNs) were chosen to classify both datasets because recent studies consider them to be a superior classification tool than many of the techniques used to classify multispectral airborne imagery in past invasive plant mapping studies, such as ISODATA or the maximum likelihood algorithm (c.f. Lee et al., 1990; Benediktsson et al., 1990; Atkinson and Tatnall, 1997).

6. 2 Artificial Neural Networks (ANNs)

ANNs have become a popular tool for the classification of remotely sensed data, largely because they are non-parametric and thus are free from the restrictive assumptions of statistical classifiers (e.g. maximum likelihood) such as requiring multivariate normal distributions. The following gives a brief explanation of the architecture, required parameters and the manner in which ANNs learn how to recognise and classify the pixels of digitally acquired imagery.

6.2.1 Network architecture and forward propagation

An ANN consists of a set of nodes (or neurons) arranged in a layered architecture that, combined, may be used to transform pixels from remotely sensed imagery into a class allocation (Foody et al., 2005). The ANN used in this research is the multilayer perceptron (MLP), which consists of an input layer, an output layer and one or more hidden layers (Figure 6.1). The number of input and output nodes is determined by the characteristics of the remotely sensed data to be classified and the desired classification scheme, respectively (Foody, 2001). Generally, the number of input nodes is equal to the number of variables (e.g. bands) used in the classification process and the number of output nodes is equal to the number of output classes (e.g. plant species) upon which the dataset is being trained on.

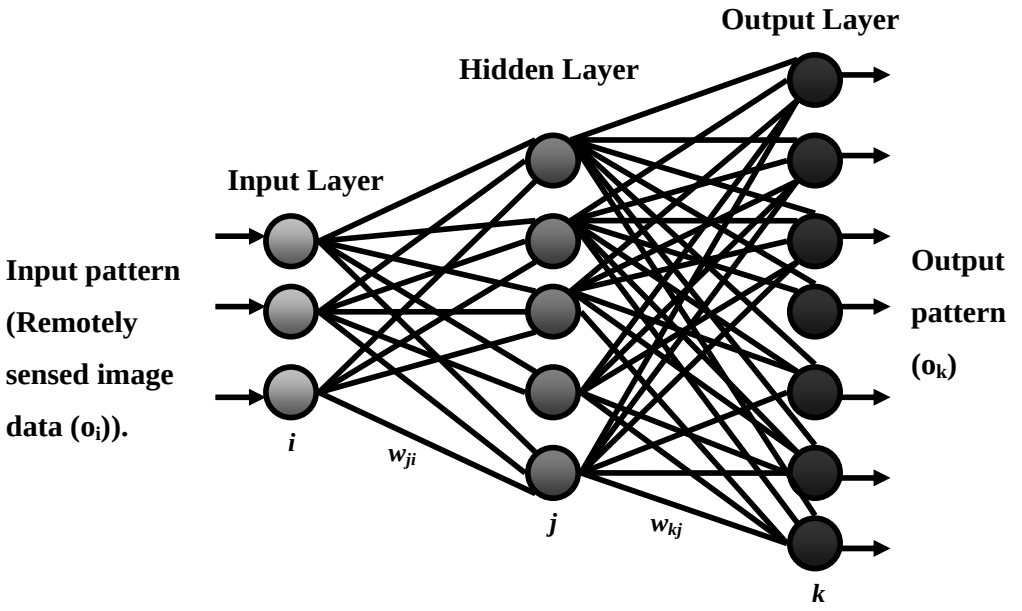

Figure 6.1 Neural network architecture of a multilayer perceptron used for the classification of remotely sensed data (adapted from Paola and Schowengerdt, 1995).

Each layer is interconnected to the following layer, but there are no interconnections within a layer (Figure 6.1). The input layer serves as a distribution structure for the data being presented to the network. No processing is done at this layer. The interconnections between each node have an associated weight. When a value (pixel) is passed down that interconnection it is multiplied by that weight. These weight values contain the distributed knowledge of the network (Paola and Schowengerdt, 1995). The role of the hidden layer nodes is to formulate the weighted sum of all of its inputs (Foody, 2001), which is achieved using Equation 6.1 (Atkinson and Tatnall, 1997; refer to Figure 6.1 for notation):

$$netj = \sum_{j=1}^{J} w_{ji}\, o_i \qquad (6.1)$$

where w_{ji} represents the weights between node i (the input layer) and node j (the hidden layer); and

o_i are the outputs from node i, the input layer.

The output from a given node, j, is then computed, typically using a non-linear sigmoid function that is applied to the weighted sum of inputs (net_j) such as (Foody, 2001):

$$o_j = 1/(1+\exp^{-\lambda netj}) \tag{6.2}$$

where λ is a constant that modifies the shape of the sigmoid.

Output unit, o_k, is computed in the same way (Murai and Omatu, 1997). This process is known as forward propagation.

6.2.2 Adjusting interconnecting weight values: Backpropagation

Once the forward propagation is completed, the activities of the output nodes are compared with their expected activities. Each node in the output layer is associated with a class. When a pattern is presented to the network it will generate a value that indicates the similarity between the input pattern and the corresponding class. A measure of error is then calculated between the actual output and the expected output using the root-mean-square error equation (Eastman, 2006):

$$RMSE = \sqrt{\frac{\sum_p \sum_k (t_{pk} - o_{pk})^2}{PN}} \tag{6.3}$$

where P is the number of nodes in the input layer;

N is the number of output nodes (classes);

t_{pk} is the target output of the p^{th} training pattern of the k^{th} node in the output layer; and

o_{pk} is the actual output of the p^{th} training pattern of the k^{th} node in the output layer.

Backpropagation, using a gradient descent function known as the generalised delta rule, is then used to continually adjust the interconnecting weight values to minimise the RMSE (Equation 6.3). Two functions are used to manipulate the different weights between the input nodes and the hidden layer nodes (Equation 6.4) and the

hidden layer nodes and the output layer nodes (Equation 6.5). Refer to Rumelhart et al. (1986) for further information and their derivation.

$$\Delta w_{ji}(n+1) = \eta(\delta o_i) + \alpha \Delta w_{ji}(n) \tag{6.4}$$

$$\Delta w_{kj}(n+1) = \eta(\delta_k o_j) + \alpha \Delta w_{kj}(n) \tag{6.5}$$

where $\Delta w_{ji}(n+1)$ is the change of a weight connecting nodes j (hidden layer nodes) and i (input layer nodes) at the $(n+1)^{th}$ iteration;

$\Delta w_{kj}(n+1)$ is the change of a weight connecting nodes j (hidden layer nodes) and k (output layer nodes) at the $(n+1)^{th}$ iteration;

n is the iteration number;

$\delta_j o_i$ is an index of the rate of change of the error with respect to the output from node i;

$\delta_k o_j$ is an index of the rate of change of the error with respect to the output from node j;

η is the learning rate parameter; and

α is the momentum parameter.

The learning rate (η) is the percentage of the step taken towards the minimum error at iteration (Paola and Schowengerdt, 1995). Low values can cause the network to converge on a solution at an unacceptably slow rate, whilst values too high may result in the best solution being stepped over and thus unrealised (Figure 6.2a). During the training phase, if the network encounters a local minimum it can get stuck and the global minimum error may not be found (Figure 6.2b). It is also possible for the system to oscillate between two points (Paola and Schowengerdt, 1995). The purpose of the momentum parameter (α) is to avoid such local minimum errors and oscillatory changes and reinforce general trends so that the network continues to descend towards the global minimum error. The process of backpropagation is repeated for a set number of iterations or until the error of the neural network is minimised or reaches a user defined acceptable magnitude, at which point it is considered to have learnt to recognise the possible patterns (Bishop, 1995).

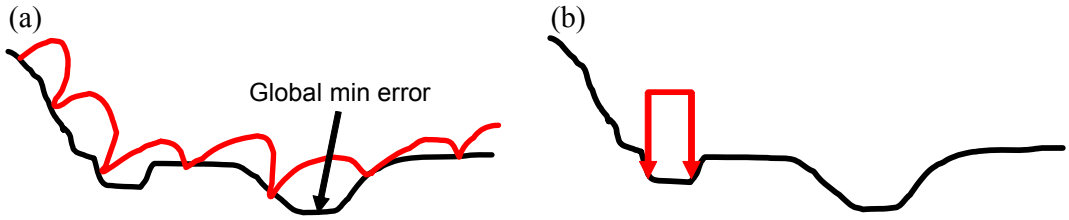

Figure 6.2 Potential errors caused by (a) poor choice of the learning rate parameter (set too high); and (b) neglecting to set the momentum parameter (see text).

6. 3 Methodology

6.3.1 Collection of training and testing data

Training and testing data were acquired in September 2005. An existing track (see Figures 3.6 and 3.7) running predominately northeast was used as a transect line to assist a convenience style sampling method (de Grujter, 1999). This sampling technique was used as it enabled sampling over the full length of the DMSI image and was relatively quick, thus allowing the gathering of an adequate number of samples. Woody vegetation present on the imagery (e.g. mesquite, eucalyptus and snakewood) that could be unambiguously identified in both the field (with the aid of a GPS) and on enlarged maps of the DMSI were labelled as to species type and later digitised and stored in a GIS. As all coexisting woody vegetation is long-lived, the delay between image acquisition and field work did not affect sample collection. Two-thirds of the sample set was used to assist in the selection of patch statistics for both the overall separation and pairwise separation approaches (see Section 6.3.6.1) and to classify both the DMSI and hyperspectral imagery using an ANN. One-third was kept aside to assess the accuracy in terms of both class allocation and size of mesquite patch that can be reliably detected from both image types. As the flight line used to collect the hyperspectral imagery was designed to overlap the DMSI imagery collected, the same plants were used as training and testing data, with some exceptions: (i) because the hyperspectral imagery has a spatial resolution of 3 m, small isolated plants could not be resolved and, therefore, had to be removed; and (ii) as different methods were used to geo-reference the different images, the training data had to be redrawn.

A total of nine sequential steps were used to classify the DMSI and hyperspectral imagery and assess their potential as a monitoring tool. These steps are described in more detail hereafter.

6.3.2 Step 1: Patch extraction

To extract the patches of all woody vegetation (mesquite, eucalyptus species and snakewood) found within the DMSI and overlapping hyperspectral strip, the raw image bands were first processed using an unsupervised classification routine (ISODATA), with required parameters found heuristically (20 iterations, 5 clusters). Woody vegetation was easily discerned from grasses and soils using this method. Only those pixels representing woody vegetation were used in subsequent analyses. All contiguous pixels were then grouped to form patches, which were then assigned patch statistics (see Section 6.3.2).

6.3.3 Step 2: Assignment of patch statistics

The assignment of patch statistics differed between the DMSI and the hyperspectral imagery. Seven patch statistics were assigned to each of the four bands of the DMSI, resulting in a total of 28 discriminatory variables (Table 6.1) for each patch. However, as the power of hyperspectral imagery is its spectral resolution, only the mean was extracted from the patches found within the hyperspectral imagery. Moreover, the assignment of 7 statistics for 126 bands would result in 882 new files, which is impractical and prohibitively too large to store and process.

Table 6.1 Description of the statistics calculated for each patch.

Statistic	Description
Maximum	The highest digital number of a patch.
Mean	The mean of all digital numbers of a patch.
Median	The median of all digital numbers of a patch.
Minimum	The minimum value of all digital numbers of a patch.
Standard Deviation	The standard deviation of all digital numbers of a patch.
Majority	The spectral response (digital number) that occurs most often for a patch. Shrubs with homogenous cover would be expected to have a stable majority throughout its population.
Variety	The number of different digital numbers of a patch. Shrubs with homogenous cover would be expected to have a low variety coefficient, as opposed to shrubs showing a high level of variation.

6.3.4 Step 3: Normalisation

The newly created patch statistics were each rescaled to be within the range of 0 and 1, by dividing each by its respective maximum value. This procedure has been shown to improve the ANNs performance (Mather, 2004) and avoid it stalling at an error level that is too high (early saturation) (Kanellopoulos and Wilkinson, 1997).

6.3.5 Step 4: Exploratory analysis

Spectral plots were analysed visually to identify the reflectances of each species at each wavelength to initially determine the likelihood of successfully differentiating mesquite from associated species.

Differences between species for each of the patch statistics were tested using analysis of variance. Tukey's HSD test was used to separate means at the 0.05 probability level. If mesquite was not significantly different from at least one species, that patch statistic was immediately excluded from further consideration.

6.3.6 Step 5: Discriminant analysis

The use of extra variables (e.g. patch statistics) usually increases the accuracy of the neural network, so long as they provide additional useful information (Kanellpoulous and Wilkinson, 1997). However, inclusion of patch statistics offering little to no discrimination between the classes can reduce the accuracy of the classification and markedly increase the time required for training (Foody and Arora, 1997). Because hyperspectral imagery is collected in many narrow contiguous bands there is usually significant spectral redundancy. While the above exploratory analysis is able to exclude some patch statistics, further exclusion of relatively uninformative patch statistics is possible by using linear discriminant analysis (LDA) (e.g. Gong et al., 1997; Foody et al., 2005). For example, patch statistics that may be individually good discriminators may share the same discriminating information with others and can be eliminated on the basis that they will likely weaken the classification or, at the very least, increase classification time with no gain in classification accuracy (i.e., variable redundancy). Therefore, backward stepwise elimination based on the F-to-remove statistic was used to eliminate redundant and relatively uninformative patch statistics (Klecka, 1980). See also Section 2.3.5.5.5 for more information on discriminant analysis and the F-to-remove statistic.

6.3.6.1 Identifying patch statistics for overall and pairwise separation

Two approaches were taken for both imagery types to identify the most suitable patch statistics for introduction to the ANN. In the first case, discriminant analysis was used to identify a set of patch statistics that best separated all three species simultaneously. This approach is referred to as overall separation. This was done because conventional methods of classification usually attempt to derive an optimum overall error (Lark, 1995). Therefore, comparisons can be made between this approach and a pairwise separation approach, which sought to identify the set of patch statistics that could best discriminate between each species in a pairwise fashion (e.g. mesquite versus snakewood and mesquite versus eucalyptus). Thus, under the pairwise separation approach, two binary classifications were derived, which involved mesquite and each of the two other classes in turn. These were then combined using a simple rule: if snakewood or eucalyptus then not mesquite. In such a case, high accuracy for the mesquite class is of primary interest; hence it is unimportant whether the non-mesquite classes are confused with each other or if the overall error is reduced as a result (Lark, 1995).

6.3.7 Step 6: Classification using an ANN

The ANN architecture comprised of one hidden layer and three output nodes for the classes of mesquite, snakewood and eucalyptus. The number of input nodes was determined from Step 5. The number of hidden nodes was determined by taking the square root of the product between the number of input nodes and the number of output nodes. This method for deriving the number of hidden nodes is said to provide a reasonable balance between over training and over generalising (Eastman, 2006). The learning rate parameter was derived using an automated adaptive algorithm, which avoids an otherwise trial and error approach. The adaptive algorithm adjusts the learning rate downward after some training interval if the overall training error has increased and upward if it has decreased. In this way, the initial value chosen for the learning rate is not crucial to the success of network training, and training speed is increased since the learning rate is adjusted to the highest value that does not cause instability (Paola and Schowengerdt, 1995). The momentum parameter (α, see Equations 6.4 and 6.5) was fixed at 0.5 so that 50% of the weight change is added at iteration. The sigmoid constant (λ, see Equation 6.2) was effectively ignored and set to 1, since alternative values are said to have little

effect on the solution (Caudill, 1988). To avoid overtraining, the process of backpropagation was terminated manually by visual examination of solution convergence shown on a continuously updated root mean square error plot.

6.3.8 Step 7: Class accuracy assessment

A patch-based accuracy assessment was performed and a confusion matrix derived using the testing data described in Section 6.3.1. Patches were used in this accuracy assessment because conventional pixel-based approaches for assessing the image classification accuracy may overestimate the accuracy. This is the case because conventional approaches assess the absolute percentage of pixels correctly classified and do not consider the spatial association (autocorrelation) of pixels (Hamada et al., 2007). For example, a large mesquite patch may be made up of 20 pixels, whereas a snakewood patch may be made up of only 4 pixels. Even if both are correctly classified the accuracy of mesquite will be deemed to be 5 times better when, in fact, it should be equal. Statistics computed from the confusion matrix included the overall accuracy, errors of commission, and errors of omission and per-class Kappa. See Section 2.3.4 for more information on these statistics.

6.3.9 Step 8: Size-class accuracy assessment

It generally follows that the higher the spatial resolution the greater the ability to resolve smaller patches. Therefore, imagery collected at different spatial resolutions may differ in their ability to map individual plants of different sizes. This study assumes that the greatest success in classification accuracy will occur as mesquite patches increase in size, as has been demonstrated by Dehaan et al. (2007) for mapping blackberry. To test this assumption, the surface area of each patch used for accuracy validation (the testing data) of the classification was calculated in the GIS. An analysis, similar to the Incremental Cover Evaluation (ICE) method discussed by Mundt et al. (2005), proceeded whereby producer's accuracy was graphed against various size classes in order to determine the minimum patch size of the mesquite class that could be reliably detected for both DMSI (1 m spatial resolution) and the hyperspectral imagery (3 m spatial resolution). The significance of the difference in accuracy between size-classes for the two approaches and image types were assessed using a two-sample difference of proportions test with at the 0.05 level of probability (Walpole and Myers, 1993).

6.3.10 Step 9: Accuracy comparisons

The preceding step was used to offer insight into the size of mesquite patch that could be reliably detected based on the imagery and approaches implemented. For comparison between the two approaches and imagery types, patches that were deemed to be unreliably detected were ignored so that the efficacy of the image types could be tested on patches that could be reliably, and therefore repeatedly, detected. Omission and commission errors were computed based on this size-class threshold and a two-sample difference of proportions test was again computed to assess the significance of the difference in accuracy between the two approaches and image types. Differences were tested at the 0.05 level of significance.

6. 4 Results

6.4.1 Exploratory analysis of DMSI

Spectral reflectance curves for mesquite and associated plant species are presented in Figure 6.3 (DMSI). These curves were derived by taking the average of the spectral response at each wavelength for each species using the training data collected. Dashed polygons identify areas of the spectrum where spectral reflectance is unique for all species, as identified by Tukey's HSD test. Figure 6.3 and Table 6.2 (see mean patch statistic) shows that all species were inseparable in the blue and green portions of the spectrum. No significant difference was found between mesquite and eucalyptus in the red portion of the spectrum although snakewood is separable from mesquite and eucalyptus in this region (Figure 6.3; Table 6.2).

The relatively high near infrared reflectance of eucalyptus species suggests that they are undergoing the greatest amount of photosynthesis of the three species (Figures 6.3). Snakewood absorbed the greatest amount of near infrared radiation, which is likely due to its erectophile canopy structure (Figures 6.3 and 6.4). This was followed by mesquite, and is likely due to a high level of leaf wilting and associated stress caused by the leaf-tying moth. All species were found to be separable in this portion of the spectrum (Figure 6.3; Table 6.2).

Table 6.2 highlights the need to explore many alternative patch statistics when using high spatial resolution multispectral imagery. For example, spectral similarity between species in the blue band (see Figure 6.3) would conventionally preclude that

band from being used as an input in any classification process, yet the mean differences of four of the seven object statistics are significantly different on all species. Half of the patch statistics explored separated all species and thus are considered candidates for introduction to the ANN under the overall separation approach. However, only the near-infrared band would be considered under conventional techniques (e.g. pixel-based classification of the raw band data). The near-infrared band contains the greatest amount of information, showing dissimilarity from all species (five out of seven were significant) and highlights its importance for mapping species on the premise of defoliation. No further variables were found to separate mesquite from eucalyptus species (pairwise separation); however, a further 13 were found that may assist separation of mesquite from snakewood (Table 6.2) and are, therefore, candidates for introduction to the ANN under the pairwise separation approach for those two species.

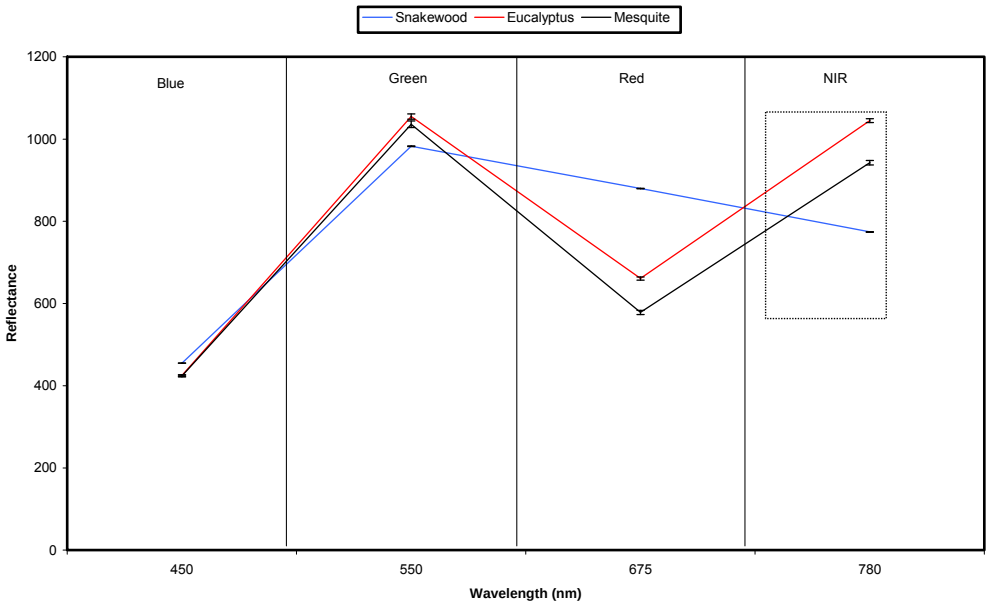

Figure 6.3 Spectral reflectance curves of mesquite and associated species derived from the DMSI. Curves represent the average spectral response at each of the four wavelengths imaged for each species as derived from the training data. The dashed polygon enclosing the spectral reflectance curves show zones of potential separation between all species. Error bars represent +/- 1 standard error.

Table 6.2 Patch statistics of mesquite and associated species derived from the DMSI after normalisation. Statistics in bold show significant differences between all species and are therefore candidates for introduction to the ANN under the overall separation approach. Species with a different letter to mesquite are candidates for introduction to the ANN under the pairwise separation approach.

Band	Patch Statistic	Mesquite	Snakewood	Eucalyptus
Blue	Maximum	0.427a	0.372b	0.421a
(450 nm)	Mean	0.454a	0.467b	0.441a
	Median	0.432a	0.448b	0.419a
	Minimum	**0.432a**	**0.504b**	**0.409c**
	Std. Dev.	**0.149a**	**0.034b**	**0.182c**
	Majority	**0.433a**	**0.464b**	**0.405c**
	Variety	**0.124a**	**0.008b**	**0.069c**
Green	**Maximum**	**0.353a**	**0.230b**	**0.337c**
(550 nm)	Mean	0.362a	0.29b	0.356a
	Median	0.356a	0.286b	0.352a
	Minimum	0.336a	0.337a	0.329a
	Std. Dev.	0.247a	0.058b	0.255a
	Majority	**0.378a**	**0.338b**	**0.364c**
	Variety	**0.135a**	**0.007b**	**0.066c**
Red	**Maximum**	**0.457a**	**0.472b**	**0.446c**
(675 nm)	Mean	0.354a	0.458b	0.354a
	Median	0.347a	0.454b	0.348a
	Minimum	0.293a	0.462b	0.294a
	Std. Dev.	0.214a	0.050b	0.214a
	Majority	0.328a	0.462b	0.319a
	Variety	**0.138a**	**0.007b**	**0.065c**
NIR	**Maximum**	**0.428a**	**0.206b**	**0.476c**
(780 nm)	**Mean**	**0.439a**	**0.291b**	**0.484c**
	Median	**0.412a**	**0.257b**	**0.462c**
	Minimum	0.425a	0.386b	0.431a
	Std. Dev.	**0.239a**	**0.053b**	**0.333c**
	Majority	0.484a	0.387b	0.483a
	Variety	**0.136a**	**0.007b**	**0.07c**

6.4.2 Exploratory analysis of hyperspectral imagery

Due to the high content of chlorophyll in its leaves, eucalyptus species had the highest green peak (Figure 6.4). Mesquite exhibited the lowest green-peak (Figure 6.4), which is likely to be caused by activity of the leaf tier causing the leaves to yellow (see Section 3.2.1); thus pigments other than chlorophyll are beginning to dominate the spectral response.

The smaller band widths and greater number of bands of the hyperspectral imagery detected separation between all species in two areas of the visible region that was not identified with the broad bandwidths of the DMSI as illustrated by the dashed polyon in the visible portion of the spectrum (Figure 6.4). Separation between mesquite and

snakewood is unlikely to occur in the short wave near infrared portion of the spectrum because their spectral signatures (and standard errors) overlap in this region (Figure 6.4). In contrast to the DMSI, eucalyptus species are more unique over most of the spectrum than both snakewood and mesquite (Figure 6.4; Appendix A).

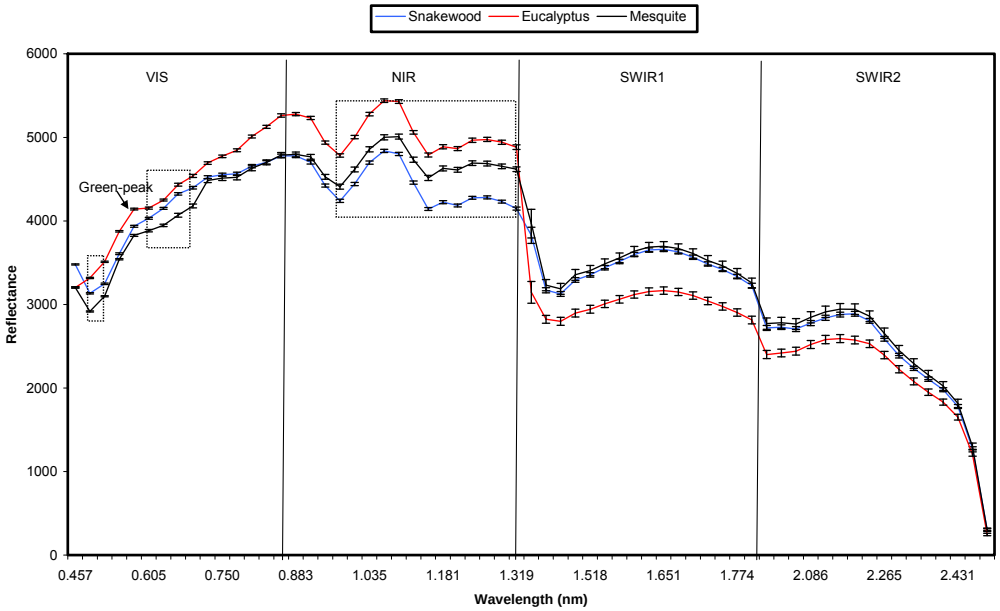

Figure 6.4 Spectral reflectance curves of mesquite and associated species derived from the hyperspectral imagery. Curves represent the average spectral response at each of the 126 wavelengths imaged for each species as derived from the training data. Dashed polygons enclosing the spectral reflectance curves show zones of potential separation between all species. Error bars represent +/- 1 standard error.

Similar to the DMSI, none of the spectral signatures and associated standard errors for all species overlapped throughout most of the near infrared portion of the spectrum (Figure 6.4). However, unlike DMSI, which only provided one band in the NIR for image processing, a total of 26 (out of 32) bands showed significant differences between all species in this region. This is confirmed by the significant differences in means of the mean patch statistics (Appendix A).

In total, 36 patch statistics (out of 126) were found to be able to separate all species (Appendix A), and are thus candidates for introduction to the ANN using the overall separation method. An additional two patch statistics are available to assist

separation of mesquite from snakewood (pairwise separation) and all of the 126 patch statistics are available to separate mesquite from eucalyptus species, including 64 from the short-wave infrared (SWIR) portion of the spectrum, which was not sampled with the DMSI.

6.4.3 Discriminant analysis

Discriminant analysis was performed on the patch statistics found to separate all species (overall separation) and those found to separate each species on a pairwise basis from the exploratory analysis performed above. Results are shown in Table 6.3 and Table 6.4, respectively. Comparisons between Table 6.3 and Table 6.4 show that many of the patch statistics used in pairwise separation of mesquite from associated species are quite different to those found from overall separation. This illustrates the need to assess such an approach.

Table 6.3 Summary of the patch statistics found from discriminant analysis that best separate all species (overall separation method).

Imagery	Band	Patch Statistic
DMSI (all bands)	Red (675 nm)	Maximum
	Green (550 nm)	Maximum
	NIR (780 nm)	Maximum
	NIR (780 nm)	Standard Deviation
Hyperspectral	NIR:53 (1208 nm)	Mean
	NIR:43 (1065 nm)	Mean
	VIS:15 (663 nm)	Mean
	VIS:11 (605 nm)	Mean

Table 6.4 Summary of the patch statistics found from discriminant analysis that best separate mesquite from each species in turn (pairwise separation method).

Imagery	Band	Patch Statistic
DMSI (all bands)	NIR (780 nm)	Standard Deviation*
Mesquite v Eucalyptus	NIR (780 nm)	Mean*
	Green (550 nm)	Maximum
	NIR (780 nm)	Maximum
DMSI (all bands)	Red (675 nm)	Maximum
Mesquite v Snakewood	Green (550 nm)	Mean*
	NIR (780 nm)	Maximum
	Blue (450 nm)	Minimum*
Hyperspectral	NIR:33 (912 nm)	Mean*
Mesquite v Eucalyptus	VIS:19 (721 nm)	Mean*
	SWIR2:103 (2122 nm)	Mean*
	SWIR2:113 (2299 nm)	Mean*
Hyperspectral	VIS:15 (663 nm)	Mean
Mesquite v Snakewood	NIR:53 (1208 nm)	Mean
	NIR:43 (1065 nm)	Mean
	NIR: 55 (1236 nm)	Mean*

*Patch statistics that were found to be different to those found from assessing the overall separation.

6.4.4 Class accuracy assessment

6.4.4.1 Overall separation approach: DMSI

The confusion matrix based on the best overall separation method of the patch statistics derived from the DMSI (Table 6.5) shows a very high overall agreement (81.5%), which indicates that all species are being reasonably well separated with the variables used. The overall Kappa value also suggests a good agreement with the testing data, based on the ranges proposed by Monserud and Leemans (1992). However, inspection of the per-class Kappa statistics shows that these values are being inflated by an excellent classification of the snakewood class, particularly from the producer's perspective. In particular, the class of most interest, mesquite, was only classified as "fair" from both perspectives.

Table 6.5 Confusion matrix and associated statistics based on the patch statistics derived from the DMSI that gave the best overall separation.

	Mesquite	Snakewood	Eucalyptus	Totals	Errors of Commission	Kappa per class (User's)
Mesquite	107	8	85	200	0.47	0.45
Snakewood	51	770	39	860	0.10	0.74
Eucalytpus	47	19	222	288	0.23	0.69
Totals	205	797	346	1348		
Errors of Omission	0.48	0.03	0.36			
Kappa per class (Producer's)	0.44	0.91	0.54			
Overall agreement (%)				81.53		
Overall Kappa				0.41		

6.4.4.2 Pairwise separation approach: DMSI

Attempting to improve the separation from mesquite and associated species using the pairwise separation approach (Table 6.6) did not result in increasing the per-class Kappa's from either perspective.

Table 6.6 Confusion matrix and associated statistics based on the patch statistics derived from the DMSI that gave the best pairwise separation.

	Mesquite	Other	Totals	Errors of Commission	Kappa per class (User's)
Mesquite	101	100	200	0.50	0.41
Snakewood	205	1044	1148	0.09	0.40
Totals	205	1144	1348		
Errors of Omission	0.51	0.09			
Kappa per class (Producer's)	0.40	0.41			
Overall agreement (%)			84.94		
Overall Kappa			0.41		

6.4.4.3 Overall separation approach: Hyperspectral imagery

Classification of the hyperspectral imagery based on overall separation (Table 6.7) showed a similar pattern to the DMSI: while the overall agreement is high, it is inflated by low omissions of the snakewood class and as expected from exploratory analysis of the spectral plot, low commission into the eucalyptus class. The hyperspectral imagery performed better than the DMSI on the mesquite class from a user's perspective, but omissions were similar to the DMSI.

Table 6.7 Confusion matrix and associated statistics based on the patch statistics derived from the hyperspectral imagery that gave the best overall separation.

	Mesquite	Snakewood	Eucalyptus	Totals	Errors of Commission	Kappa per class (User's)
Mesquite	70	7	22	99	0.29	0.62
Snakewood	30	162	35	227	0.29	0.57
Eucalytpus	19	5	168	192	0.13	0.78
Totals	119	174	225	518		
Errors of Omission	0.41	0.07	0.25			
Kappa per class (Producer's)	0.49	0.88	0.60			
Overall agreement (%)				77.22		
Overall Kappa				0.65		

6.4.4.4 Pairwise separation approach: Hyperspectral imagery

Unlike DMSI, patch statistics chosen from pairwise separation (Table 6.8) assisted in reducing the number of omissions in the mesquite class and also further reducing the commission rate.

Table 6.8 Confusion matrix and associated statistics based on the patch statistics derived from the hyperspectral imagery that gave the best pairwise separation.

	Mesquite	Other	Totals	Errors of Commission	Kappa per class (User's)
Mesquite	76	23	99	0.23	0.70
Snakewood	43	376	419	0.10	0.55
Totals	119	399	518		
Errors of Omission	0.36	0.06			
Kappa per class (Producer's)	0.55	0.70			
Overall agreement (%)			87.26		
Overall Kappa			0.62		

6.4.5 Size-class accuracy assessment

Identification of mesquite patches smaller than 36 m^2 was relatively low (43-51%) for both image types regardless of whether overall or pairwise separation was used to choose patch statistics (Figures 6.5a,b). Accuracy improved for patches >36 m^2 (66-94%) with both approaches and image types. Both approaches used on the hyperspectral imagery were more reliable at capturing patches >36 m^2 than the DMSI using either the overall or pairwise separation approaches. However, the best approach was found using pairwise separation on the hyperspectral imagery, which was significantly more accurate than DMSI using an overall separation approach ($Z=2.78$, $P<0.05$) (Figure 6.5a).

6.4.6 Accuracy comparisons

The size-class accuracy assessment revealed that, in general, regardless of image type or approach, errors of omission were only likely to be of an acceptable magnitude for mesquite patches >36 m^2. Therefore, to identify the best approach (image and method of selecting patch statistics), patches <36 m^2 were masked out and assessment of omission and commission errors was assessed only for patches >36 m^2 (Table 6.9). Although not directly comparable, it can be seen that both errors of commission and omission were much reduced when only patch sizes above 36 m^2 were included (Table 6.9 vs. Tables 6.5-6.8).

(a)

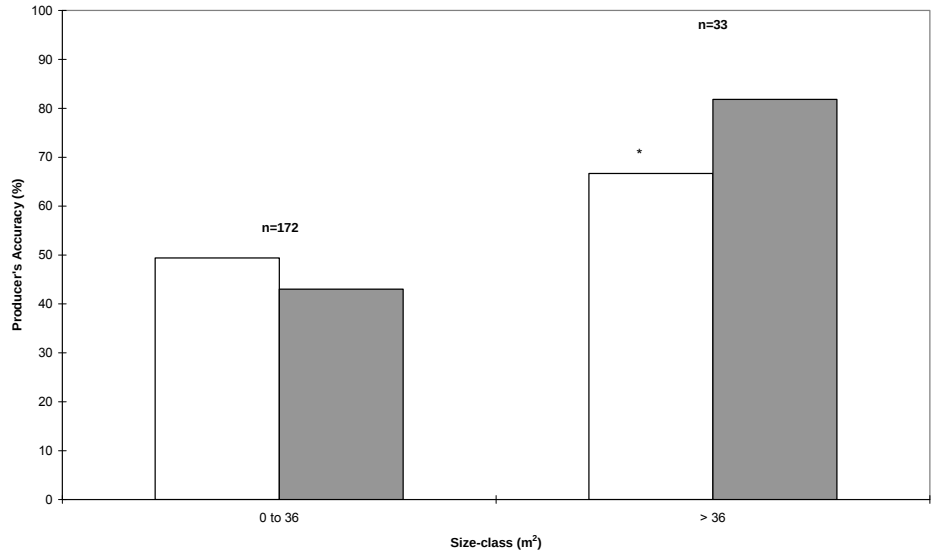

(b)

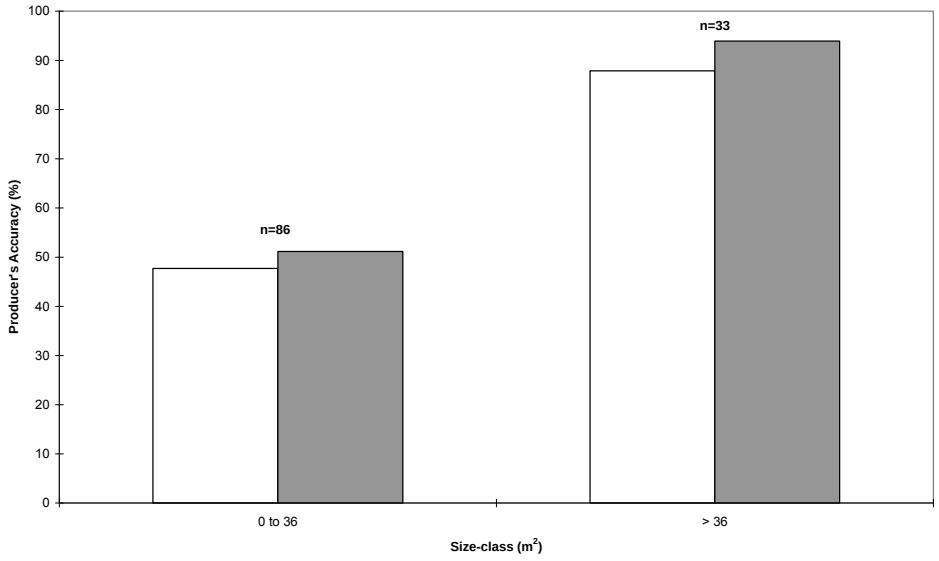

Figure 6.5 Percentage of mesquite patches correctly detected (producer's perspective) for two size-classes for a) the DMSI and b) the hyperspectral imagery. Open bars represent classification using patch statistics found from the best overall separation method; grey bars represent classification using patch statistics found from pairwise separation. *Indicates accuracy values that were significantly poorer than the best accuracy for that size-class using either overall or pairwise separation on either image type.

The hyperspectral imagery, using patch statistics found from pairwise separation produced the lowest omission and commission rates. However, omission rates were only significantly better than DMSI processed using patch statistics found from overall separation ($Z=2.78$, $P<0.05$). Consequently, all methods and imagery types except for DMSI processed using overall separation are capable of accurately mapping mesquite patches >36 m^2. However, hyperspectral imagery processed using pairwise separation appears to be superior, even though not statistically better than hyperspectral imagery processed using overall separation or DMSI processed using pairwise separation at the 95% confidence level (Table 6.9).

Table 6.9 Errors of omission and commission for both image types and both approaches for patches >36 m^2.

Approach	Statistic	Hyperspectral	DMSI
Overall separation	Omission	1-(27/33) = 18%	1-(22/33) = 33%*
	Commission	10/98 = 10%	8/98 = 8%
Pairwise separation	Omission	1-(31/33) = 6%	1-(27/33) = 18%
	Commission	6/98 = 6%	6/98 = 6%

*Indicates accuracy significantly poorer than the highest accuracy found for that statistic.

A sample map output showing a portion of the integrated trial, classified using the hyperspectral imagery with patch statistics identified from pairwise separation is shown in Figure 6.6. Black polygons show areas that were only controlled via the leaf tier. That is, no other form of mechanical removal was performed in these areas. As can be seen, the areas that were not controlled were correctly labelled as mesquite. Areas that have been controlled by mechanical removal are free of mesquite and correctly labelled as other species.

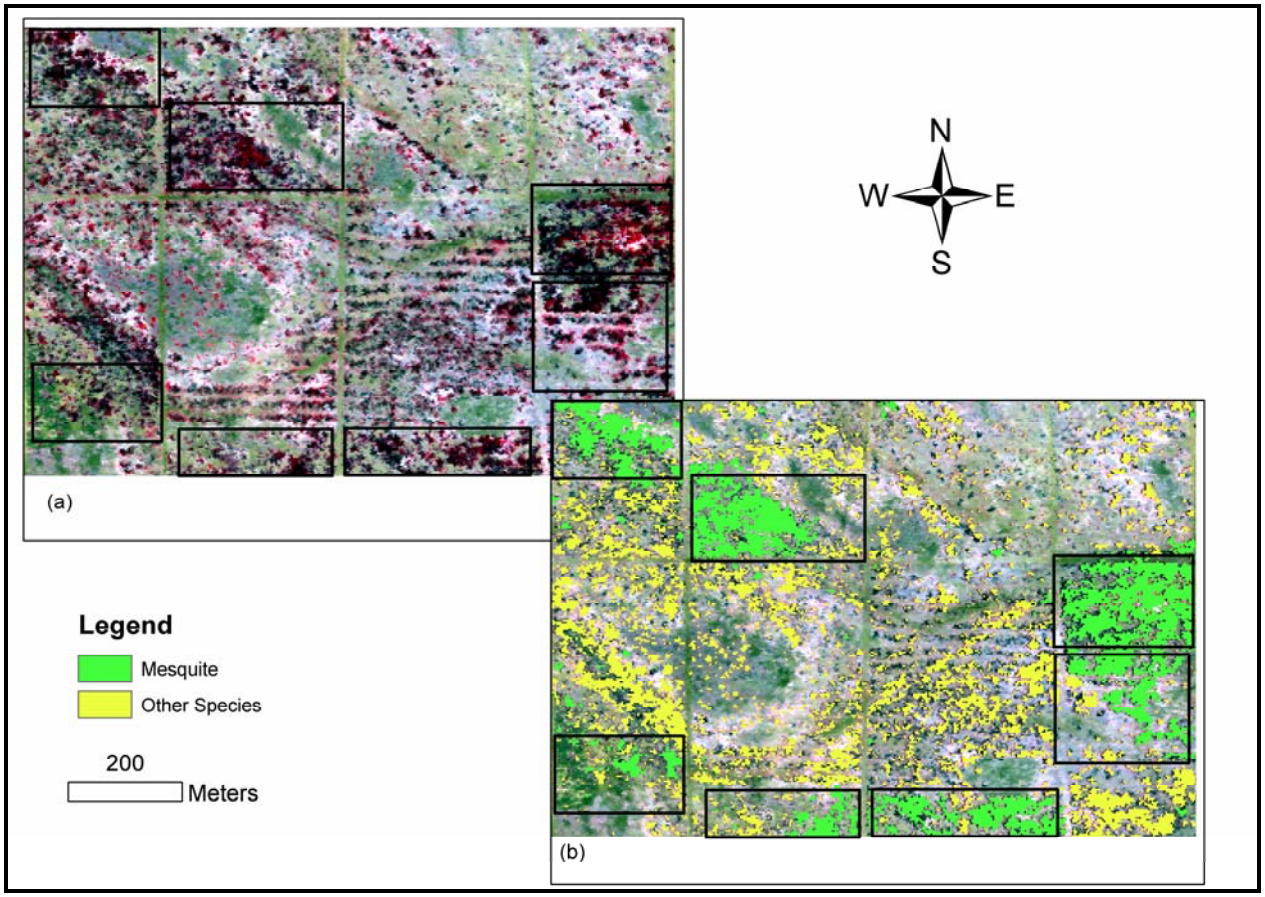

Figure 6.6 Sample map of the hyperspectral imagery classified using patch statistics identified by pairwise separation for a portion of the integrated trial. The black polygons represent areas not controlled by mechanical removal.

6. 5 Discussion

Assessment of class accuracy using confusion matrices has been the subject of much debate (e.g. Foody et al., 2002). At least two issues can be identified as to their inadequacy to reliably identify the best imagery and approach for the classification of invasive species from high spatial resolution data source. Firstly, assessment of the accuracy at distinguishing between different woody plant species that form easily delineable patches should not use a per-pixel approach. Such an approach does not take into account the fact that a patch may occupy many pixels and thus ignores local spatial autocorrelation. This will optimistically bias the accuracy of plants that are large and grow in thickets and pessimistically bias plants that have relatively small canopies. The per-class Kappa statistic only partially compensates for this fact. Therefore, in this study patches were used to construct the confusion matrix to mitigate this bias. However, per-pixel approaches have been used extensively to indicate classification accuracy throughout the weed mapping literature and thus need to be interpreted critically if they are mapping woody plants of vastly different sizes.

Secondly, confusion matrices do nothing to explain why there are errors or where they are occurring. For instance, growth habit, such as thicket formation, assists discrimination from coexisting species and, as has been shown in previous studies, classification accuracy generally increases as patches increase in size (e.g. Frazier, 1998; Dehaan et al., 2007; Hamada et al., 2007). Therefore, a higher proportion of large patches in the testing data, as opposed to small juveniles, is likely to optimistically bias the class accuracy. Subsequently, the confusion matrices and accuracy comparisons of DMSI versus the hyperspectral imagery must be considered critically. For example, the poorer accuracy of the DMSI in Section 6.4.3 is mainly an artefact of having been computed with more smaller patches (e.g. more were resolvable due to its higher spatial resolution). This is confirmed by non-significant differences between, for example, the hyperspectral imagery processed using patch statistics found from overall separation and the DMSI processed using patch statistics found from pairwise separation. Per-class Kappa only partially compensates for this difference in sample size, yet such comparisons between imagery are common (Congalton and Green, 1999). Significant differences are therefore predominantly

due to the approach for choosing patch statistics and the power of the imagery to differentiate mesquite from other species. Therefore, it is argued that an accuracy assessment of different size classes offers greater insight and confusion matrices should be derived from patches that can be reliably detected from each image type. In this study, reliable detection for both image types was found to be patches >36 m^2.

If the user is prepared to only craft management strategies based on patches that can be reliably detected then confusion matrices based on this threshold may be useful at indicating expected commission and omission error rates. Mapping invasive species in areas with poor access limits the tolerance of commission errors because of the cost and time taken for transport of removal crews and equipment (Lass and Prather, 2004). In this study, the best commission rate found was 6% (based on a pairwise separation of the patch statistics extracted from the hyperspectral imagery for patches >36 m^2), which effectively means that 6% of patches classed as mesquite will not be mesquite in the field. Comparisons between studies are difficult given a lack of information on the patch sizes used in other studies. However, the commission rate found in this study is similar to that found from previous studies using ANNs (e.g. Foody et al., 2005) but significantly better than other studies using unsupervised classification and thresholding routines (e.g. Frazier et al., 1998). The similar accuracy to the study by Foody et al. (2005) is likely to be a result of assessing accuracy with similarly large patch sizes (e.g. average = 77.7 m^2).

High omission errors can also be costly to management. For example, the more mesquite that is not detected and therefore not controlled, the higher the likelihood for reinvasion. In this study the lowest percentage of omission was 6%, for patches >36 m^2. This figure is lower than that found for mapping blackberry thickets using classification routines such as spectral angle mapper (SAM), matched filtering (MF) (Dehaan et al., 2007) and supervised and unsupervised classification (e.g Frazier et al., 1998); however, again, this is inconclusive given a lack of information on shrub/thicket sizes used for accuracy testing in those studies. For example, the inclusion of smaller shrubs inflated the errors of omission to levels as high as 51%. Mixture-tuned matched filtering (MTMF) is one method that may assist in the reduction of omission errors (Boardmand, 1998), which has been demonstrated by

Dehaan et al. (2007) for mapping blackberry thickets (e.g. 9% commission error) and, therefore, may be useful to trial in future studies for those patch sizes.

Neither DMSI nor hyperspectral imagery appears capable of reliably mapping mesquite patches less than 36 m^2 and this appears consistent with other studies on invasive woody plants that grow in thickets using similar spatial resolution imagery (e.g. Ullah et al., 1989; Frazier, 1998). However, accuracy increased to a very high level for patches >36 m^2, particularly using the pairwise separation approach on the hyperspectral dataset. As most individual mesquite plants (i.e., those that have not formed coalesced stands) in the study area are under 25 m^2 (van Klinken et al., 2006), this may be inadequate for mapping individual shrubs, for monitoring frontal population expansion or recent outbreaks from within the main population. Instead, this is still likely to rely on ground traverses and/or visual airborne surveys flown at low speed and altitude. A previous airborne survey of the region (van Klinken et al., 2007; Section 3.3.1) was capable of mapping shrubs down to 1.5 m^2. Alternatively, improvements in spatial resolution in such equipment as Unmanned Aerial Vehicles (UAVs; e.g. <5 cm) may be explored, with current research showing them to be an extremely attractive option for this task (e.g. Rango et al., 2006). Furthermore, there is potential to tune multispectral imagery such as DMSI, which can achieve a spatial resolution of 25 cm, to the wavelengths deemed to best separate species from hyperspectral imagery (Hamada et al., 2007); however, this may not suffice as the appearance of mesquite and associated species may change between image acquisitions. The option with the most potential therefore appears to be UAVs coupled with the same spectral resolution of hyperspectral instruments.

The results of this study demonstrate that the various patch statistics used enhance the ability to map large mesquite patches to quite a high accuracy even with coarse spectral resolution imagery. Exploratory analysis of the patch statistics introduced (e.g. majority and variety) in this study show the ability to separate mesquite from one or more species using this imagery. However, they were not used as input into the ANN classification procedure as they were excluded by the linear discriminant analysis step. Nonetheless, they may prove to be useful variables in future studies of this and other species of interest.

Choosing variables based on pairwise separation appears to be marginally better than choosing variables based on overall separation for both image types, particularly when assessed for patches >36 m^2. However, this needs further assessment and may be further explored in several ways. Firstly, if the map user is willing to accept a degree of commission error, omissions can be removed by increasing the prior probability that a patch is classified as mesquite (e.g. movement of the discriminatory plane (c.f. Lark, 1995)). The commissioned cases may then be removed by other means, such as direct field evaluation (Foody et al., 2005). Secondly, more complex operations (other than the Boolean OR) may be used to derive the "other" class. This may involve the use of fuzzy operators assigned to the activation layers of the ANN or the addition of complex weights (Foody et al., 2005). Thirdly, exploration of additional patch statistics such as size and shape may add further discriminatory power to enhance classification accuracy. Finally, rather than using mesquite as the target species for identifying patch statistics that separate it from each coexisting species in turn, patch statistics that separate eucalyptus from mesquite and eucalyptus from snakewood can be trialled to identify if its accuracy improves over the overall separation approach. Likewise, this can be done by using snakewood as the target class.

6. 6 Summary

Exotic plants pose a significant threat to biodiversity, ecosystem functioning and productivity on both local and global scales. A key requirement for effective management of invasive species is the ability to reliably identify their location and distribution across landscapes. Remote sensing is a potential data source for extracting this information. This study tested the use of four-band (red, green, blue and near infrared) digital multispectral imagery (DMSI) acquired at a resolution of 1 m and 126 band hyperspectral imagery acquired with a spatial resolution of 3 m for mapping mesquite. Various patch statistics were computed on patches extracted from the imagery. Two approaches were taken for identifying the patch statistics offering the greatest information for classification using a multilayer perceptron (MLP) artificial neural network. These were termed overall separation and pairwise separation. Overall separation sought to identify the patch statistics offering greatest overall separation from all three species (mesquite, eucalyptus and snakewood). Under pairwise separation, patch statistics were selected based on the separation

between mesquite and all species in turn. Two binary classifications were carried out comparing mesquite to each of the non-mesquite classes, which were then combined using a rule based approach (if snakewood or eucalyptus then not mesquite). Patches that were not identified as mesquite for either of the binary classifications were designated into the "other" class. Comparisons between the two image types suggested that hyperspectral imagery, particularly using the pairwise separation approach, was the most accurate. Analysis of the accuracy rates for different size classes showed that most of the error occurred for patches <36 m^2 and, therefore, neither imagery is likely to be able to resolve new outbreaks until they exceed that threshold. However, the use of either image type is likely to enable accurate classification of patches >36 m^2, particularly if a pairwise separation approach is adopted. Notwithstanding, hyperspectral imagery is likely to offer better results and greater flexibility under different defoliation regimes. Higher spatial resolution, most likely coupled to the same spectral resolution of hyperspectral instruments should be explored for its ability to map patches smaller than 36 m^2.

7 SUMMARY AND RECOMMENDATIONS

7. 1 Introduction

When dealing with plant invasions, land managers and policy makers require detailed information on which to base management action. However, labour intensive surveys are becoming less practical and prohibitively expensive. Spatial sciences offer a contemporary way in which to derive much of the necessary information in a timely and nonintrusive fashion. The research presented in this thesis demonstrates three kinds of information that can be developed or derived:

(i) historical aerial photographs can be analysed to reconstruct the spatial rates and patterns of invasion over time;
(ii) models can be produced to predict the suitability of a region to invasion; and
(iii) high spatial and spectral resolution remotely sensed imagery may assist in mapping and monitoring the distribution and spread of woody invasive plants, although issues with respect to the size of patch that can be detected and that which is required to be detected need further consideration. Only airborne imagery was used in this study – no satellite based remote sensed imagery was considered.

A summary of these three modules of research are presented hereafter, followed by recommendations for further research in these areas.

7. 2 Spatial and Temporal Invasion Rates and Patterns

Chapter 4 studied invasion rates and patterns through space and time over a 450 ha test area using a temporal series of aerial photography. This type of information is important for determining current and future levels of invasion over different land types, methods of expansion, and causes of spread, which can all assist in developing strategies and practices to reduce the likelihood of invasion in suitable, but currently unoccupied areas (e.g. through extrapolation over regional areas (see Section 7. 3)).

Woody plant patches were extracted from the temporal datasets of aerial photography using an unsupervised classification routine. Native vegetation was

masked out using an image acquired prior to invasion in this area. The spatial and temporal rates and patterns of mesquite invasion since introduction were then studied and revealed that:

(i) mesquite domination over grasses had been as rapid as areas occupied in its native range;
(ii) net mesquite cover increased from 2.4 % in 1970 to 24.4 % in 2001 over the 450 ha test area examined;
(iii) rates of mesquite invasion varied for each land type. Mesquite cover increased from 3 % in 1970 to 36 % in 2001 over the riparian zone; 2.6 % to 24.2 % over red loamy soils; and 0.4% to 11.1 % over stony soils;
(iv) recruitment will occur over all land types, however, canopies will coalesce more rapidly over the riparian zone and red-loamy soils than stony flats; and
(v) early successional patterns, such as high patch initiation followed by coalescence is similar to where mesquite is native, but patch mortality did not occur.

7.2.1 Recommendations

The availability of aerial photography prior to mesquite invasion in this study enabled post-processing of the unsupervised classification outputs to mask out native vegetation. This technique may be transferrable to other studies where aerial photography exists prior to the introduction of an invasive and long lived plant. However, because of the unique shape of mesquite relative to other species in the studied environment, object-oriented software (e.g. e-Cognition), which can include such variables as shape (and size, scale and colour) is recommended for trial, particularly in areas where aerial photography is not available prior to mesquite invasion. Additional samples in the 60-90 % cover range may be sought to better quantify the accuracy of the technique employed for this class.

7. 3 Modelling the Suitability of the Pilbara to Mesquite Invasion

Chapter 5 implemented a novel approach for predicting the suitability of the Pilbara Region to mesquite invasion. Such an output is useful for identifying priority areas to control and to monitor for outbreaks to enable early intervention strategies.

The model implemented in this study attempted to overcome many of the short-comings observed of commonly used techniques, particularly in ecological applications. For example, the modelling approaches that are typically used for conservation planning are also often used for predicting the suitability ranges of invasive plants. However, these applications have polarised objectives:

(i) conservative models need to limit (or, preferably, exclude) the number of false positives detected (i.e., underestimate the suitable habitat); and
(ii) invasive species prediction models need to limit false negatives (i.e., overestimate the suitable habitat).

While some models are often more conservative in their estimation than others, this level of conservatism cannot be directly controlled. Therefore, ordered weighted averaging was introduced to demonstrate its ability to directly alter the amount of risk assumed in each model.

A second limitation of commonly used models has been the assumption that there is no range of suitability within those defined to represent the variables used to model suitability. This study incorporated the use of fuzzy membership functions to better illustrate that within a suitability range there are different levels of favourability and these levels are continuous.

Thirdly, some of the methods used for modelling invasion suitability do not assign greater importance to variables likely to have more influence in defining areas suitable for invasion (e.g. BIOCLIM, WISP). Therefore, pairwise comparison, incorporating expert knowledge, was used to derive weights with respect to the importance of each variable.

Three models were derived, which varied the amount of conservatism from conservative to risk taking. Models were validated using 1000 random points (500 presence/500 absence) from an airborne helicopter survey of the core infestation. The area under the curve of relative operating characteristic (ROC) plots and the maximum Kappa method were used to quantify the accuracy of the models. Both

methods agreed that the model assuming the most risk gave the most representative result.

7.3.1 Recommendations

The approach to regional predictive modelling used in this study was robust and informative. It could capitalise on the relatively limited spatial data that were available for the Pilbara Region. Spatial data are typically limited for rangelands throughout the world and, therefore, the model developed in this thesis has a potentially wide application.

Data collected at a finer scale over areas of most interest are recommended to explore local variation. This would enable the derivation of a relationship between the density recordings of the aerial survey and the continuous outputs of the model so that a series of cut-points could be constructed showing various levels of suitability, rather than a simple Boolean output.

As the mesquite population is still expanding, repeat sampling and model refinement through iteration may be required. For example, it is possible that observed absences were only the result of not having sufficient time to invade there and not due to lack of necessary conditions. If this is identified to be the case, then variables can be directly updated by modifying the fuzzy membership functions.

The ROC plots and maximum Kappa method gave identical or nearly identical results. It is suggested, however, that the maximum Kappa method is more easily interpreted, while the ROC plot gives more information over the range of possible values. Therefore, it is recommended that both statistics should be presented in all model validations, particularly if the prevalence of data is equal (e.g. split equally between presence and absence records).

7. 4 Development of a Mapping and Monitoring Tool

Chapter 6 examined the effectiveness of DMSI and hyperspectral imagery for discriminating between mesquite and coexisting species. Accuracy in terms of the patch size reliably indentified was also investigated. Various summary statistics were applied to the patches of woody vegetation within the DMSI in order to garner

more discriminatory information. Only the mean spectral response was extracted from the hyperspectral imagery.

Both image types were useful at discriminating mesquite from coexisting species, particularly where patch statistics were chosen using pairwise separation of mesquite and associated species. However, neither DMSI nor hyperspectral imagery appears capable of reliably mapping mesquite patches less than 36 m^2 (ca 50 % accuracy) and this appears consistent with other studies on invasive woody plants that grow in thickets using similar spatial resolution imagery (e.g. Ullah et al., 1989; Frazier, 1998). Accuracy increased to a very high level for patches >36 m^2 (6 % omission) particularly using the pairwise separation approach on the hyperspectral dataset. As most individual mesquite plants (i.e., those that have not formed coalesced stands) in the study area are under 25 m^2 (van Klinken et al., 2006), this may be inadequate for mapping individual shrubs, for monitoring frontal population expansion or recent outbreaks from within the main population, although it is sufficient for mapping thickets and above average adults. Instead, this is still likely to rely on ground traverses and/or visual airborne surveys flown at low speed and altitude (e.g. van Klinken et al., 2007). Overall, the best approach identified in this research appears to be hyperspectral imagery processed using patch statistics found from pairwise separation of mesquite and each of the coexisting species in turn.

7.4.1 Recommendations

As mentioned above, the imagery and techniques used in this study could only reliably detect patches >36 m^2, with patches smaller than this only discernible for 50% of cases. This is unlikely to be acceptable for reliably mapping sparse, isolated shrubs or for monitoring new outbreaks. A previous airborne survey of the region (van Klinken et al., 2007) was capable of mapping shrubs down to 1.5 m^2, and may be an alternative method for recording individuals; however, this technique suffers from having to aggregate shrub counts into an 18.5 ha quadrat. A preferred solution would be to identify presence within smaller grid cells (e.g. <1 m^2). To this end, it is recommended that a pilot study using unmanned aerial vehicles (UAVs), which are capable of spatial resolutions <5 cm, be used, coupled with a hyperspectral instrument. The techniques described in Chapter 6 would be directly transferrable to such imagery, including the use of ANNs for classification.

Further exploration of the spectral signatures of mesquite plants/patches of different sizes (potentially grouped into size-classes) could be investigated as a source of error in detecting smaller patches. For example, it is possible that even when highly defoliated, thickets appear more vigorous (e.g. less sun flecks) than an isolated shrub even with the same percentage of defoliation. Consequently, different patch statistics may be appropriate for different size classes, which may aid in their discrimination from species of similar size and appearance (e.g. a heavily defoliated mesquite shrub versus the erectophile canopy structure of snakewood).

Further research on the use of choosing patch statistics using pairwise separation (e.g. mesquite versus each of the coexisting classes in turn) should be conducted. A useful test may involve changing the target species from mesquite to each of the other two species present in the study area. Patch statistics can then be selected that best separate these species from the each of the other two species. Studies using this technique on other species in different environments would also assist in confirming or denying it as a better approach than choosing patch statistics that best separate all species at once (overall separation).

The DMSI and hyperspectral imagery were collected at different spatial resolutions (1 m and 3 m, respectively). A more robust comparison of the two image types might best be undertaken by resampling the DMSI to a resolution of 3 m to match that of the hyperspectral imagery.

REFERENCES

Altman, D. G., Lausen, B., Sauerbrei, W. and Schumacher, M. (1994) Dangers of using 'optimal' cutpoints in the evaluations of prognostic factors, *Journal of the National Cancer Institute*, Vol. 86, pp. 829-835.

Anderson, G. L., Everitt, J. H., Richardson, A. J. and Escobar, D. E. (1993) Using satellite data to map false broomweed (*Ericameria austrotexana*) infestations on south Texas rangelands, *Weed Technology*, Vol. 7, pp. 865-871.

Anderson, J. and Cobb, N. (2004) Tree cover discrimination in panchromatic aerial imagery of Pinyon-Juniper Woodlands, *Photogrammetric Engineering and Remote Sensing*, Vol. 70, pp. 1063-1068.

Andrew, M. H. (1988) Grazing impact in relation to livestock watering points, *Trends in Ecology and Evolution*, Vol. 3, pp. 336-339.

Ansley, R. J., Wu, X. B., and Kramp, B. A. (2001) Observation: long-term increases in mesquite canopy cover in a north Texas savanna, *Journal of Range Management*, Vol. 54, pp. 171-176.

Archer, S., Scifres, C. J., Bassham, C. R., and Maggio, R. (1988) Autogenic succession in a subtropical savanna: conversion of grassland to thorn woodland, *Ecological. Monographs*, Vol. 58, pp. 111-127.

Archer, S. (1989) Have Southern Texas savannas been converted to woodlands in recent history? *The American Naturalist*, Vol. 134, pp. 545-561.

Archer, S. (1994) Woody plant encroachment into southwestern grasslands and savannas: Rates, patterns and proximate causes, in: Vavra, M., Laycock, W. and Pieper, R (eds), Ecological Implications of Herbivory in the West, Society for Range Management, Denver, pp. 13-68.

Archer, S. (1995) Tree-grass dynamics in a *Prosopis*-thornscrub savanna parkland: reconstructing the past and predicting the future, *Ecoscience*, Vol. 2, pp. 83-99.

Archer, S., Schimel, D. S. and Holland, E. A. (1995) Mechanisms of shrubland expansion: Land use, climate or CO_2?, *Climatic Change*, Vol. 29, pp. 91-99.

Aspinall, R. J., Marcus, W. A., Boardman, J. W. (2002) Considerations in collecting, processing, and analysing high spatial resolution hyperspectral data for environmental investigations, *Journal of Geographical Systems*, Vol. 4, pp. 15-29.

Asner, G. P., Archer, S., Hughes, R. F., Ansley, R. J., and Wessman, C. A. (2003) Net changes in regional woody vegetation cover and carbon storage in Texas Drylands, 1937-1999, *Global Change Biology*, Vol. 9, pp. 316-335.

Atkinson, P. M. and Tatnall, A. R. L. (1997) Neural networks in remote sensing, *International Journal of Remote Sensing,* Vol. 18, pp. 699-709.

Ayalew, L. and Yamagishi, H. (2005) The application of GIS-based logistic regression for landslide susceptibility mapping in the Kakuda-Yahiko mountains, Central Japan, *Geomorphology*, Vol. 65, pp. 15-31.

Baars, J. (2002) Biological control initiatives against *Lantana camera* L. (Verbenaceae) in South Africa: An assessment of the present status of the programme, and an evaluation of *Coelocephalapion camarae* Kissinger (Coleoptera: Brentidae) and *Falconia intermedia* (Distant) (Hemiptera: Miridae), two new candidate enemies for release on the weed. *PhD Thesis*, Rhodes University, Grahamstown.

Ball, G. L. (1994) Ecosystem modelling with GIS, *Environmental Management*, Vol. 18, pp. 345-349.

Beard, J.S. (1975) Pilbara, 1:1,000,000 Vegetation series: the vegetation of the Pilbara area. University of Western Australia Press, Australia.

Benediktsson, J. A., Swain, P. H. and Esroy, O. K. (1990) Neural network approaches versus statistical methods in classification of multisource remote sensing data, *IEEE Transactions on Geoscience and Remote Sensing,* Vol. 28, pp. 540-551.

Bishop, C. M. (1995) *Neural networks for pattern recognition*, Oxford University Press, Oxford, 482 pp.

Boardman, J. W. (1998) Leveraging the high dimensionality of AVIRIS data for improved sub-pixel target unmixing and rejection of false positives: Mixture tuned matched filtering, AVIRIS 1998 Proceedings, JPL, California, 6 pp.

Bonham-Carter, G. (1994) Geographic Information Systems for Geoscientists: Modelling with GIS, Pergamon Press, Netherlands, Tarrytown, N. Y., 398 pp.

Bowman, D. M. J. S. (1998) Tansley Review No. 101. The impact of Aboriginal landscape burning on the Australian biota, *New Phytologist*, Vol. 140, pp. 385-410.

Bowman, D. M. J. S., Walsh, A., and Milne, D. J. (2001) Forest expansion and grassland contraction within a eucalyptus savanna matrix between 1941 and 1994 at Litchfield National Park in the Australian monsoon tropics. *Global Ecology and Biogeography*, Vol. 10, pp. 535-548.

Brandtberg, T. (2002) Individual tree-based species classification in high spatial resolution aerial images of forests using fuzzy sets, *Fuzzy Sets and Systems*, Vol. 132, pp. 371-387.

Brown, J. R. and Archer, S. (1987) Woody plant seed dispersal and gap formation in a North-American sub-tropical savanna woodland: the role of domestic herbivores, *Vegetatio*, Vol. 73, pp. 73-80.

Brown, J. R. and Archer, S. (1989) Woody plant invasion of grasslands: establishment of honey mesquite (*Prosopis glandulosa* var. *glandulosa*) on sites differing in herbaceous biomass and grazing history, *Oecologia*, Vol. 80, pp. 19-26.

Brown, J. R., and Carter, J. (1998) Spatial and temporal patterns of exotic shrub invasion in an Australian tropical grassland. *Landscape Ecology,* Vol. 13, pp. 93-102.

Bureau of Meteorology, 2006. Tropical cyclones affecting inland Pilbara towns, Available: http://www.bom.gov.au/weather/wa/cyclone/about/inland_pilbara_index.shtm.

Burks, T. F., Shearer, S. A. Heath, J.R., and Donohue, K.D. (2005) Evaluation of neural –network classifiers for weed species discrimination, *Biosystems Engineering*, Vol. 91, pp. 293-304.

Burnett, C. and Blaschke, T. (2003) A multi-scale segmentation/object relationship modeling methodology for landscape analysis, *Ecological Modelling*, Vol. 168, pp. 233-249.

Busby, J. R. (1991) BIOCLIM – A bioclimatic analysis and prediction system, in: Nature conservation: cost effective biological surveys and data analysis (Margules, C. R. and Austin, M. P. eds), CSIRO, Melbourne, pp. 64-68.

Cantor, S. B., Sun, C. C., Tortolero-Luna, G., Richards-Kortum, R. and Follen, M. (1999) Comparison of C/B ratios from studies using receiver operating characteristic curve analysis, *Journal of Clinical Epidemiology*, Vol. 52, pp. 885-892.

Carleer, A. and Wolff, E. (2004) Exploitation of Very High Resolution Satellite Data for Tree Species Identification, *Photogrammetric Engineering and Remote Sensing*, Vol. 70, pp. 135-140.

Carson, H. W., Lass, L. W. and Callihan, R. H. (1995) Detection of Yellow Hawkweed (*Hieracium pretense*) with high resolution multispectral digital imagery, *Weed Technology*, Vol. 9, pp. 477-483.

Caudill, M. (1988) Neural networks primer: Part III, *AI Expert,* June, pp. 53-59.

Chavez, P. S. (1988) An improved dark-object subtraction technique for atmospheric scattering correction of multispectral data, *Remote Sensing of Environment,* Vol. 24, pp. 459-479.

Clark University (2006) IDRISI Andes V 15.01, Clark Laboratories, Worcester MA, USA.

Cocks, T., Jenssen, R., Stewart, R., Wilson, I., Shields, T. (1998) The HyMap airborne hyperspectral sensor: The system, calibration and performance, Proceedings of the 1st EARSEL Workshop on Imaging Spectrometry, Zurich, 6-8 October, pp. 37-42.

Cohen, J. (1960) A coefficient of agreement for nominal scales, *Educational and Psychological measurement*, Vol. 20, pp. 37-46.

Collingham, Y. C., Wadsworth, R. A., Huntley, B., and Hulme, P. E. (2000) Predicting the spatial distribution of non-indigenous riparian weeds: issues of spatial scale and extent, *The Journal of Applied Ecology*, Vol. 37, Supplement 1: NERC/SERAD Special Issue, pp. 13-27.

Congalton, R. G. and Green, K. (1999) Assessing the accuracy of remotely sensed data: principles and practices, Boca Raton, Lewis Publishers.

Cox, J. R., De Alba-Avila, A., Rice, R. W., and Cox, J. N. (1993) Biological and physical factors influencing *Acacia constricta* and *Prosopis velutina* establishment in the Sonoran Desert, *Journal of Range Management*, Vol. 46, pp. 43-48.

de Gruijter, J. (1999) Spatial sampling schemes for remote sensing, in: A. Stein, F. Van Der Meer & B. Gorte, (eds.), *Spatial Statistics for Remote Sensing*, Springer, p. 325.

Dehaan, R., Louis, J., Wilson, A., Hall, A. and Rumbachs, R. (2007) Discrimination of blackberry (*Rubus fruticosus* sp. agg.) using hyperspectral imagery in Kosciuszko National Park, NSW, Australia, *Photogrammetry and Remote Sensing*, Vol. 62, pp. 13-24.

Derner, J. D., Tischler, C. R., Polley, H. W. and Johnson, H. B. (2005) Seedling growth of two honey mesquite varieties under CO_2 enrichment, *Rangeland Ecology and Management*, Vol. 58, pp. 292-298.

Dewey, S. A., Price, K. P. and Ramsey, D. (1991) Satellite remote sensing of Dyer's woad (*Isatis tinctoria*), *Weed Technology*, Vol. 5, pp. 479-484.

Eastman, J. R. (2006) IDRISI Andes: Guide to GIS and image processing, Clark Laboratories, Worcester, 327 pp.

Eckhardt, H. C., van Wilgen, B. W. and Biggs, H. C. (2000) Trends in woody vegetation cover in the Kruger National Park, South Africa, between 1940 and 1998, *African Journal of Ecology*, Vol. 38, pp. 108-115.

Elith, J., Graham, C. H., Anderson, R. P., Dudik, M., Ferrier, S., Guisan, A., Hijmans, R. J., Huettmann, F., Leathwick, J. R., Lehmann, A., Li, J., Lohmann, L. G., Loisell, B. A., Manion, G., Moritz, C., Nakamura, M., Nakazawa, Y., Overton, J., Peterson. A. T., Phillips, J., Richardson, K., Scahetti-Pereira, R., Schapire, R. E., Soberon, J., Williams, S., Wisz, M. S. and Zimmermann, N. E.

(2006) Novel methods to improve prediction of species' distributions from occurrence data, *Ecography*, Vol. 29, pp. 129-151.

El-Keblawy, A. and Al-Rawai, A. (2005) Effects of salinity, temperature and light on germination of invasive *Prosopis juliflora* (Sw.) D.C., Journal of Arid Environments, Vol. 61, pp. 555-565.

Erikson, M. (2004) Species classification of individually segmented tree crowns in high-resolution aerial images using radiometric and morphologic image measures, *Remote Sensing of Environment,* Vol. 91, pp. 469-477.

Esch, T., Roth, A., Strunz, G. and Desch, S. (2003) Object-oriented classification of Landsat-7 data for regional planning purposes. *The International Archives of the Photogrammetry, Remote Sensing and Spatial Information Sciences* (CD-ROM), Vol. XXXIV-7/W9, Regensburg, Germany, 27-29, June, 2003.

ESRI (2004) Environmental Systems Research Institute, ArcGIS Version 9, Environmental Systems Research Institute Incorporated, Redlands, California.

Everitt, J. H. and Villarreal, R. (1987) Detecting Huisache (*Acacia farnesiana*) and Mexican Palo-verde (Parkinsonia aculeate) by aerial photography, *Weed Science*, Vol. 35, pp. 427-432.

Everitt, J. H. and DeLoach, C. J. (1990) Remote sensing of Chinese Tamarisk (*Tamarix chinensis*) and associated vegetation, *Weed Science,* Vol. 38, pp. 273-278.

Everitt, J. H., Alaniz, M. A., Escobar, D. E. and Davis, M. R. (1992a) Using remote sensing to distinguish common (*Isocoma coronopifolia*) and Drummond Goldenweed (*Isocoma drummondii*), *Weed Science*, Vol. 40, pp. 621-628.

Everitt, J. H., Escobar, D. E., Alaniz, M. A., Villarreal, R. and Davis, M. R. (1992b) Distinguishing brush and weeds on rangelands using video remote sensing, Weed Technology, Vol. 6, pp. 913-921.

Everitt, J. H., Anderson, G. L., Escobar, D. E., Davis, M. R., Spencer, N. R. and Andrascik, R. J. (1995) Use of remote sensing for detecting and mapping Leafy Spurge (Euphorbia esula), *Weed Technology*, Vol. 9, pp. 599-609.

Everitt, J. H., Escobar, D. E., Alainz, M. A., Davis, M. R. and Richerson, J. V. (1996) Using spatial information technologies to map Chinese Tamarisk (*Tamarix chinensis*) infestations, *Weed Science,* Vol. 44, pp. 194-201.

Everitt, J. H., Escobar, D. E., Appel, D. N., Riggs, W. G. and Davis, M. R. (1999) Using airborne digital imagery for detecting oak wilt disease, *Plant Disease* Vol. 83, pp. 502–505.

Everitt, J. H., Yang, C., Racher, B. J., Briton, C. M. and Davis, M. R. (2001) Remote sensing of Redberry Juniper in the Texas Rolling Plains, *Journal of Range Management,* Vol. 54, pp. 254-259.

Everitt, J. H., Yang, C., Helton, R. J., Hartmann, L. H. and Davis, M. R. (2002) Remote sensing of giant salvinia in Texas waterways, *Journal of Aquatic Plant Management*, Vol,. 40, pp. 11-16.

Everitt, J. H., Yang, C. and Flores, D. (2003) Light reflectance characteristics and remote sensing of waterlettuce, *Journal of Aquatic Plant Management*, Vol. 41, pp. 39-44.

Everitt, J. H., Yang, C., Alaniz, M. A., Davis, M. R., Nibling, F. L. and Deloach, C. J. (2004) Canopy spectra of giant reed and associated vegetation, *Journal of Range Management*, Vol. 57, pp. 561-569.

Fensham, R. J., Fairfax, R. J., Holman, J. E., and Whitehead, P. J. (2002) Quantitative assessment of vegetation structural attributes from aerial photography, *International Journal of Remote Sensing*, Vol. 23, pp. 2293-2317.

Fensham, R. J. and Fairfax, R. J. (2003) Assessing woody vegetation cover change in north-west Australian savanna using aerial photography, *International Journal of Wildland Fire*, Vol. 12, pp. 359-367.

Fielding, A. H. and Bell, J. F. (1997) A review of methods for the assessment of prediction errors in conservation presence/absence models, *Environmental Conservation*, Vol. 24, pp. 38-49.

Foody, G. M. and Arora, M. K. (1997) An Evaluation of Some Factors Affecting the Accuracy of Classification by an Artificial Neural Network, *International Journal of Remote Sensing,* Vol. 18, pp. 799-810.

Foody, G. M. (2001) Thematic Mapping from Remotely Sensed Data with Neural Networks: MLP, RBF and PNN based Approaches, *Journal of Geographical Systems,* Vol. 3, pp. 217-232.

Foody, G. M. (2002) Status of land cover classification accuracy assessment, *Remote Sensing of Environment*, Vol. 80, pp. 185-201.

Foody, G. M., Atkinson, P. M., Gething, P. W., Ravenhill, N. A. and Kelly, C. K. (2005), Identification of Specific Tree Species in Ancient Semi-Natural Woodland from Digital Aerial Sensor Imagery, *Ecological Applications,* Vol. 15, pp. 1233-1244.

Frazier, P. (1998) Mapping blackberry thickets in Kosciuszko National Park using airborne video data, *Plant Protection Quarterly*, Vol. 13, pp 145-148.

Gao, B. C., Goetz, A. F. H. (1990) Column atmospheric water vapour and vegetation liquid water retrievals from airborne imaging spectrometer data, *Journal of Geophysical Research*, Vol. 95, pp. 3549-3564.

Gao, B. C., Heidebrecht, K. B. and Goetz, A. F. H. (1993) Derivation of scaled surface reflectances from AVIRIS data, *Remote Sensing of Environment*, Vol. 44, pp. 165-178.

Gao, B. C. Heidebrecht, K. B. and Goetz, A. F. H. (1999) *ATmosphere REMoval Program (ATREM) User's Guide, Version 3.1*, Center for the Study of Earth from Space (CSES), Cooperative Institute for Research in Environmental Sciences (CIRES), University of Colorado, Boulder, CO.

Gardiner, D. B., Tupper, G. J. and Dudgeon, G. S. (1998) A quantitative appraisal of woody shrub encroachment in western New South Wales, *The Rangeland Journal*, Vol. 20, pp. 26-40.

Gessler, P. E., I.D. Moore, N. J., McKenzie and P. J. Ryan (1995) Soil-landscape modelling and spatial prediction of soil attributes, *International Journal of GIS*, Vol. 9, pp. 421-432.

Gibbens, R. P., Beck, R. F., McNeely, R. P., and Herbel, C. H. (1992) Recent rates of mesquite establishment in the Northern Chihuahan Desert, *Journal of Range Management*, Vol. 45, pp. 585-588.

Gibbens, R. P., and Lenz, J. M. (2001) Root systems of some Chihuahuan Desert plants, *Journal of Arid Environments*, Vol. 49, pp. 221-263.

Gile, L. H., Gibbens, R. P., and Lenz, J. M. (1997) The near-ubiquitous pedogenic world of mesquite roots in an arid basin floor, *Journal of Arid Environments*, Vol. 35, pp. 39-58.

Gillham, J. H., Hild, A. L., Johnson, J. H., Hunt, E. R. Jr, and Whitson, T. D. (2004) Weed invasion susceptibility prediction (WISP) model for use with Geographic Information Systems, *Arid Land Research and Management*, Vol. 18, pp. 1-12.

Glendening, G. E. (1952) Some quantitative data on the increase of mesquite and cactus on a desert grassland range in Southern Arizona, *Ecology,* Vol. 33, pp. 319-328.

Glenn, N. F., Mundt, J. T., Weber, K.T., Prather, T. S., Lass, L.W. and Pettingill, J. (2005) Hyperspectral data processing for repeat detection of leafy spurge, *Remote Sensing of Environment*, Vol. 95, pp. 399-412.

Gong, P., Pu, R. and Yu, B., (1997) Conifer Species Recognition: An Exploratory Analysis of *In Situ* Hyperspectral Data, *Remote Sensing of Environment,* Vol. 62, pp. 189-200.

Gorsevski, P. V., Gessler, P. E. , Foltz, R. B., and Elliot, W. J. (2006) Spatial prediction of landslide hazard using logistic regression and ROC Analysis, *Transactions in GIS*, Vol. 10, pp. 395-415.

Goslee, S. C., Havstad, K. M., Peters, D. P. C., Rango, A., and Schlesinger, W. H. (2003) High-resolution images reveal rate and pattern of shrub encroachment

over six decades in New Mexico, U.S.A., *Journal of Arid Environments*, Vol. 54, pp. 755-767.

Goslee, S. C., Peters, D. P. C., and Beck, K. G. (2006) Spatial prediction of invasion success across heterogeneous landscapes using an individual-based model, *Biological Invasions*, Vol. 8, pp. 193-200.

Green, A. A., Berman, M., Switzer, P. and Craig, M. (1988) A transformation for ordering multispectral data in terms of image quality with implications for noise removal, *IEEE Transactions on Geoscience and Remote Sensing*, Vol. 26, pp. 65-74.

Greig-Smith, P., 1983. Quantitative Plant Ecology, 3rd ed. Blackwell Scientific, Oxford.

Grice, A. C., Radford, I. J., and Abbott, B. N. (2000) Regional and landscape-scale patterns of shrub invasion in tropical savannas, *Biological Invasions*, Vol. 2, 187-205.

Griffiths, M. and Barker, R. D. (1966) The plants eaten by sheep and by kangaroos grazing together in a paddock in south-western Queensland, *CSIRO Wildlife Research*, Vol. 11, pp. 145-167.

Guisan, A. and Zimmermann, N.E. (2000) Predictive habitat distribution models in ecology, *Ecological Modelling*, Vol. 135, pp. 147-186.

Haara, A. and Haarala, M. (2002) Tree Species Classification using Semi-Automatic Delineation of Trees on Aerial Images, *Scandanavian Journal of Forest Research,* Vol. 17, pp. 556-565.

Hair, J. F. Jr., Black, W. C., Babin, B. J., Anderson, R. E., and Tatham, R. L. (2006) Multivariate Data Analysis (6th ed), Pearson Education International, Australia, 899 pp.

Hamada, Y., Stow, D. A., Coulter, L. L., Jafolla, J. C. and Hendricks, L. W. (2007) Detecting Tamarisk species (Tamarix spp.) in riparian habitats of Southern California using high spatial resolution hyperspectral imagery, *Remote Sensing of Environment*, Vol. 109, pp. 237-248.

Harding, G. B. and Bate, G. C. (1991) The occurrence of invasive *Prosopis* species in the north-western Cape, South Africa, *South African Journal of Science*, Vol. 87, pp. 188-192.

Hay, G. J., Blaschke, T., Marceau, D. J. and Bouchard, A. (2003) A comparison of three image-object methods for the multiscale analysis of landscape structure, *Photogrammetry and Remote Sensing*, Vol. 57, pp. 327-345.

Harsanyi, J. C. and Chang, C. I. (1994) Hyperspectral image classification and dimensionality reduction: an orthogonal subspace projection approach, *IEEE Transactions on Geoscience and Remote Sensing*, Vol. 32, pp. 779–785.

Hennessy, J. T., Gibbens, R. P., Tromble, J. M., and Cardenas, M. (1983) Vegetation changes from 1935 to 1980 in mesquite dunelands and former grasslands of southern New Mexico, *Journal of Range Management*, Vol. 36, pp. 370-374.

Heuvelink, G. B. M. and Burrough, P. A. (1993) Error propagation in cartographic modelling using Boolean logic and continuous classification, International Journal of *Geographical Information Science*, Vol. 7, pp. 231-246.

Higgins, S. I., Richardson, D. M., Cowling, R. M., and Trinder-Smith, T. H. (1999) Predicting the landscape-scale distribution of alien plants and their threat to plant diversity, *Conservation Biology*, Vol. 13, pp. 303-313.

Highland Statistics LTD (2006), Software package for multivariate analysis and multivariate time series analysis, version 2.5.1 (computer program).

Huberty, C. J. (1994) Applied Discriminant Analysis, New York, USA, Wiley, 466 pp.

Hudak, A. T. and Wessman, C. A. (1998) Textural analysis of historical aerial photography to characterise woody plant encroachment in South African savanna, *Remote Sensing of Environment*, Vol. 66, pp. 317-330.

Hulme, P. E. (2003) Biological invasions: winning the science but losing the conservation war?, *Oryx*, Vol. 37, pp. 178-193.

Hunt, E. R., Everitt, J. H., Ritchie, J. C., Moran, S., Booth, D. T., Anderson, G. L., Clark, P. E. and Seyfried, M. S. (2003) Applications and Research Using Remote Sensing for Rangeland Management, *Photogrammetric Engineering and Remote Sensing,* Vol. 69, pp. 675-693.

Hunt, E.R., Everitt, J. H., and Hamilton, R. (2005) A weed manager's guide to remote sensing and GIS-mapping and monitoring, Remote Sensing Applications Center, USDA Forest Service, Salt Lake City, UT, available: http:www.fs.fed.us/eng/rsac/invasivespecies/documents/mapping.pdf

Hutchinson, C. F., Unruh, J. D. and Bahre, C. J. (2000) Land Use vs. Climate as Causes of Vegetation Change: A Study in SE Arizona, *Global Environmental Change,* Vol. 10, pp. 47-55.

Jensen, J. R., 1996. Introductory Digital Image Processing: A Remote Sensing Perspective, Prentice Hall, New Jersey.

Kadmon, R., and Harari-Kremer, R. (1999) Studying long-term vegetation dynamics using digital processing of historical aerial photographs, *Remote Sensing of Environment*, Vol. 68, pp. 164-176.

Kanellopoulos, I. and Wilkinson, G. G. (1997) Strategies and Best Practice for Neural Network Image Classification, *International Journal of Remote Sensing,* Vol. 18, pp. 711-725.

Kendrick, P. and Stanley, F. (2001) Pilbara 4 – Roebourne synopsis, A biodiversity audit of Western Australia's 53 biogeographical subregions in 2002, pp. 581-593.

Klecka, W.R. (1980) *Discriminant Analysis*, Quantitative Applications in the Social Sciences, Sullivan, J.L. (ed), Sage University Papers, 71 pp.

Kramp, B. A., Ansley, R. J., and Tunnell, T. R. (1998) Survival of mesquite seedlings emerging from cattle and wildlife feces in a semi-arid grassland, *The Southwestern Naturalist*, Vol. 43, pp. 300-312.

Kruse, F. A. Lefkoff, A. B., Boardman, J. W., Heidebrecht, K. B., Shapiro, A. T., Barloon, P. J., and Goetz, A. F. H. (1993) The Spectral Image Processing System (SIPS) – Interactive visualisation and analysis of imaging spectrometer data, *Remote Sensing of Environment*, Vol. 44, pp. 145-163.

Lahav-Ginott, S., Kadmon, R. and Gersani, M. (2001) Evaluating the viability of *Acacia* populations in the Negev Desert: A remote sensing approach, *Biological. Conservation*, Vol. 98, 127-137.

Laliberte, A., Rango, A., Havstad, K. M., Paris, J. F., Beck, R. F., McNeely, R. P., and Gonzalez, A. L. (2004) Object-oriented image analysis for mapping shrub encroachment from 1937 to 2003 in southern New Mexico, *Remote Sensing of Environment*, Vol. 93, pp. 198-210.

Landis, J. R. and Koch, G. C. (1977) The measurement of observer agreement for categorical data, *Biometrics*, Vol. 33, pp. 159-174.

Lark, R. M. (1995) Components of Accuracy of Maps with Special Reference to Discriminant Analysis of Remote Sensor Data, *International Journal of Remote Sensing,* Vol. 16, pp. 1461-1480.

Lass, L. W., Carson, H. W. and Callihan, R. H. (1996) Detection of Yellow Starthistle (Centaurea solstitialis) and Common St. Johnswort (Hypericum perforatum) with multispectral digital imagery, *Weed Technology*, Vol. 10, pp. 466-474.

Lass, L. W., Thill, D. C., Shafii, B. and Prather, T. S. (2002) Detecting Spotted Knapweed (Centaurea maculosa) with hyperspectral remote sensing technology, *Weed Technology*, Vol. 16, pp. 426-432.

Lass, L. W. and Prather, T. S. (2004) Detecting the locations of Brazilian Pepper Trees in the Everglades with a hyperspectral sensor, *Weed Technology*, Vol. 18, pp. 437-442.

Lass, L. W., Prather, T. S., Glenn, N. F., Weber, K. T., Mundt, J. T. and Pettingill, J. (2005) A review of remote sensing of invasive weeds and example of early detected of Spotted Knapweed (*Centaurea maculosa*) and Babysbreath

(*Gypsophila paniculata*) with a hyperspectral sensor, *Weed Science*, Vol. 53, pp. 242-251.

Lawerence, R. L., Wood, S. D. and Sheley, R. L. (2006) Mapping invasive plants using hyperspectral imagery and Breiman Cutler classifications (RandomForest), *Remote Sensing of Environment*, Vol. 100, pp. 356-362.

Lawes, R. A. and Wallace, J. F. (2006) Using temporal sequences of Landsat imagery to detect trends in *Acacia nilotica* in the Mitchell grass plains, in: Preston, C., Watts, J. H. and Crossman, N. D. (eds) *Proceedings of the 15th Australian Weeds Conference,* Weed Management Society of South Australia, Adelaide, pp. 474-476.

Leckie, D. G., Yuan, X., Ostaff, D. P., Piene, H., MacLean, D. A. (1992) Analysis of high resolution multispectral MEIS imagery for Spruce Budworm damage assessment on a single tree basis, *Remote Sensing of Environment*, Vol. 40, pp. 125-136.

Lee, J., Weger, R. C., Sengupta, S. K. and Welch, R. M. (1990) A neural network approach to cloud classification, *IEEE Transactions on Geoscience and Remote Sensing*, Vol. 15, pp. 3263-3270.

Leighton, K. A., Zappelli, S. A., Godden, P. T., MacDonagh, A. F., van Vreeswyk, A. M. E., Payne, A. L., Mitchell, A. A., and Hennig, P. (2004) Land systems of the Pilbara rangeland survey (includes Roebourne Plains survey area, mapped 1987). Maps to accompany Western Australian Department of Agriculture, Technical Bulletin No. 92.

Lillesand, T. M. and Kiefer, R. W. (2000) Remote Sensing and Image Interpretation, 4th Ed, John Wiley and Sons, Inc., New York.

Liu, C, Berry, P. M., Dawson, T. P., and Pearson, R. G. (2005) Selecting thresholds of occurrence in the prediction of species distributions, *Ecography*, Vol. 28, pp. 385-393.

Loiselle, B. A., Howell, C. A., Graham, C. H., Goerck, J. M., Brooks, T., Smith, K. G. and Williams, P. H. (2003) Avoiding pitfalls of using species distribution models in conservation planning, *Conservation Biology*, Vol. 17, pp. 1591-1600.

Lopez-Portillo, J. and Montana, C. (1999) Spatial distribution of *Prosopis glandulosa* var. *torreyana* in vegetation stripes of the Southern Chihuahuan Desert, *Acta Oecologica*, Vol. 20, pp. 197-208.

Mack, R. N., Simberloff, D., Lonsdale, W. M., Evans, H., Clout, and M., Bazzaz, F. A. (2000) Biotic invasions: causes, epidemiology, global consequences, and control, *Ecological Applications*, Vol. 10, pp. 689-710.

Mack, R. N. (2005) Assessing biotic invasions in time and space: The second imperative, in: *Invasive alien species: A new synthesis*, Mooney, H. A., Mack,

R. N., McNeely, J. A, Neville, L. E., Sche, P. J., Waage, J. K. (eds), Island Press, Washington, 368 pp.

Malczewski, J. (1999) GIS and mutlicriteria decision analysis, John Wiley and Sons, Brisbane, 392 pp.

Manson, F. J., Loneragan, R., McLeod, M. and Kenyon, R. A. (2001) Assessing Techniques for Estimating the Extent of Mangroves: Topographic Maps, Aerial Photographs and Landsat TM Images, *Marine and Freshwater Research,* Vol. 52, pp. 787-792.

Martin, M. E., Newmann, S. D., Aber, J. D. and Congalton, R. G. (1998) Determining forest species composition using high spectral resolution remote sensing data, *Remote Sensing of Environment*, Vol. 65, pp. 249-254.

Mather, P. M., 2004. Computer processing of remotely-sensed images: an introduction, 3rd Ed., John Wiley & Sons Ltd.

McDonald RC, Isbell RF, Speight JG, Walker J, Hopkins MS (1990) (Eds.) *Australian soil and land survey handbook – field handbook* (2nd ed), Inkata Press: Melbourne).

McGarigal, K., Cushman, S. A., Neel, M. C. and Ene, E. (2002) FRAGSTATS: Spatial Pattern Analysis Program for Categorical Maps. Computer Software Program Produced by the Authors at the University of Massachusetts, Amherst. Available at the following web site: www.umass.edu/landeco/research/fragstats/fragstats.html.

McGlynn, I.O. and Okin, G.S. (2006) Characterization of shrub distribution using high spatial resolution remote sensing: Ecosystem implications for a former Chihuahuan Desert grassland, *Remote Sensing of Environment*, Vol. 101, pp. 554-566.

Meadly, G. R. W. (1962) Weeds of Western Australia – mesquite, *Journal of Agriculture. WA*, Vol. 3, pp. 729-739.

Medlin, C. R, Shaw, D. R., Gerard, P. D. and LaMastus, F. E. (2000) Using remote sensing to detect weed infestations in *Glycine max*, *Weed Science*, Vol. 48, pp.393-398.

Miao, X., Gong, P., Swope, S. Pu, R., Carruthers, R., Anderson, G. L., Heaton, J. S. and Tracey, C. R. (2006) Estimation of yellow starthistle abundance through CASI-2 hyperspectral imagery using linear spectral mixture models, *Remote Sensing of Environment*, Vol. 101, pp.329-341.

Mitchell, A. A. and Wilcox, D. G. (1994) *Arid shrubland plants of Western Australia* (2nd and enlarged edition), University of Western Australia Press in Association with the Department of Agriculture Western Australia, 478 pp.

Monserud, R. A. and Leemans, R. (1992) Comparing global vegetation maps with the Kappa statistic, *Ecological Modelling*, Vol. 62, pp. 275-293.

Moody, M. E. and Mack, R. N. (1988) Controlling the spread of plant invasions: the importance of nascent foci, *Journal of Applied Ecology*, Vol. 25, pp. 1009-1021.

Morisette, J. T., Jarnevich, C. S., Ullah, A., Cai, W., Pedelty, J. A., Gentle, J. E., Stohlgren, T. J., and Schnase, J. L. (2006) A tamarisk habitat suitability map for the continental United States, *Frontiers in Ecology and the Environment*, Vol. 4, pp. 11-17.

Mullerova, J., Pysek, P., Jarosik, V. and Pergl, J. (2005) Aerial photographs as a tool for assessing the regional dynamics of the invasive plant species *Heracleum mantegazzianum*, *Journal of Applied Ecology*, Vol. 42, pp. 1042-1053.

Mundt, J., Glenn, N. F., Weber, K. T., Prather, T. S., Lass, L. W., and Pettingill, J. (2005) Discrimination of hoary cress and determination of its detection limits via hyperspectral image processing and accuracy assessment techniques, *Remote Sensing of Environment*, Vol. 96, pp. 509-517.

Murai, H. and Omatu, S. (1997) Remote sensing image analysis using a neural network and knowledge-based processing, *International Journal of Remote Sensing*, Vol. 18, pp. 811-828.

Olivera, F., Furnans, J. Maidment, D., Djokic, D. and Ye, Z. (2002) Drainage Systems, in: ArcHydro: GIS for Water resources, Maidment, D. (ed), ESRI Press, Redlands, California, pp. 55-86.

Osmond, R., March, N., Campbell, S., van Klinken, R., Cobon, R., and Jeffrey, P. (2003) Mesquite: best practice manual, The State of Queensland, Department of Natural Resources and Mines, 90 pp.

Paola, J. D. and Schowengerdt, R. A. (1995) A Review and Analysis of Backpropagation Neural Networks for Classification of Remotely-Sensed Multi-spectral Imagery, *International Journal of Remote Sensing,* Vol. 16, pp. 3033-3058.

Papanastasis, V. P. (1977) Optimum size and shape of quadrat for sampling herbage weight in grasslands of northern Greece, *Journal of Range Management*, Vol. 30, pp. 446-449.

Parker-Williams, A. and Hunt, E. R. –Jr. (2002) Estimation of leafy spurge cover from hyperspectral imagery using mixture tuned matched filtering, *Remote Sensing of Environment*, Vol. 82, pp. 446-456.

Pasiecznik, N. M., Felker, P., Harris, P. J. C., Harsh, L. N., Cruz, G., Tewari, J. C., Cadoret, K., and Maldonado, L. J. (2001) The *Prosopis juliflora* - *Prosopis pallida* complex: a monograph, HDRA Coventry, UK.

Payne, A. L. and Mitchell, A. A. (2002) Pastoral condition guides for the Pilbara. Miscellaneous Publication 19/2002. Perth, Australia: Department of Agriculture, 83 pp.

PCI Geomatica (2003) *Orthoengine User Guide, Geomatica Version 9*, PCI Geomatics, Richmond Hill, Ontario, Canada, 158 pp.

Pontius, R. G. Jr and Schneider, L. C. (2001) Land-cover change model validation by an ROC method for the Ipswich watershed, Massachusetts, USA, *Agriculture Ecosystems and Environment*, Vol. 85, pp. 239-248.

Polley, H. W., Johns, H. B. and Mayeux, H. S. (1994) Increasing CO_2: Comparitive responses of the C4 grass *Schizachyrium* and grassland invader *Prosopis*, *Ecology*, Vol. 75, pp. 976-988.

Polley, H. W. (1997) Implications of rising atmospheric carbon dioxide concentration for rangelands, *Journal of Range Management*, Vol. 50, pp. 563-577.

Rango, A., and Havstad, K. (2003) The utility of historical aerial photographs for detecting and judging the effectiveness of rangeland remediation treatments, *Environmental Practice*, Vol. 5, pp. 107-118.

Rango, A., Laliberte, A., Steele, C., Herrick, J.E., Bestelmeyer, B., Schmugge, T., Roanhorse, A., and Jenkins, V. (2006) Using Unmanned Aerial Vehicles for Rangelands: Current Applications and Future Potentials, *Environmental Practice*, Vol. 8, pp. 159-168.

Ramsey, E. W. III, Nelson, G. A., Sapkota, S. K., Seeger, E. B. and Martella, K. D. (2002) Mapping Chinese Tallow with colour-infrared photography, *Photogrammetric Engineering and Remote Sensing*, Vol. 68, pp. 251-255.

Rejmanek, M. and Pitcairn, M. J. (2002) When is eradication of exotic pest plants a realistic goal? In: Veitch, C.R. and Clout, M. N. (eds), *Turning the tide: The eradication of invasive species*, IUCN SSC Invasive Species Specialist Group, Gland, Switzerland, and Cambridge, UK, pp. 249-252.

Richards, J. A. and Jia, X. (1999) *Remote sensing digital image analysis: An introduction,* Springer-Verlag, Berlin, 363 pp.

Robertson, M. P., Peter, C. I., Villet, M. H., and Ripley, B. S. (2003) Comparing models for predicting species' potential distributions: a case study using correlative and mechanistic predictive modelling techniques, *Ecological Modelling*, Vol. 164, pp. 153-167.

Robertson, M. P., Villet, M. H. and Palmer, A. R. (2004) A fuzzy classification technique for predicting species' distributions: applications using invasive alien plants and indigenous insects, *Diversity and Distributions*, Vol. 10, pp. 461-474.

Robinson, T. P., van Klinken, R. D., and Metternicht, G. I. (2008) Spatial and temporal rates and patterns of mesquite (*Prosopis* spp.) invasion in Western Australia, *Journal of Arid Environments*, Vol. 72, pp. 175-188.

Rossiter, D. G. (2004) Technical Note: Statistical methods for accuracy assessment of classified thematic maps, Department of Earth Systems Analysis, International Institute for Geo-information Science and Earth Observation (ITC), Enschede (NL), 46 pp.

Rouget, M., Richardson, D. M., Nel, J. L., Le Maitre, D. C., Egoh, B. and Mgidi, T. (2004) Mapping the potential ranges of major plant invaders in South Africa, Lesotho and Swaziland using climatic suitability, *Diversity and Distributions*, Vol. 10, pp. 475-484.

Roujean, J. L., Leroy, M. and Deschamps, P. Y. (1992) A bidirectional reflectance model of the Earth's Surface for the Correction of Remote Sensing Data, *Journal of Geophysical Research*, Vol. 20, pp. 455-468.

Rumelhart, D. E., Hinton, G. E. and Williams, R. J. (1986) Learning Internal Representations by Error Propagation, in D. E. Rumelhart & McClelland, (eds.), *Parallel Distributed Processing: Explorations in the Microstructures of Cognition*, vol. 1, MIT Press, Cambridge, pp. 318-362.

Saaty, T. L. (1977) A scaling method for priorities in hierarchical structures, *Journal of Mathematical Phycology*, Vol. 15, pp. 234-281.

Saaty, T. L. (1990) How to make a decision: the analytic hierarchy process, European *Journal of Operational Research*, Vol. 48, pp. 9-26.

Scanlan, J. C., and Archer, S. (1991) Simulated dynamics of succession in a North American subtropical Prosopis savanna, *Journal of Vegetation Science*, Vol. 2, pp. 625-634.

Schlesinger, W. H., Reynolds, J. F., Cunningham, G. L., Huenneke, L., Jarrell, W. M., Virginia, R. A. and Whiteford, W. G. (1990) Biological Feedbacks in Global Desertification, *Science,* Vol. 247, pp. 1043-1048.

Schmidt, K. S. and Skidmore, A. K. (2003) Spectral discrimination of vegetation types in a coastal wetland, Remote Sensing of Environment, Vol. 85, pp. 92-108.

Schoener, T. W. (1990) The ecological niche, In: Ecological concepts: the contribution of ecology to an understanding of the natural world (Cherrett, J. M. ed), Blackwell Scientific Publications, Oxford, pp. 79-113.

Scholes, R. J. and Archer, S. R. (1997) Tree-grass interactions in savannas, *Annual Review of Ecology and Systematics*, Vol. 28, pp. 517-544.

Sharp, B. R. and Bowman, D. M. J. S. (2004a) Net Woody Vegetation Increase Confined to Seasonally Inundated Lowlands in an Australian Tropical Savanna,

Victoria River District, Northern Territory, *Austral Ecology,* Vol. 29, pp. 667-683.

Sharp, B. R. and Bowman, D. M. J. S., (2004b) Patterns of Long-Term Woody Vegetation Change in a Sandstone-Plateau Savanna Woodland, Northern Territory, Australia, *Journal of Tropical Ecology,* Vol. 20, pp. 259-270.

Shearer, G., Kohl, D. H., Virginia, R. A., Bryan, B. A., Skeeters, J. L. Nilsen, E. T., Sharifi, M. R. and Rundel, P. W. (1983) Estimates of N2-fixation from variations in the natural abundance of 15N in Sonora Desert ecosystems, Oecologia, Vol. 56, pp. 365-373.

SpecTerra Services (2003) *DMSI Technical Specifications and Costs*, SpecTerra Services Pty LTd, Leederville, Western Australia, 2 pp.

Stehman, S. V. (1999) Comparing thematic maps based on map value, *International Journal of Remote Sensing*, Vol. 20, pp. 2347-2366.

Stephenson, C. M., MacKenzie, M. L., Edwards, C. and Travis, J. M. J. (2006) Modelling establishment probabilities of an exotic plant, *Rhododendron ponticum*, invading a heterogenous, woodland landscape using logistic regression with spatial autocorrelation, *Ecological Modelling*, Vol. 193, pp. 747-758.

Stewart, J., 1995. Calculus, 3rd ed. Brooks/Cole Publishing Company, Melbourne.

Stromberg, J. C., Wilkins, S. D., and Tress, J. A. (1993) Vegetation-hydrology models: implications for management of *Prosopis velutina* (velvet mesquite) riparian ecosystems, *Ecological Applications*, Vol. 3, pp. 307-314.

Taylor, J. E. (1990) Feasibility of remote sensing for monitoring bracken fern in eastern Australia, In: Thompson, J. A. and Smith, R. T. (eds), *Bracken Biology and Management*, The Australian Institute of Agricultural Science, Sydney, Australia, pp. 133-139.

Thorp, J. R. and Lynch, R. (2000) The determination of weeds of national significance, National Weeds Strategy Executive Committee, Launceston.

Tso, B. and Mather, P. M. (2001) *Classification methods for remotely sensed data*, Taylor and Francis, London, 352 pp.

Ullah, E., Field, R. P., McLaren, D. A. and Peterson, J. A. (1989) Use of airborne thematic mapper (ATM) to map the distribution of blackberry (*Rubus fruticosus* agg.) (Rosaceae) in the Strzelecki Ranges, south Gippsland, Victoria, *Plant Protection Quarterly*, Vol. 4, pp. 149-154.

Underwood, E., Ustin, S. and DiPietro, D. (2003) Mapping nonnative plants using hyperspectral imagery, *Remote Sensing of Environment,* Vol. 86, pp. 150-161.

USGS (2003) Monitoring changes in vegetation and land surfaces by remote sensing – Detecting infestations of Cheatgrass on the Colardo Plateau Available: http://climchange.cr.usgs.gov/info/sw/monitor/remote1.html)

Van Auken, O. W. (2000) Shrub invasions of North American semiarid grasslands, *Annual Review of Ecology and Systematics*, Vol. 31, pp. 2-20.

van Klinken, R. D. and Campbell, S. D. (2001). The biology of Australian weeds 37. *Prosopis* L. species, *Plant Protection Quarterly*, Vol. 16, pp. 2-20.

van Klinken, R. D., Fichera, G. and Cordo, H. (2003) Targeting biological control across diverse landscapes: the release, establishment and early success of two insects on mesquite (Prosopis) in rangeland Australia, *Biological Control*, Vol. 26, pp. 8-20.

van Klinken, R. D., Graham, J., and Flack, L. K. (2006) Population ecology of hybrid mesquite (*Prosopis* species) in Western Australia: how does it differ from native range invasions and what are the implications for impacts and management?, *Biological Invasions*, Vol. 8, pp. 727-741.

van Klinken, R. D., Shepherd, D., Parr, R., Robinson, T. P. and Anderson, L. (2007) Mapping mesquite (*Prosopis*) distribution and density using visual aerial surveys, *Rangeland Ecology & Management*, Vol. 60, pp. 408–416.

Van Vreeswyk, A. M. E., Payne, A. L., Leighton, K. A. and Hennig, P. (2004) Technical bulletin No. 92: An inventory and condition survey of the Pilbara Region, Western Australia, Department of Agriculture, Western Australia, 424 pp.

Vogelmann, T. C. (1993) Plant tissue optics, *Annual Review of Plant Physiology and Plant Molecular Biology*, Vol. 44, pp. 231-251.

Walpole, R. E. and Myers, R. H. (1993) Probability and statistics for engineers and scientists, 5th Edition, Macmillan Publishing Company, Sydney, 766 pp.

Wang, L., Sousa, W. P., Gong, P., Biging, G. S. (2004) Comparison of IKONOS and QuickBird images for mapping mangrove species on the Caribbean coast of Panama, *Remote Sensing of Environment*, Vol. 91, pp. 432-440.

Wang, C., Menenti, M. Stoll, M-P., Belluco, E., Marani, M. (2007) Mapping mixed vegetation communities in salt marshes using airborne spectral data, *Remote Sensing of Environment*, Vol. 107, pp. 559-570.

Warren, A., Holechek, J., and Cardenas, M. (1996) Honey mesquite influences on Chihuahuan Desert vegetation, *Journal of Range Management*, Vol. 49, pp. 46-52.

Wright, H. A., Bunting, S. C. and Neuenschwander, L. F. (1976) Effect of fire on honey mesquite, *Journal of Range Management*, Vol. 29, pp. 567-571.

Yager, R. R. (1988) On ordered weighted averaging aggregation operators in multi-criteria decision making, *IEEE Transactions on Systems, Man and Cybernetics*, Vol. 18, pp. 183-190.

Zadeh, L. A. (1965) Fuzzy sets, *Information and Control*, Vol. 8, pp. 338-353.

Zadeh, L. A. (1987) Fuzzy sets as a basis for a theory of possibility, In: *Fuzzy sets and applications: selected papers by LA Zadeh*, Yager, R. R., Ovchinnikov, S. Tong, R. M. and Nguyen, H. T. (eds), John Wiley and Sons, New York, pp. 193-218.

Zweig, M. H. and Campbell, G. (1993) Receiver-operating characteristic (ROC) plots: a fundamental evaluation tool in clinical medicine, *Clinical Chemistry*, Vol.39,pp.561-577.

APPENDIX A

Patch statistics of mesquite and associated species derived from the hyperspectral imagery after normalisation. Statistics in bold show significant differences between all species.

Band	Patch Statistic	Mesquite	Standard Deviation	Snakewood	Standard Deviation	Eucalyptus	Standard Deviation
VIS:1 (456 nm)	Mean	0.679a	0.033	0.737b	0.049	0.755b	0.053
VIS:2 (471 nm)	Mean	0.672a	0.033	0.728b	0.049	0.754b	0.054
VIS:3 (486 nm)	**Mean**	**0.666a**	0.033	**0.72b**	0.050	**0.753c**	0.055
VIS:4 (501 nm)	**Mean**	**0.670a**	0.036	**0.716b**	0.054	**0.758c**	0.056
VIS:5 (515 nm)	**Mean**	**0.673a**	0.037	**0.711b**	0.058	**0.762c**	0.060
VIS:6 (531 nm)	Mean	0.690a	0.041	0.717a	0.061	0.767b	0.061
VIS:7 (545 nm)	Mean	0.707a	0.045	0.723a	0.071	0.772b	0.066
VIS:8 (560 nm)	Mean	0.716a	0.054	0.736a	0.073	0.778b	0.072
VIS:9 (575 nm)	Mean	0.726a	0.060	0.749a	0.074	0.785b	0.074
VIS:10 (590 nm)	Mean	0.729a	0.077	0.755a	0.075	0.784b	0.082
VIS:11 (605 nm)	**Mean**	**0.732a**	0.083	**0.761b**	0.076	**0.783c**	0.088
VIS:12 (619 nm)	**Mean**	**0.727a**	0.083	**0.759b**	0.076	**0.780c**	0.088
VIS:13 (634 nm)	**Mean**	**0.722a**	0.083	**0.758b**	0.076	**0.777c**	0.088
VIS:14 (648 nm)	**Mean**	**0.713a**	0.108	**0.751b**	0.082	**0.771c**	0.118
VIS:15 (663 nm)	**Mean**	**0.704a**	0.126	**0.744b**	0.091	**0.765c**	0.132
VIS:16 (677 nm)	**Mean**	**0.713a**	0.129	**0.752b**	0.095	**0.774c**	0.138
VIS:17 (692 nm)	**Mean**	**0.722a**	0.135	**0.759b**	0.099	**0.784c**	0.141
VIS:18 (706 nm)	Mean	0.758a	0.135	0.778a	0.113	0.808b	0.123
VIS:19 (721 nm)	Mean	0.794a	0.135	0.796a	0.121	0.831b	0.116
VIS:20 (735 nm)	Mean	0.801a	0.157	0.805a	0.131	0.843b	0.122
VIS:21 (749 nm)	Mean	0.808a	0.157	0.814a	0.131	0.855b	0.122
VIS:22 (763 nm)	Mean	0.806a	0.159	0.806a	0.133	0.855b	0.128
VIS:23 (778 nm)	Mean	0.805a	0.163	0.797a	0.135	0.855b	0.131
VIS:24 (792 nm)	Mean	0.800a	0.164	0.796a	0.136	0.857b	0.134
VIS:25 (806 nm)	Mean	0.794a	0.165	0.796a	0.137	0.859b	0.137
VIS:26 (821 nm)	Mean	0.790a	0.165	0.791a	0.137	0.859b	0.137
VIS:27 (835 nm)	Mean	0.787a	0.165	0.786a	0.137	0.859b	0.143
VIS:28 (849 nm)	Mean	0.784a	0.165	0.783a	0.137	0.859b	0.143

VIS:29 (863 nm)	Mean	0.782a	0.166	0.780a	0.138	0.859b	0.148
VIS:30 (876 nm)	Mean	0.781a	0.166	0.778a	0.138	0.858b	0.148
NIR:31 (882 nm)	Mean	0.780a	0.165	0.776a	0.138	0.858b	0.151
NIR:32 (898 nm)	Mean	0.780a	0.165	0.772a	0.138	0.857b	0.151
NIR:33 (912 nm)	Mean	0.779a	0.164	0.767a	0.135	0.856b	0.151
NIR:34 (928 nm)	Mean	0.782a	0.164	0.768a	0.135	0.856b	0.151
NIR:35 (944 nm)	Mean	0.786a	0.161	0.768a	0.127	0.857b	0.153
NIR:36 (959 nm)	Mean	0.785a	0.161	0.762a	0.127	0.854b	0.153
NIR:37 (974 nm)	**Mean**	**0.784a**	0.161	**0.756b**	0.126	**0.852c**	0.156
NIR:38 (989 nm)	**Mean**	**0.788a**	0.161	**0.758b**	0.126	**0.855c**	0.156
NIR:39 (1005 nm)	**Mean**	**0.791a**	0.164	**0.761b**	0.128	**0.858c**	0.158
NIR:40 (1020 nm)	**Mean**	**0.792a**	0.164	**0.764b**	0.128	**0.860c**	0.158
NIR:41 (1035 nm)	**Mean**	**0.794a**	0.168	**0.768b**	0.130	**0.863c**	0.161
NIR:42 (1050 nm)	**Mean**	**0.795a**	0.168	**0.768b**	0.130	**0.864c**	0.161
NIR:43 (1065 nm)	**Mean**	**0.796a**	0.169	**0.769b**	0.130	**0.866c**	0.163
NIR:44 (1079 nm)	**Mean**	**0.800a**	0.169	**0.769b**	0.130	**0.868c**	0.163
NIR:45 (1094 nm)	**Mean**	**0.803a**	0.170	**0.769b**	0.129	**0.871c**	0.166
NIR:46 (1108 nm)	**Mean**	**0.811a**	0.170	**0.770b**	0.129	**0.874c**	0.166
NIR:47 (1123 nm)	**Mean**	**0.819a**	0.170	**0.772b**	0.128	**0.876c**	0.166
NIR:48 (1137 nm)	**Mean**	**0.813a**	0.170	**0.756b**	0.128	**0.866c**	0.174
NIR:49 (1152 nm)	**Mean**	**0.807a**	0.168	**0.739b**	0.116	**0.855c**	0.184
NIR:50 (1166 nm)	**Mean**	**0.810a**	0.168	**0.741b**	0.116	**0.857c**	0.184
NIR:51 (1180 nm)	**Mean**	**0.814a**	0.167	**0.743b**	0.119	**0.859c**	0.188
NIR:52 (1194 nm)	**Mean**	**0.816a**	0.167	**0.742b**	0.119	**0.860c**	0.188
NIR:53 (1208 nm)	**Mean**	**0.817a**	0.165	**0.742b**	0.116	**0.862c**	0.189
NIR:54 (1222 nm)	**Mean**	**0.820a**	0.165	**0.746b**	0.116	**0.866c**	0.189
NIR:55 (1236 nm)	**Mean**	**0.822a**	0.163	**0.750b**	0.117	**0.870c**	0.190
NIR:56 (1250 nm)	**Mean**	**0.822a**	0.163	**0.750b**	0.117	**0.871c**	0.190
NIR:57 (1264 nm)	**Mean**	**0.821a**	0.159	**0.749b**	0.119	**0.872c**	0.191
NIR:58 (1278 nm)	**Mean**	**0.818a**	0.158	**0.745b**	0.122	**0.869c**	0.197

NIR:59 (1291 nm)	**Mean**	**0.815a**	0.158	**0.741b**	0.121	**0.866c**	0.198
NIR:60 (1305 nm)	**Mean**	**0.812a**	0.158	**0.732b**	0.121	**0.859c**	0.198
NIR:61 (1319 nm)	**Mean**	**0.810a**	0.161	**0.724b**	0.123	**0.852c**	0.211
NIR:62 (1389 nm)	**Mean**	**0.628a**	0.161	**0.578b**	0.123	**0.605c**	0.211
SWIR1:63 (1404 nm)	Mean	0.447a	0.963	0.432a	0.655	0.358b	1.000
SWIR1:64 (1419 nm)	Mean	0.590a	0.376	0.575a	0.209	0.500b	0.372
SWIR1:65 (1433 nm)	Mean	0.734a	0.376	0.718a	0.209	0.643b	0.372
SWIR1:66 (1447 nm)	Mean	0.730a	0.369	0.715a	0.205	0.640b	0.369
SWIR1:67 (1462 nm)	Mean	0.727a	0.363	0.712a	0.196	0.638b	0.367
SWIR1:68 (1476 nm)	Mean	0.740a	0.363	0.726a	0.196	0.645b	0.365
SWIR1:69 (1490 nm)	Mean	0.753a	0.366	0.739a	0.189	0.652b	0.364
SWIR1:70 (1504 nm)	Mean	0.758a	0.366	0.746a	0.189	0.657b	0.359
SWIR1:71 (1518 nm)	Mean	0.764a	0.343	0.753a	0.182	0.662b	0.353
SWIR1:72 (1531 nm)	Mean	0.770a	0.343	0.760a	0.182	0.667b	0.353
SWIR1:73 (1545 nm)	Mean	0.777a	0.330	0.766a	0.178	0.672b	0.346
SWIR1:74 (1558 nm)	Mean	0.781a	0.330	0.770a	0.178	0.674b	0.346
SWIR1:75 (1572 nm)	Mean	0.785a	0.322	0.774a	0.177	0.676b	0.341
SWIR1:76 (1585 nm)	Mean	0.791a	0.320	0.781a	0.177	0.681b	0.341
SWIR1:77 (1598 nm)	Mean	0.797a	0.318	0.788a	0.177	0.686b	0.340
SWIR1:78 (1611 nm)	Mean	0.800a	0.313	0.791a	0.177	0.687b	0.340
SWIR1:79 (1624 nm)	Mean	0.804a	0.309	0.794a	0.176	0.688b	0.336
SWIR1:80 (1637 nm)	Mean	0.806a	0.307	0.796a	0.176	0.690b	0.336
SWIR1:81 (1650 nm)	Mean	0.807a	0.305	0.798a	0.177	0.692b	0.335
SWIR1:82 (1663 nm)	Mean	0.804a	0.307	0.795a	0.182	0.690b	0.335
SWIR1:83 (1675 nm)	Mean	0.801a	0.309	0.792a	0.176	0.689b	0.335
SWIR1:84 (1688 nm)	Mean	0.796a	0.313	0.787a	0.177	0.686b	0.338
SWIR1:85 (1700 nm)	Mean	0.791a	0.316	0.782a	0.177	0.682b	0.340
SWIR1:86 (1713 nm)	Mean	0.788a	0.318	0.778a	0.177	0.680b	0.341
SWIR1:87 (1725 nm)	Mean	0.784a	0.322	0.773a	0.179	0.677b	0.342
SWIR1:88 (1737 nm)	Mean	0.781a	0.322	0.771a	0.179	0.674b	0.342

SWIR1:89 (1750 nm)	Mean	0.778a	0.320	0.769a	0.180	0.672b	0.343
SWIR1:90 (1762 nm)	Mean	0.774a	0.319	0.764a	0.180	0.668b	0.344
SWIR1:91 (1774 nm)	Mean	0.769a	0.319	0.759a	0.180	0.664b	0.344
SWIR1:92 (1786 nm)	Mean	0.760a	0.319	0.752a	0.186	0.658b	0.344
SWIR1:93 (1798 nm)	Mean	0.752a	0.318	0.745a	0.195	0.652b	0.349
SWIR1:94 (1952 nm)	Mean	0.724a	0.359	0.713a	0.199	0.628b	0.369
SWIR2:95 (1971 nm)	Mean	0.695a	0.386	0.681a	0.195	0.603b	0.374
SWIR2:96 (1990 nm)	Mean	0.701a	0.369	0.687a	0.189	0.609b	0.366
SWIR2:97 (2009 nm)	Mean	0.707a	0.367	0.693a	0.189	0.615b	0.361
SWIR2:98 (2028 nm)	Mean	0.697a	0.367	0.683a	0.195	0.611b	0.361
SWIR2:99 (2047 nm)	Mean	0.687a	0.365	0.673a	0.200	0.607b	0.362
SWIR2:100 (2067 nm)	Mean	0.679a	0.369	0.664a	0.206	0.602b	0.364
SWIR2:101 (2085 nm)	Mean	0.671a	0.379	0.654a	0.206	0.597b	0.367
SWIR2:102 (2104 nm)	Mean	0.670a	0.379	0.653a	0.209	0.596b	0.367
SWIR2:103 (2122 nm)	Mean	0.670a	0.384	0.652a	0.209	0.596b	0.377
SWIR2:104 (2140 nm)	Mean	0.678a	0.384	0.662a	0.201	0.602b	0.372
SWIR2:105 (2158 nm)	Mean	0.687a	0.372	0.671a	0.195	0.608b	0.368
SWIR2:106 (2176 nm)	Mean	0.696a	0.359	0.682a	0.190	0.614b	0.358
SWIR2:107 (2193 nm)	Mean	0.705a	0.353	0.693a	0.190	0.620b	0.358
SWIR2:108 (2212 nm)	Mean	0.702a	0.348	0.689a	0.189	0.620b	0.353
SWIR2:109 (2229 nm)	Mean	0.699a	0.347	0.685a	0.195	0.620b	0.349
SWIR2:110 (2246 nm)	Mean	0.678a	0.347	0.663a	0.196	0.607b	0.341
SWIR2:111 (2264 nm)	Mean	0.658a	0.351	0.641a	0.196	0.594b	0.341
SWIR2:112 (2281 nm)	Mean	0.653a	0.343	0.636a	0.191	0.592b	0.327
SWIR2:113 (2299 nm)	Mean	0.648a	0.338	0.630a	0.185	0.590b	0.326
SWIR2:114 (2316 nm)	Mean	0.644a	0.328	0.627a	0.182	0.585b	0.313
SWIR2:115 (2332 nm)	Mean	0.640a	0.321	0.624a	0.174	0.580b	0.309
SWIR2:116 (2349 nm)	Mean	0.640a	0.318	0.624a	0.173	0.581b	0.302
SWIR2:117 (2365 nm)	Mean	0.641a	0.306	0.625a	0.167	0.582b	0.295
SWIR2:118 (2382 nm)	Mean	0.641a	0.293	0.626a	0.167	0.582b	0.283

SWIR2:119 (2399 nm)	Mean	0.641a	0.293	0.626a	0.167	0.581b	0.283
SWIR2:120 (2415 nm)	Mean	0.633a	0.282	0.619a	0.159	0.578b	0.266
SWIR2:121 (2431 nm)	Mean	0.625a	0.273	0.612a	0.158	0.575b	0.261
SWIR2:122 (2447 nm)	Mean	0.606a	0.231	0.594a	0.128	0.562b	0.204
SWIR2:123 (2462 nm)	Mean	0.586a	0.206	0.575a	0.126	0.548b	0.196
SWIR2:124 (2478 nm)	Mean	0.472a	0.154	0.470a	0.077	0.423b	0.122
SWIR2:125 (2494 nm)	Mean	0.359a	0.117	0.366a	0.068	0.298b	0.114
SWIR2:126 (2500 nm)	Mean	0.180a	0.033	0.183a	0.049	0.149b	0.053